The Proteinase-activated receptor 1 in mesenchymal stem cells – Importance for the progression of hepatocellular carcinoma

Dissertation

To Fulfill the Requirements for the Degree of

“Doctor rerum naturalium” (Dr. rer. nat.)

seit 1558

Submitted to the Council of the Faculty of Biology and Pharmacy of the

Friedrich Schiller University Jena

by

Graduate Biochemist Matthias Ditze

born on April 25, 1987, in Gera

Jena, March 2017

Gutachter:

1. ***Prof. Dr. rer. nat. Frank-Dietmar Böhmer***
   Institut für Molekulare Zellbiologie
   Hans-Knöll-Str. 2, 07745 Jena

2. ***Prof. Dr. rer. nat. Bruno Christ***
   Klinik und Poliklinik für Visceral-, Transplantations-, Thorax- und Gefäßchirurgie
   Liebigstraße 20, 04103 Leipzig

3. ***Prof. Dr. med. Utz Settmacher***
   Klinik für Allgemein-, Viszeral- und Gefäßchirurgie
   Am Klinikum 1, 07747 Jena

Tag der öffentlichen Verteidigung: 26.01.2017

List of contents

List of abbreviations

Ang	angiopoietin
Ang-1/2	angiogenin 1/2
APS	ammonium persulfate
AT-MSC	adipose tissue-derived mesenchymal stem cell
Ato	Atopaxar
BAPTA-AM	1,2-Bis(2-aminophenoxy)ethane-N,N,N′,N′-tetraacetic acid tetrakis(acetoxymethyl ester)
BCA	bicinchoninic acid
BIM-1	bisindolylmaleimide 1
BM-MSC	bone marrow-derived mesenchymal stem cell
BSA	bovine serum albumin
cat. no.	catalog number
cDNA	complementary deoxyribonucleic acid
C_q	quantification cycle
CT	computed tomography
DAG	diacylglycerol
ddH_2O	double-distilled water
DMEM	Dulbecco's Modified Eagle Medium
DMEM10	DMEM with 10 % (v/v) fetal calf serum and 1 % (v/v) penicillin/streptomycin
DMSO	dimethyl sulfoxide
DNA	deoxyribonucleic acid
E. coli	*Escherichia coli*
EDTA	ethylenediaminetetraacetic acid
EF	exoplasmic fracture face
ELISA	enzyme-linked immunosorbent assay
EM6F	MSC culture growth medium
EM6F15	EM6F with 15 % (v/v) fetal calf serum
ERK 1/2	extracellular-signal regulated kinase 1/2
ESC	embryonal stem cells
FCS	fetal calf serum
Fluo-4-AM	Fluo-4-acetoxymethyl ester
FRIL	freeze-fracture replica immunolabeling
GFP	green fluorescent protein
G protein	guanine nucleotide-binding protein
GAPDH	glyceraldehyde 3-phosphate dehydrogenase
GOI	gene of interest
GPCR	G protein-coupled receptor
HBV	hepatitis B virus
HCC	hepatocellular carcinoma
HCV	hepatitis C virus
HE	hematoxylin/eosin
HEK293T	transformed human embryogenic kidney cell line
Hep3B	HCC cell line
HEPES	4-(2-hydroxyethyl)-1-piperazineethanesulfonic acid
HGF	hepatocyte growth factor
HRP	horse radish peroxidase
IL-6/8	Interleukin 6/8
iPSC	induced pluripotent stem cells
MAPK	mitogen-activated protein kinase
MCP-1	monocyte chemotactic protein 1
MEK	MAPK/ERK kinase
Met	HGF receptor
MMP	matrix metalloproteinase
mRNA	messenger ribonucleic acid
MSC	mesenchymal stem cell
NF-κB	nuclear factor kappa-light-chain-enhancer of activated B cells
NIH-U	National Institute of Health unit
$PAR_{1/2/3/4}$	proteinase-activated receptor 1/2/3/4
$PAR_{1/2/4}$-AP	$PAR_{1/2/4}$-activating peptide
PBS	phosphate-buffered saline
PCR	polymerase chain reaction
PDGFR	platelet-derived growth factor receptor
PEI	polyethylenimine
PI_3K	phosphatidylinositide 3-kinase
PKC	protein kinase C
PLC-β	phosphoinositide phospholipase C β
PVDF	polyvinylidene fluoride
qPCR	quantitative real-time polymerase chain reaction
RhoA	Ras homolog gene family member A
RNA	ribonucleic acid
RPMI	Roswell Park Memorial Institute medium
RT	room temperature
SCID	severe combined immunodeficiency
SD	standard deviation
SDS-PAGE	sodium dodecyl sulfate polyacrylamide gel electrophoresis
shRNA	small hairpin ribonucleic acid
T_A	annealing temperature
TACE	trans-arterial chemoembolization
TBST	Tris-buffered saline/Tween
TEMED	N,N,N',N'-tetramethyl-ethylenediamine
temp.	temperature
TIMP-1	tissue inhibitor of matrix metalloproteinases
T_M	melting temperature
TRC	The RNAi Consortium
TSP-1	thrombospondin 1
VEGF	vascular endothelial growth factor
α-SMA	alpha-smooth muscle actin

Summary

Mesenchymal stem cells (MSCs) are unspecialized cells with the capability to differentiate into various cell entities. They also secrete many biologically active factors with regenerative potential, making them a potentially suitable option for the treatment of chronic liver diseases. However, the chronically damaged liver is susceptible to the formation of hepatocellular carcinoma (HCC), whose potential interaction with therapeutically applied exogenous MSCs is unknown. In this context, the family of proteinase-activated receptors (PARs) deserves special attention, which occupies a promoting role in the progression of HCC, cirrhosis and cholangiocarcinoma through activation in different cell entities of the liver parenchyma. PARs are currently insufficiently characterized in MSCs. Hence, we hypothesized that PARs may also exert a biologically relevant role in MSCs, as well in the potential interaction with HCC initiation and progression.

For assessing the role of the PAR family in MSCs, we employed primary human adipose tissue-derived MSCs (AT-MSCs). Our results indicated that PAR_1 is the predominantly expressed PAR subtype in AT-MSCs, which exerted a strong increase in the intracellular free Ca^{2+} concentration upon stimulation with thrombin or the subtype-specific PAR_1-activating peptide (PAR_1-AP) TFLLRN-NH_2. Activation of other PAR subtypes caused only a comparatively weak (PAR_2) or no Ca^{2+} response (PAR_4). Hence, we focused the additional characterization on PAR_1. We initially verified its presence on the plasma membrane of AT-MSCs via the freeze-fracture replica immunolabeling technique. Furthermore, PAR_1 activation in AT-MSCs caused no effects on the cells' proliferation rate, but significantly reduced their rate of migration across a collagen-coated porous polycarbonate membrane. Moreover, we identified a large number of biologically active proteins in conditioned media of AT-MSCs, among them interleukin (IL)-6, IL-8 and monocyte chemotactic protein 1 (MCP-1). PAR_1 activation led to an elevated expression and secretion of these cytokines. The PAR_1 antagonist Atopaxar, the Ca^{2+} chelator BAPTA-AM and the protein kinase C (PKC) inhibitor BIM-1 reduced the secretion of IL-8 and IL-6, thus implying PAR_1 specificity and dependency on the Ca^{2+}/PKC pathway of the observed expression and secretion events.

The MSCs' secretory activity is likely to affect adjacent cells, e.g. aberrant hepatocytes in the HCC microenvironment, during potential cellular therapy. We assessed the biologic relevance of such cell interactions *in vivo* using a xenotransplantation mouse model. To this end, we subcutaneously co-injected AT-MSCs and cells from the HCC cell line Hep3B into immunocompromised mice. Hep3B cells and AT-MSCs together caused a strong formation of tumors with typical histologic HCC characteristics, while Hep3B cells alone only occasionally caused tumors of significantly smaller size and AT-MSCs

alone caused no tumors. To track down the stem cells in the tumors, we employed green fluorescent protein (GFP)-labeled AT-MSCs in this tumor model, but we were not able to detect GFP in the formed Hep3B tumors. These results implied that the AT-MSC-derived promoting effect on the Hep3B cells' growth affected initial tumor developmental stages.

Furthermore, the shRNA-mediated stable knockdown of PAR_1 in AT-MSCs had no significant impact on the observed tumor formation by the co-injection of Hep3B cells and AT-MSCs. Therefore, the potentially PAR_1-triggered signaling in AT-MSCs did not seem to have an influence on the tumor formation in the employed mouse model.

In conclusion, we could demonstrate that the PAR family is expressed in AT-MSCs and that PAR_1 has a significant impact on the biology of these stem cells via affecting their migratory behavior and by regulating the expression and secretion of proteins with potentially tumor-promoting effects. Furthermore, the *in vivo* interaction of AT-MSCs with HCC cells seems to favor HCC tumor growth in the subcutaneous mouse model studied. However, additional experimental efforts will aid to verify and assess the importance of these *in vivo* findings for the MSC-based therapy of HCC.

Zusammenfassung

Mesenchymale Stammzellen (MSCs) sind unspezialisierte Zellen mit der Fähigkeit, sich in verschiedene Zelltypen differenzieren zu können. Zudem sezernieren sie viele biologisch aktive Faktoren mit regenerativem Potential, welche sie potenziell für die Behandlung von Lebererkrankungen geeignet erscheinen lassen. Die chronisch geschädigte Leber ist jedoch anfällig für die Entwicklung des hepatozellulären Karzinoms (HCC). Welchen Einfluss eventuell applizierte exogene MSCs auf die Entwicklung eines HCC haben könnten, ist bislang ungeklärt. In diesem Zusammenhang könnte die Familie der Proteinase-aktivierbaren Rezeptoren (PARs) von besonderer Bedeutung sein. Frühere Arbeiten haben gezeigt, dass die Aktivierung von PARs in verschiedenen Zellarten des Leberparenchyms stattfindet und eine fördernde Rolle in der Entwicklung des HCCs, der Zirrhose und des Cholangiokarzinoms einnimmt. Daher vermuteten wir, dass die in MSCs unzureichend charakterisierten PARs ebenfalls eine Rolle sowohl für die biologischen Eigenschaften dieser Zellen selbst als auch für die potentielle Interaktion mit der HCC Initiation und Progression haben könnten.

Diese Fragestellungen wurden an primären MSCs, die aus humanem Fettgewebe isoliert wurden (AT-MSCs), untersucht. Unsere Ergebnisse zur PAR-Expression in diesen Zellen deuteten darauf hin, dass PAR_1 der prädominant exprimierte PAR-Subtyp in den AT-MSCs ist. Die PAR_1-Aktivierung mit Thrombin oder dem subtyp-spezifischen PAR_1-aktivierenden Peptid (PAR_1-AP) TFLLRN-NH_2 führte zu einer starken Erhöhung der intrazellulären freien Ca^{2+}-Konzentration, während die Stimulation anderer PAR-Subtypen nur eine schwache (PAR_2) oder keine (PAR_4) Ca^{2+}-Antwort erzeugten. Aus diesem Grund fokussierten wir unsere weiteren Untersuchungen auf PAR_1 und verifizierten zunächst dessen Expression auf der Plasmamembran mittels Elektronenmikroskopie von PAR_1-immunmarkierten Gefrierbruch-Replikas von AT-MSCs. Die PAR_1-Aktivierung in AT-MSCs hatte keinen Einfluss auf die Proliferationsrate der Zellen, führte jedoch zu einer signifikant reduzierten Migration der AT-MSCs durch eine Kollagen-beschichtete poröse Polycarbonat-Membran. Zudem identifizierten wir eine Vielzahl an biologisch aktiven Proteinen im Kulturüberstand der AT-MSCs, darunter Interleukin (IL)-6, IL-8 und Monozyten-chemotaktisches Protein 1 (MCP-1). Die PAR_1-Aktivierung führte zu einer erhöhten Expression und Sekretion dieser Zytokine. Der Einsatz des PAR_1-Antagonisten Atopaxar, des Ca^{2+}-Chelators BAPTA-AM und des Protein Kinase C (PKC)-Inhibitors BIM-1 reduzierte die Sekretion von IL-8 und IL-6, was eine PAR_1-Spezifität und Abhängigkeit vom Ca^{2+}/PKC-Signalweg für die beobachteten Expressions- und Sekretionsereignisse impliziert.

Die sekretorische Aktivität der MSCs könnte, im Zuge der potentiellen zellulären Therapie von Lebererkrankungen, Auswirkungen auf benachbarte Zellen, wie z.B. entartete Hepatozyten in der HCC-Mikroumgebung, haben. Die Möglichkeit einer solchen Zellinteraktion prüften wir in einem *in vivo*

Xenotransplantations-Mausmodell. AT-MSCs und Zellen der HCC-Zelllinie Hep3B wurden dazu gemeinsam subkutan in immundefiziente Mäuse injiziert. Die Hep3B-Zellen und AT-MSCs zusammen führten zu einer starken Tumorbildung mit typischen histologischen HCC-Charakteristiken. Hep3B-Zellen alleine bildeten nur gelegentlich Tumore mit deutlich geringerer Größe. Die alleinige Injektion von AT-MSCs bewirkte keine Tumorbildung. Um die Stammzellen in den Tumoren aufzuspüren, setzten wir grün fluoreszierendes Protein (GFP)-markierte AT-MSCs in diesem Tumormodel ein, jedoch konnten wir kein GFP in den gebildeten Hep3B-Tumoren detektieren. Dieser Befund impliziert, dass der stimulierende Effekt der AT-MSCs auf das Wachstum der Hep3B-Zellen während der initialen Tumorentwicklungsstadien auftrat.
Weiterhin hatte der stabile Knockdown von PAR_1 mittels shRNA in AT-MSCs keinen signifikanten Effekt auf die beobachtete Tumorbildung bei Koinjektion von Hep3B-Zellen und AT-MSCs. Daher schienen potenziell durch PAR_1-ausgelöste Signalwege in AT-MSCs keinen Einfluss auf die Tumorformation in dem angewendeten Mausmodel gehabt zu haben.

Zusammenfassend konnten wir zeigen, dass die PAR-Familie in AT-MSCs exprimiert wird und dass PAR_1 von Bedeutung für die Biologie dieser Stammzellen ist. PAR_1 hat einen Einfluss auf das Migrationsverhalten und auf die Regulation der Expression und Sekretion von potentiell tumorfördernden Proteinen. Weiterhin scheint in dem untersuchten Mausmodel die *in vivo* Interaktion von AT-MSCs und HCC-Zellen das HCC-Tumorwachstum zu fördern. Um die Wichtigkeit dieser *in vivo* Daten für die Behandlung des HCC mit MSCs beurteilen zu können, werden jedoch weitere experimentelle Bemühungen als Verifikation benötigt.

1 Introduction

Mesenchymal stem cells (MSCs) are emerging players in clinical research for the treatment and curation of tissue diseases, which fail to heal through natural mechanisms. Especially liver diseases can cause chronic damage and inflammation to the liver parenchyma, which potentially progress to cirrhosis and/or hepatocellular carcinoma (HCC). While conventional treatments of late stage liver diseases battle with relapse of HCC, the treatments with MSCs have recently shown promising curative effects. Notably, tremendous beneficial effects were observed with respect to the curation of liver failure and cirrhosis *in vivo* in animal models. However, the impact of MSCs on HCC and tumorous tissue in general remains controversial. HCC is one of the prevalent carcinomas and leading tumor-related causes of death worldwide. Several malignant features of HCC cells have been shown to be promoted by the guanine nucleotide-binding protein (G protein)-coupled receptor family of proteinase-activated receptors (PARs). PARs have also been linked to the promotion of liver fibrosis and cholangiocarcinoma through their activation in hepatic stellate cells or cholangiocytes of the liver parenchyma. Therefore, PARs might promote liver diseases through the activation of other cell entities as well. The external addition of large quantities of MSCs as means of cell-based therapy would add another cell population into the liver, with an insufficiently assessed biological relevance of the PAR family and impact on HCC. (Adams et al. 2011; Farazi & DePinho 2006; Hass & Otte 2012; Nakanuma et al. 2010).

1.1 Hepatocellular carcinoma

Hepatocellular carcinoma (HCC) is the major primary carcinoma event in liver tissue and comprises up to 90 % of all cases of primary liver cancer. Although precise numbers about the worldwide epidemiology of HCC are rather inconsistent between the references, it is clear that HCC ranks as the fifth or sixth most common cancer in the world. Especially Southeast Asia and sub-Saharan countries are affected, and HCC is the second or third most cancer-related cause of death. HCC especially occurs in patients above 40 years, with incidence peaking at the age of 70. Moreover, men are affected 2.4 times more often than women. (El-Serag 2011; European Association for the Study of the Liver & European Organisation for Research and Treatment of Cancer 2012; Farazi & DePinho 2006).

1.1.1 Causes for HCC

HCC has various underlying causes, which contribute to liver and hepatocyte aberrations. The liver is a major site for the storage of nutrients, a station for cleansing the body from harmful substances, and a general place of metabolite turnover and production. Hence, it is exposed to a variety of external

and internal influences that may cause sudden or slow changes in tissue integrity. Major influences for the onset of liver diseases include the following:

(1) Viral infections: Hepatitis B and C virus (HBV, HCV), Epstein-Barr virus, cytomegalovirus and adenovirus. 30-50 % of HBV-caused deaths are due to HCC, 2.5 % of HCV patients develop HCC. (Adams & Hubscher 2006; Farazi & DePinho 2006; Rehermann & Nascimbeni 2005).

(2) Steatohepatitis and alcohol: Excessive accumulation of cholesterols and triglycerides as a result of the metabolic syndrome (non-alcoholic steatohepatitis) or prolonged heavy alcohol intake (alcoholic liver disease). Additionally, the breakdown of alcohol in the liver leads to shortages of the oxygen and energy supply, and eventually damage of mitochondria and hepatocytes. (Ahmed 2015; Cunningham & Van Horn 2003; O'Shea, Dasarathy, & McCullough 2009).

(3) Obstructed bile and blood flow.

(4) Inherited diseases: Haemochromatosis and Wilson's disease express metabolic changes leading to a toxic accumulation of excess hepatic iron or copper, respectively. (Ulvik 2015; Wu et al. 2015).

(5) Chemical compounds: drugs, food additives, herbal compounds, aflatoxin B1-contaminated food or high dosages of vitamin A can cause liver intoxication and mutagenic events. (Chen et al. 2015a; Lopez & Hendrickson 2014).

(6) Cirrhosis: Scarring of liver tissue as an advanced stage of liver diseases, characterized by massive deposition of extracellular matrix (fibrosis) by activated hepatic stellate cells into the liver lobules, which leads to hardening and loss of function of the liver. (Tsochatzis, Bosch, & Burroughs 2014).

While HBV infections make up the major risk factors for liver diseases in countries with limited access to socialized medicine, developed countries largely face problems of drug and alcohol abuse and diseases linked to obesity. All causes may potentially lead to more severe liver disease stages with chronic inflammation, cirrhosis and HCC. (El-Serag 2011; Farazi & DePinho 2006).

1.1.2 Characteristics of HCC

The variety of HCC risk factors creates the basis for a phenotypic and large molecular heterogeneity among cases of HCC. Genomic analyses revealed that a set of 48 genes was frequently mutated in advanced stage HCCs. These genomic alterations are acquired through the chronic pro-inflammatory state in the diseased liver, accompanied by a constant demise of hepatocytes, necrosis, and hyperproliferation of adjacent cells. It was estimated that in a liver parenchyma with chronic hepatitis 1-3 % of hepatocytes die per day, in contrast to 0.01 % in healthy liver tissue. The liver is capable of growing to its full mass within five to ten days when two third of it is removed. However, the

permanent loss of hepatocytes during chronic inflammation may overcome the liver's self-regeneration potential, and may lead to genomic aberrations and eventually organ failure.

The high cellular turnover in the diseased liver favors the selection of pro-oncogenic genomic lesions in hepatocytes or progenitor cells. These genomic alterations can occur during replication errors, oxidative stress, and integration of the HBV genome or DNA intercalation of mutagenic aflatoxin B1. Major common events during HCC formation include the activation of telomerase activity, promotion of Wingless Int-1 (Wnt), mitogen-activated protein kinase (MAPK) and Janus kinase-signal transducer and activator of transcription (JAK-STAT) pathways, alterations of cell-cycle genes and inactivation of the tumor suppressor p53. (Aravalli 2010; Farazi & DePinho 2006; Marquardt, Andersen, & Thorgeirsson 2015; Taub 2004).

The progression of HCC is promoted by a large variety of autocrine and paracrine stimuli. Recent reports frequently described the involvement of receptors like epidermal growth factor receptor (EGFR), platelet-derived growth factor receptor (PDGFR), vascular endothelial growth factor receptor (VEGFR), hepatocyte growth factor (HGF) receptor (Met) and PARs in the promotion of HCC proliferation, invasion and migration. Especially PARs seem to play a central role in liver diseases since their implications in fibrosis, HCC and cancer were demonstrated by our and other research groups previously (for detailed information refer to paragraph 1.3.3, page 14). Cytokines like VEGF, HGF, monocyte chemotactic protein 1 (MCP-1), Interleukin (IL) 6 and IL-8 were also described in various publications to promote HCC through autocrine and paracrine mechanisms. The PAR family, as well as IL-6, IL-8 and MCP-1, were integral elements of this study and will be introduced in detail in paragraph 1.3 (page 10) and 1.2.3 (page 7), respectively. (Farazi & DePinho 2006; Marquardt, Andersen, & Thorgeirsson 2015).

The interplay of these molecular events in the liver causes the formation of a highly vascularized HCC, which forms single solid tumors with little or no tumor stroma during early stages. Advanced and terminal stages are characterized by an aggressive tumor state with multifocal lesions, vascular invasion and the formation of metastases. (European Association for the Study of the Liver & European Organisation for Research and Treatment of Cancer 2012; Schlachterman et al. 2015).

1.1.3 Diagnosis and treatment of HCC

The diagnosis of HCC is usually achieved through regular surveillance of high-risk patient groups with underlying pronounced hepatitis, non-alcoholic steatohepatitis, alcoholic liver disease or cirrhosis, or until HCC reveals itself. However, HCC may often not be perceived in early stages since it bears no pathognomonic symptoms and is prone to false diagnosis. Diagnosis tools include ultra-sonographic, computed tomographic and magnetic resonance imaging. In addition, percutaneous liver biopsies can be gathered to verify the diagnosis. Serum markers like alpha-fetoprotein (AFP) are upregulated in HCC

patients, but lack high specificity and may only serve as a hint for diagnosis. (Attwa & El-Etreby 2015; Schlachterman et al. 2015).

About one-third of HCC patients are diagnosed in early stages and face good prognosis. Early stages comprise single tumor sites with up to three nodules and are eligible for resection, ablation with high frequencies or ethanol, or liver transplantation. The choice of treatment highly depends on the location of the lesion, cirrhotic background, and organ donor availability. Another 20 % of patients are diagnosed in intermediate stages with multiple lesions and are treated with transarterial chemoembolization (TACE), in which HCC tissue is flushed with cytotoxic agents like doxorubicin. HCC tissue is mainly supplied by hepatic arteries, which allows embolization of affected areas while the main supply of the remaining tissue is still achieved via the portal vein. The remaining 50 % of patients face a poor prognosis and are diagnosed with advanced stages of HCC including metastasis. These patients are treated with TACE, radioembolization with $Yttrium^{90}$ loaded beads, radiation therapy or molecular approaches with specific monoclonal antibodies to block VEGFR, PDGFR, angiopoietin receptor 2 (Tie2) and others that drive vascularization of HCC. The multi-kinase inhibitor sorafenib is currently the only chemotherapeutic drug to increase the survival rate of advanced stage HCC patients. (Attwa & El-Etreby 2015; Chan & Yeo 2012; European Association for the Study of the Liver & European Organisation for Research and Treatment of Cancer 2012; Schlachterman et al. 2015; Xiu et al. 2015).

Despite the wide range of treatment techniques, the median overall survival rate amounts to five years for early stage HCC patients, less than two years for advanced stage HCC patients and few months for terminal stage HCC patients. Even after transplantation, resection or ablation therapy, the supposed healthy tissue is still able to bring back the disease yet again and with stronger impact. The responsible mechanisms are uncertain. Metastasis below thresholds of detection sensitivity or residing cancer stem cells may cause recurrence and formation of new lesions, and mediate resistance to chemotherapy.

In recent years, medical research explored novel treatment techniques for the curation of liver diseases, with a focus on the treatment with stem cells and derived techniques. The opportunities and risks of the employment of this cell-based approach will be elucidated in paragraph 1.2. (Aravalli 2010; Bayo et al. 2013; European Association for the Study of the Liver & European Organisation for Research and Treatment of Cancer 2012; Romano et al. 2015; Schlachterman et al. 2015).

1.2 Mesenchymal stem cells in the HCC microenvironment

Stem cells are unspecialized cells, which fulfill essential roles in embryogenesis, tissue homeostasis, repair and regeneration. In recent years, particularly mesenchymal stem cells have become an attractive target for medical research to transfer their unique properties on the treatment and curation of chronic wounds and fibrosis, as in the case of liver diseases. (Bayo et al. 2013; Hass & Otte 2012; Liang et al. 2014).

1.2.1 Stem cell entities and common characteristics

The term stem cells comprises a variety of fibroblast-like shaped cell entities of different origins, which possess the feature of 'stemness'. It describes the capability to undergo an indefinite or vast amount of cell divisions and yet keeping an undifferentiated state by continuous self-renewal, and the ability to specialize into a variety of tissues.

Today, stem cells of many different origins are known and applied in medical research and therapy. Embryonal stem cells (ESCs) form the inner mass of the blastocyst during embryogenesis. They are pluripotent and thus able to differentiate into any cell type of the three germ layers. In contrast, adult stem cells reside in small quantities in stem cell niches inside tissues or organs in order to maintain tissue homeostasis, regulation of inflammation, and wound repair. Adult stem cells are not pluripotent, but still multipotent, which means they are able to differentiate into a limited range of different tissues like connective tissue (mesenchymal stem cells, MSCs), hematopoietic cells (hematopoietic stem cells), neural cells (neural stem cells), skin and hair (epidermal stem cells), or epithelial tissues of the gastrointestinal tract (epithelial stem cells). (Martello & Smith 2014; National Institutes of Health 2015; Zipori 2004).

MSCs were initially isolated from bone marrow and termed colony forming units-fibroblasts in 1976. Apart from the bone marrow niche, researchers were able to isolate MSCs from perivascular niches in the periphery, e.g. adipose tissue, placenta, umbilical cord, muscles, lungs and others. The presence of a putative human liver stem cell is still under discussion, but stem- or progenitor-like cells were found in liver parenchyma of several other species. (Aravalli 2010; Bayo et al. 2013; Christ & Pelz 2013; Friedenstein, Gorskaja, & Kulagina 1976; Ma et al. 2014).

Finally, apart from naturally occurring stem cells, researchers were able to show that many differentiated adult cells, which are usually non-proliferative, could be reprogrammed to regain stemness characteristics. These so-called induced pluripotent stem cells (iPSC) are generated by the insertion and overexpression of a combination of few specific genes that can cause adult cells to regain pluripotency and proliferative capability. (Aravalli 2010; Malik & Rao 2013).

As pointed out in paragraph 1.1.2, the reprogramming of adult cells may also occur naturally through the selective pressure of a diseased tissue microenvironment. Cells that accumulate inheritable genetic aberrations may undergo malignant transformation and form so-called cancer stem cells (CSCs). They have been described for several types of cancer and are currently being considered as a source of tumor initiation, recurrence and metastasis. (Aravalli 2010; Garnier et al. 2010; Kreso & Dick 2014).
ESCs and iPSCs may offer unlimited possibilities and elaborate tools to support clinical therapy of many diseases, but they bear burdens of ethical issues, a high risk to form stem cell tumors (teratomas) and issues of xenotransplant rejection when applied in cell-based therapies. However, MSCs might fulfill the requirements for safe employment in such therapies since they can be relatively easily acquired from the human body without major procedures and show fewer problems with histocompatibility. While bone marrow-derived MSCs (BM-MSCs) still play a major role in research to unveil signaling and cellular actions on *in vitro* and *in vivo* models, adipose tissue-derived MSCs (AT-MSCs) may be an, even more, valuable resource since adipose tissue harbors more stem cells than bone marrow and is easily accessible. One gram of adipose tissue harbors around 5,000 to 200,000 MSCs, which is approx. 1,000- to 10,000-fold more than an equal amount of bone marrow tissue. Hence, the employment of MSCs from patient's adipose tissues, which can be propagated *ex vivo* and injected back into the patient's diseased tissues and organs, is a valuable tool for autologous MSC-guided therapies. (Baer & Geiger 2012; Ma et al. 2014).

The variety of sources for MSCs and the lack of a unique MSC-marker or surface protein gave rise to a panel of minimal criteria for defining MSCs *in vitro*, set up by the International Society for Cellular Therapy. In general, MSCs must (1) show plastic adherence *in vitro*, (2) express a set of stem cell surface markers and lack the expression of hematopoietic markers, and (3) show the ability to differentiate into osteoblasts, adipocytes and chondroblasts under standard conditions. These criteria clearly discriminate BM-MSCs from hematopoietic stem cells, which are both present in the bone marrow. Functionally, MSCs are also able to differentiate into various specialized cell entities including hepatocytes, which makes them an attractive tool for cell-based therapy of liver diseases. (Dominici et al. 2006; Stock et al. 2010).

1.2.2 MSCs as therapeutic approach for the treatment of HCC

The employment of MSCs in therapeutic approaches to cure various diseases is based on the findings that they can support survival, regeneration and repopulation of damaged tissue through:

(1) mitochondrial transfer to or cell fusion with damaged cells.
(2) the release of microvesicles and exosomes filled with RNA, miRNA and proteins; and the secretion of biologically active proteins, which will be introduced in closer detail in paragraph 1.2.3.

(3) transdifferentiation into various cell entities of the ectodermal, mesodermal and endodermal lineage. (Liang et al. 2014).

Therefore, MSCs open up many possibilities for the treatment of liver diseases. Applications include the transplantation of (genetically engineered) MSCs, MSC-derived differentiated target tissue or progenitor cells, or the injection of MSC-conditioned media at the sites of interest in order to cure the damaged tissue.

Reports about the systemic administration of labeled MSCs into mice revealed that the cells accumulated within lungs and liver after injection, but relocated to locations of injury, inflammation and cancer within the following one to three days, a process called 'homing.' Though the engraftment of MSCs into diseased tissue was quantified to have an efficiency of less than 0.01 %, the local injection into the tissue of interest had 3.5 % efficiency. These numbers may seem small, but even the administration of conditioned MSC media caused protective effects on liver tissue in a radiation model in rats. (Chen et al. 2015b; Reagan & Kaplan 2011; Rustad & Gurtner 2012).

The transplantation of MSCs or MSC-derived hepatic progenitor cells into the liver was successfully applied in a model of chemically induced acute liver failure in mice. Kuo et al. could demonstrate that intraspleenically or intravenously injected MSCs were able to engraft into the host liver and help liver survival by regeneration of the affected damaged tissue, probably due to anti-oxidative, anti-apoptotic and paracrine properties of the injected cells. Furthermore, they showed that MSCs were more effective than the MSC-derived hepatic progenitor cells.

However, studies focusing on the interaction of MSCs and tumor cells indicated that MSCs could promote tumorigenic microenvironments as well. Studeny et al. and Niess et al. demonstrated that systemically injected MSCs were able to home to melanoma or HCC tumor models and contribute to tumor formation *in vivo* in mouse experiments. In a second step, they took advantage of the tumor-specific homing and employed genetically engineered MSCs. Despite the demonstrated tumor-promotion by MSCs, the coupling of MSCs with the expression of anti-proliferative proteins and drugs at the sites of tumor-incorporation resulted in an overall reduction of the tumor sizes. (Bayo et al. 2013; Kuo et al. 2008; Niess et al. 2011; Studeny et al. 2002).

1.2.3 Paracrine activity of MSCs and the potential impact on HCC

Current reviews pointed out that the paracrine activity of MSCs might be the major factor in causing the regenerative impact of MSCs on diseased tissue *in vivo*. MSCs are known to secrete a cocktail of immunoregulatory, anti-apoptotic, pro-angiogenic and growth-promoting factors. Although comprehensive data on potential differences among populations of MSCs from different origins are currently lacking, BM- and AT-MSCs share approx. 91 % homology concerning transcriptome data

conducted by Jansen et al. This similarity seems to translate into the factors that are being secreted by MSCs since a study from Hsiao et al. found a similar secretion of several biologically active factors for both BM- and AT-MSCs. Some of those factors included VEGF, IL-6, IL-8, HGF and MCP-1. They are prominent players in physiological and pathological conditions and may present pivotal targets for the assessment of the experimental interplay of MSCs and HCC in order to understand MSCs impact for cell-based therapies. Their features and relevance for the HCC are briefly outlined below. (Bayo et al. 2013; Hsiao et al. 2012; Jansen et al. 2009; Liang et al. 2014; Yagi & Kitagawa 2013).

VEGF

Vascular endothelial growth factor (VEGF) is a major stimulus for endothelial cells to cause physiological and pathological angiogenesis and an increase in vascular permeability. Moreover, it was found to play crucial roles in the onset and development of cancer in general. VEGF is described to promote growth and survival of cancer cells and to cause epithelial to mesenchymal transition, i.e. promotion of dedifferentiation, migration and invasion.

VEGF has been shown to be secreted by HCC cells at elevated levels compared to other chronic liver diseases. Excessive amounts of VEGF in the liver may promote the connection of HCC to the highly oxygenated blood supply from hepatic arteries and cause cirrhosis-promoting sinusoidal capillarization. (Goel & Mercurio 2013; Iavarone et al. 2007; Yang & Poon 2008).

HGF

Hepatocyte growth factor (HGF) is important for epithelial, neuronal and organ development, latter especially for liver and placenta, and targets multiple cell types throughout the organism. HGF is expressed by mesenchymal cells in general and is a chemoattractant for MSCs.

The impact of HGF on the liver comprises mitogenic, motogenic and survival stimuli on hepatocytes, by potently enhancing chemoattraction and migration, evasion of apoptosis/necrosis, thus reducing inflammation, induction of apoptosis of fibrosis-causing myofibroblasts and breakdown of extracellular matrix. (Forte et al. 2006; Nakamura et al. 2011; Neuss et al. 2004).

MCP-1

Monocyte chemotactic protein 1 (MCP-1) is a chemoattractant for monocytes, memory T cells and natural killer cells. It is expressed by endothelial cells, fibroblasts, smooth muscle cells, epithelial cells and others, but mainly by monocytes/macrophages. MCP-1 is also secreted by cancer cells and tumor-associated macrophages and was found to correlate with the progression of breast carcinoma and poor prognosis. Patients with HCC also show significantly upregulated serum amounts of MCP-1 compared to chronic HBV patients without HCC, thus making MCP-1 an additional serum marker for

improved diagnosis. Moreover, myofibroblast-derived MCP-1 was found to increase migration and invasion of HCC cells. (Dagouassat et al. 2010; Deshmane et al. 2009; Wang et al. 2013).

IL-8

Interleukin 8 (IL-8) is a chemoattractant and activator for neutrophil granulocytes. Apart from neutrophils, its receptors are especially expressed in endothelial cells and macrophages. IL-8-activated macrophages secrete growth factors. The activation of endothelial cells favors chemotaxis, survival, and proliferation in order to promote angiogenesis and wound healing. However, cancer cells were also found to express IL-8 and its receptors, thus additionally stimulating the tumor microenvironment in an autocrine and paracrine manner. Patients with HCC were found to possess significantly increased serum levels of IL-8, 17.6 pg/ml versus 1 pg/ml in healthy patients, which correlated with tumor size. Also, IL-8 stimulates the proliferation and survival of cancer cells. Chemotherapy was found to increase the secretion of IL-8 from cancer cells. (Ren et al. 2003; Waugh & Wilson 2008).

IL-6

Interleukin 6 (IL-6) mediates and contributes to a variety of different biologic actions, including B cell differentiation and T cell proliferation, stimulation of lymphocyte trafficking, elevation of lipolysis, and enhanced secretion of an iron metabolism-limiting compound by the liver. Moreover, it stimulates the secretion of acute phase proteins, fibrinogen and other factors by the liver and contributes to liver regeneration. Furthermore, it stimulates the secretion of IL-8, MCP-1 and other chemokines from various cell entities and is involved in angiogenesis via activation of VEGF.

These multi-faceted effects might explain why IL-6 was found to play major roles in autoimmune and inflammatory diseases. Like many other factors, its elevated levels in patient sera were found to correlate with cirrhosis, cancer development and especially metastasis. Increased IL-6 expression rates were demonstrated in HCC cells compared to cirrhotic liver cells, which led to an autocrine stimulation of survival, proliferation and metastasis. Increased levels of IL-6 were also correlated with the progression from chronic hepatitis to HCC. On molecular level, HCC was demonstrated to show hypermethylation of IL-6 signaling suppressors SOCS (suppressors of cytokine signaling), making IL-6 a key player in the progression of HCC. Furthermore, elevated IL-6 serum levels were linked to obesity and a higher risk of developing HCC, which might explain the rise of HCC from steatohepatitis (see paragraph 1.1.1). Moreover, men are more frequently affected by HCC than women, which is thought to be due to the inhibitory effect of estrogens on IL-6-producing Kupffer cells, which are macrophages of the liver that reside in the sinusoids of the liver parenchyma. (Johnson et al. 2012; Mihara et al. 2012).

1.3 Proteinase-activated receptors in the HCC microenvironment

As pointed out in paragraph 1.1 and 1.2.3, the development of liver diseases, and HCC in particular, is a complex phenomenon with multiple involved causes, cells, biologically active proteins and signaling pathways. The proteinase-activated receptor (PAR) family, however, seems to be involved in the mediation of key mechanisms of liver diseases in general, since it has been demonstrated to contribute to the progression of cholangiocarcinoma, cirrhosis and especially HCC (refer to paragraph 1.3.3, page 14).

1.3.1 PAR family

PARs are G protein-coupled receptors (GPCR), which share the common feature of seven transmembrane α-helices that are linked by extra- and intracellular loops, and the feature of transmitting extracellular signals onto intracellular-coupling G proteins. The PAR family comprises four members named in order of discovery, $PAR_{1\text{-}4}$. The unique identity of PARs lies in their mode of activation. PARs comprise an extracellular N-terminal peptide chain that is prone to cleavage by proteinases from the serine and metalloproteinase families. They cleave at distinct positions of the N-terminal peptide chain and cause the formation of a new N-terminus, which in turn serves as a 'tethered ligand' and activates the receptor through binding at its second extracellular loop.
Artificially generated peptide sequences, which have been raised according to the respective tethered ligand sequences of a specific PAR subtype, were found to activate PARs as well, with similar cellular responses as their corresponding proteinases. (Macfarlane et al. 2001; Ramachandran et al. 2012; Soh et al. 2010; Zhao, Metcalf, & Bunnett 2014).

Proteinase- and activating peptide-guided receptor activation lead to binding and activation of heterotrimeric G proteins (subunits Gα, β, γ), which couple to the PAR's intracellular situated C-terminus. The activated receptor promotes the exchange of guanosine diphosphate (GDP) to guanosine triphosphate (GTP) in the active center of the Gα subunit, thus activating the G protein to trigger further distinct signaling cascades. PARs couple to $G\alpha_q$, $G\alpha_i$ and $G\alpha_{12/13}$, which are more or less frequently activated depending on the activating proteinase or activating peptide. Other directly coupling effectors include β-arrestin 1 and 2, which serve as another platform for the activation of downstream signaling. (DeFea et al. 2000; Gieseler et al. 2013; Lin & Trejo 2013; Ramachandran & Hollenberg 2008; Ramachandran et al. 2012; Soh et al. 2010; Zhao, Metcalf, & Bunnett 2014).

The major signaling cascades being activated by PARs comprise:

(1) $G\alpha_{12/13} \rightarrow$ RhoGEFs $\rightarrow$ RhoA

(2) $G\alpha_q \rightarrow$ PLC-β $\rightarrow IP_3$/DAG $\rightarrow Ca^{2+}$, PKC, MAPKs, RTKs

(3) $G\alpha_i \rightarrow$ MAPK, inhibition of adenylyl cyclase

(4) β-arrestins $\rightarrow$ ERK1/2, Rac1

(5) $G\beta\gamma \rightarrow PI_3K$, Rac1, GRKs, K^+ channels, PLC-β, Src

DAG - diacylglycerol; ERK1/2 - extracellular-signal regulated kinase 1/2; GRK - G protein-coupled receptor kinase; IP_3 - inositol triphosphate; MAPK - mitogen-activated protein kinase; PI_3K - phosphatidylinositide 3-kinase; PKC - protein kinase C; PLC-β - phosphoinositide phospholipase C β; Rac1 - Ras-related C3 botulinum toxin substrate 1; RhoA - Ras homolog gene family member A; RhoGEF - Ras homolog gene family member guanine nucleotide exchange factor; RTK - receptor tyrosine kinase; Src - sarcoma, proto-oncogene tyrosine-protein kinase Src

The cross-activation of receptor tyrosine kinases like EGFR, Met, VEGFR and PDGFR may cause further activation of MAPKs, PI_3K, PLC-β and JAK-STAT signaling pathways. (Gieseler et al. 2013; Ramachandran & Hollenberg 2008; Regad 2015; Soh et al. 2010; Zhao, Metcalf, & Bunnett 2014).

PAR knockout studies have revealed insights into their biological functions. Genetic inactivation of the PAR_1 gene in mice caused mortality at embryonic day nine; however, half of the knockout mice seemed to develop normally, but with altered response to vascular injuries. PAR_2 and PAR_3 knockout mice developed normally without overt phenotypes, whereas PAR_4 knockout mice had an impaired platelet function. (Hamilton, Cornelissen, & Coughlin 2004; O'Brien et al. 2000).

A lack of strong phenotypes for $PAR_{2\text{-}4}$ knockouts is likely related to a considerable functional redundancy of PARs as they are often expressed simultaneously. In general, the PAR family members are seen as sensors of wounds and contribute to the inflammation and healing processes during the different phases. Detailed analyses have revealed that they play roles in platelet aggregation and secretion ($PAR_{1,\ 3,\ 4}$), vasoregulation ($PAR_{1\text{-}4}$), inflammation, gastrointestinal tract, nociception (hyperalgesia, PAR_2; analgesia, $PAR_{1\ +\ 4}$) and the central nervous system (PAR_2). With respect to their involvement in diseases, the contribution to arthritis (PAR_2) and tumor progression of various cancer entities ($PAR_{1,\ 2}$) need to be mentioned. In addition to tissue distribution, the subcellular locations like lipid rafts or caveolae, availability of interacting proteinases, receptor homo/heterodimerization and cross-activation of other receptor entities like receptor tyrosine kinases were found to be relevant for PAR signal transduction. (Adams et al. 2011; Ramachandran & Hollenberg 2008; Ramachandran et al. 2012; Zhao, Metcalf, & Bunnett 2014).

The attenuation of PAR signaling is of general medical interest, e.g. to limit activation of platelets and hence the formation of blots clots, which can cause thromboembolism after effects like ischemic stroke or myocardial infarction. However, the blood coagulation is of systemic importance, and blocking core aspects of it requires well-balanced and -established antagonists. In general, PAR signaling may be

limited by blocking PAR-activating proteinases, proteinase cleavage sites of PARs, or the intracellular C-terminus to prevent binding of effectors. Moreover, antagonists that interact with the receptor at the second extracellular loop provide promising features. (Ramachandran et al. 2012).

1.3.2 PAR_1 – the prototypical PAR

PAR_1 was discovered in 1991 by the Coughlin group and has become the prototypical subtype of the PAR family since then. However, it differs in several features from $PAR_{2\text{-}4}$, which will be briefly outlined along the following characterization of PAR_1. (Vu et al. 1991; Zhao, Metcalf, & Bunnett 2014).

$PAR_{1, 3, 4}$ are activated with the highest efficacy by thrombin, and PAR_2 by trypsin. Though thrombin is not able to cleave PAR_2, trypsin can cleave and activate PAR_1 and PAR_3 with low efficiency, and PAR_4 with approximately similar potential as thrombin. Thrombin possesses an anion-binding exosite that enables transient binding to the negatively charged region of the PAR_1 N-terminus (amino acids D^{51}-F^{56}), which leads to conformational changes of thrombin and greatly enhances its ability to cleave at PAR_1's R^{41}/S^{42} of about 25-fold. PAR_3 offers a shorter thrombin-binding region as PAR_1, but with similar dose-responses to thrombin as PAR_1. PAR_4 offers no such binding site for thrombin, thus causing the requirement of higher thrombin concentrations for PAR_4 activation. (Coughlin & Camerer 2003; Macfarlane et al. 2001; Zhao, Metcalf, & Bunnett 2014).

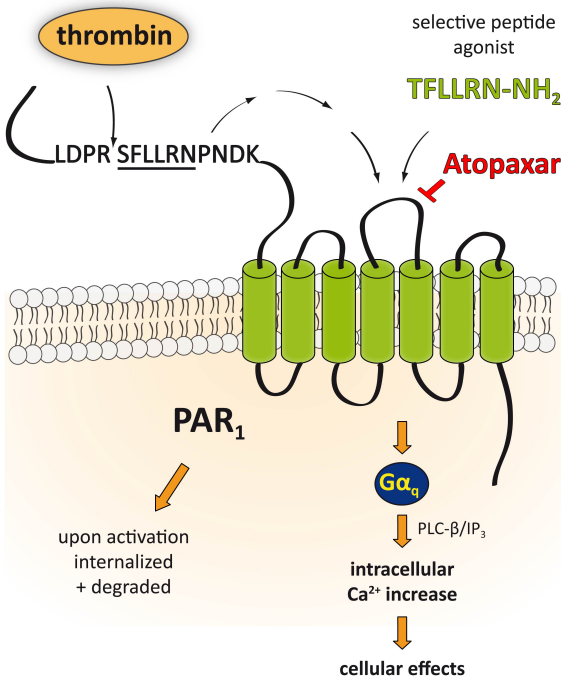

Figure 1-1: Basic concept of PAR_1 signaling and research tools

Serine proteinases like thrombin are able to cleave the N-terminal PAR_1 peptide chain and thereby revealing a newly formed tethered ligand that activates the receptor. Artificial subtype-specific agonist peptides mimic this tethered ligand and trigger characteristic signaling of respective proteinases. Atopaxar is an antagonist that blocks PAR_1 activation.

A major common PAR-activated pathway is the $G\alpha_q$ mediated activation of phospholipase C β (PLC-β), thus leading to generation of diacylglycerol (DAG) and inositol triphosphate (IP_3), which causes an increase in the free intracellular Ca^{2+} concentration.

The activation via the newly formed N-terminus can be mimicked by artificial peptides. These selective peptide agonists activate the receptor without cleavage. As illustrated in Figure 1-1, the subtype-specific PAR_1 activating peptide TFLLRN-NH_2 is based on the receptor's tethered ligand sequence SFLLRN. In general, slight modifications of the peptide's amino acid sequence or the addition of chemical moieties may improve the efficacy. (Macfarlane et al. 2001; Zhao, Metcalf, & Bunnett 2014).

Major activators of PAR_1 are thrombin, activated factor X (FXa) and plasmin, which cleave at the same site and cause activation of $G\alpha_q$, $G\alpha_{12/13}$ and β-arrestin 1-mediated signaling pathways. Activated protein C (APC), matrix metalloproteinase (MMP) 1 and 13, neutrophil elastase and neutrophil proteinase 3 cleave PAR_1 at distinct positions of the N-terminus, which causes different preferential contribution of the in paragraph 1.3.1 mentioned signaling pathways. (Ramachandran & Hollenberg 2008; Soh et al. 2010; Zhao, Metcalf, & Bunnett 2014).

The PAR_1 signaling is terminated via rapid phosphorylation of the intracellular C-terminus by G protein-coupled receptor kinases (GRKs), protein kinase A (PKA) or PKC, thus inhibiting further coupling of G proteins. Although β-arrestins play a major role in PAR_2 signaling and desensitization, β-arrestin 1 seems to contribute to PAR_1's signaling, but only little to its desensitization. The receptor is then internalized via clathrin and dynamin-dependent processes. PAR_1 is rapidly replenished on the plasma membrane through intracellular PAR_1 reservoirs. Unlike PAR_2, PAR_1 was demonstrated to cycle constitutively between the plasma membrane and endosomal vesicles, thus establishing intracellular reservoirs. Ubiquitinylation of the PAR_1 C-terminus seems to contribute to PAR_1's subcellular distribution and prevents its phosphorylation and thus desensitization. (Gieseler et al. 2013; Soh et al. 2010; Zhao, Metcalf, & Bunnett 2014).

PAR_1 was shown to form heterodimers with all other subtypes, which alters and enhances the triggered signaling of the involved subtypes. Intriguingly, the heterodimerization with PAR_3, the subtype that is least known about and does not seem to create intracellular signals on its own, enhances the activation of PAR_1 and PAR_4 by thrombin and reduces their agonism via the $G\alpha_q$ pathway. Moreover, PAR_3 seems to compensate the lack of PAR_1 in murine platelets. Human platelets express PAR_1 and PAR_4. In murine platelets, however, only PAR_4 and PAR_3 are found. (Gieseler et al. 2013; Ramachandran & Hollenberg 2008; Soh et al. 2010; Zhao, Metcalf, & Bunnett 2014).

PAR_1's role in the activation of human platelets and accompanied pathologic events gave rise to extensive research on finding specific antagonists. The PAR_1 antagonists Vorapaxar and Atopaxar completed clinical trials phase III and phase II respectively and revealed to be beneficial for the treatment of cardiovascular diseases and the inhibition of platelet aggregation. However, they also caused increased possibilities of moderate and severe bleeding and intracranial bleeding events (Vorapaxar) or hepatic abnormalities (Atopaxar). While the attribution of the utility and the complex *in vivo* interactions and side effects is ongoing, these antagonists already provide useful tools for *in vitro* research purposes. (Al-Khafaji et al. 2015; Cui et al. 2012; Moschonas, Goudevenos, & Tselepis 2015; Ramachandran 2012; Tello-Montoliu et al. 2011).

Atopaxar is a commercially available PAR_1 antagonist that was developed by the Japanese pharmaceutical company Eisai Co., Ltd. It has shown to attenuate PAR_1 activation via thrombin and specific PAR_1-APs in a concentration-dependent manner. Hence, it presumably interferes with the second extracellular loop (Figure 1-1), which is supposed to facilitate ligand binding and receptor activation. (Al-Khafaji et al. 2015; Cui et al. 2012; Matsuoka et al. 2004; Serebruany et al. 2009; Tello-Montoliu et al. 2011; Wurster & May 2012).

1.3.3 The role of PAR activation in liver diseases

The disruption of the vascular endothelial barrier, as it occurs during the course of e.g. fibrosis, cirrhosis and cancerous liver diseases, causes the activation of various potentially PAR-activating proteinases of the blood coagulation cascade. These comprise activated factor VII (FVIIa; activates PAR_2), FXa ($PAR_{1\text{-}4}$), thrombin ($PAR_{1,3,4}$), APC ($PAR_{1,3}$), and plasmin (PAR_1), which are mainly produced by the liver. Tumor microenvironments have been reported to show an enhanced and less limited activation of the blood coagulation cascade, thus leading to increased concentrations of thrombin and presumably prerequisite FVIIa and FXa. HCC tissue and cell lines were demonstrated to express and secrete elevated amounts of thrombin, which correlated with HCC metastasis and recurrence in affected patients and with metastatic features of established HCC cell lines. In the context of liver diseases, it is, therefore, likely that PARs are activated throughout the affected liver parenchyma. (Coughlin 2000; Falanga 2011; Garnier et al. 2010; Licari & Kovacic 2009; Madhusudhan, Kerlin, & Isermann 2015; ten Cate & Falanga 2008; Xue et al. 2010; Zacharski, Hommann, & Kaufmann 2004).

Recent publications of our group and other researchers could demonstrate that PARs are relevant for the progression of liver diseases:

(1) Cholangiocarcinoma – intrahepatic cancer of the bile ducts – was demonstrated to be promoted in growth and migration via activation of PAR_2 (Kaufmann et al. 2012; Nakanuma et al. 2010).

(2) Liver fibrosis and cirrhosis: PAR_1 and PAR_2 were demonstrated to mediate activation of hepatic stellate cells, thus leading to enhanced proliferation, promotion of myofibroblast differentiation, and enhanced collagen secretion. Hepatic stellate cells reside in the perisinusoidal space of the liver lobules and are the major contributors to liver fibrosis. (Borensztajn et al. 2010; Duplantier et al. 2004; Fiorucci et al. 2004; Gaça, Zhou, & Benyon 2002; Knight et al. 2012; Lu et al. 2014; Mercer & Chambers 2013).

(3) HCC: PAR_2 has been demonstrated to promote the invasiveness of HCC cells involving the cross-activation of the HGF receptor Met while PAR_1 and PAR_4 promoted migration of HCC cells via cross-activation of Met and PDGFR (Kaufmann et al. 2007, 2009; Mußbach et al. 2014).

Hence, it seems that PARs play a pivotal role in the development and progression of liver diseases via stimuli arising from the different cell entities of the liver parenchyma. In conclusion, regarding the in paragraph 1.2.2 (page 6) presented emerging cell-based techniques to cure liver diseases, PARs may also get activated in exogenously employed stem cells and hepatic precursor cells.

1.4 Hypothesis and objective

MSCs are considered as a valuable resource for the treatment of diseases associated with chronic tissue damage, as it occurs in liver fibrosis and cirrhosis. The biological properties of MSCs are still incompletely understood. The administration of MSCs as means of cellular therapy of liver diseases would add large quantities of a multifaceted and multipotent cell entity to diseased microenvironments. The consequences of the arising cell interactions are likewise insufficiently understood. To obtain better insights into these processes, the assessment of the role of PARs in MSCs appears of great interest. On the one hand, PAR expression has been detected in MSCs and is likely to affect their functions, but a detailed characterization of the different PAR subtypes and their biologic impact on the MSCs and surrounding cell entities is currently lacking. On the other hand, MSCs have shown beneficial effects on chronically inflamed liver tissues in experimental mouse models. Exposure of MSCs to an inflamed microenvironment is likely to activate resident PARs. Moreover, the interaction of MSCs and cancerous tissue remains controversial, and PAR activation may play a relevant role in it. Hence, we hypothesized that PARs may play a crucial role in MSCs, and assumingly alter their paracrine activity with an impact on the development of HCC. As illustrated in Figure 1-2, our goals were therefore to (1) characterize the PAR subtypes in MSCs, (2) to assess the biological relevance of PARs in MSCs, and (3) to assess the effect of MSCs on HCC cells *in vitro*, and *in vivo* in a xenotransplantation mouse model – with consideration of the impact of PARs.

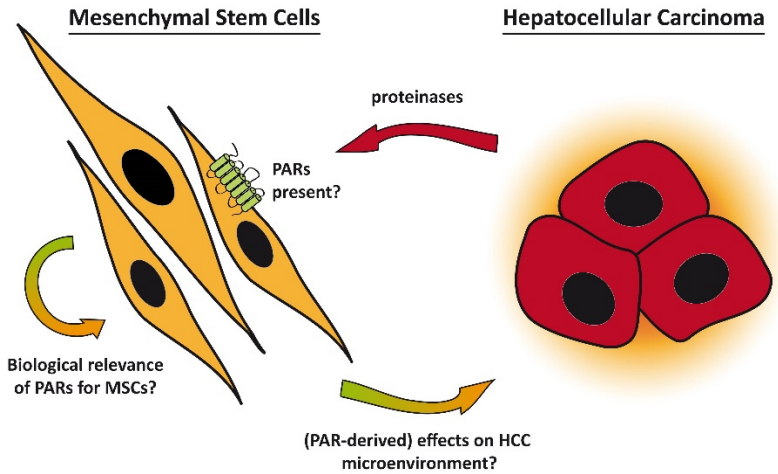

Figure 1-2: Hypothesis of the PAR-mediated impact of MSCs on the HCC microenvironment

MSCs are currently under investigation for cell-based curation of chronic liver diseases. Tumor microenvironment- and inflammation-derived proteinases might activate PARs in MSCs. Our goal was to assess the presence and biological relevance of the different PAR subtypes in MSCs. Furthermore, we wanted to assess the impact of MSCs on HCC and whether MSCs' PARs contribute to it.

2 Methods

2.1 Basic cell maintenance

The link between hepatocellular carcinoma (HCC), mesenchymal stem cells (MSCs) and proteinase-activated receptors (PARs) was addressed with *in vitro* and *in vivo* assays. All assays were conducted using primary human MSCs and cells from the permanent HCC cell line Hep3B. All cells were cultured at standard conditions of 37 °C, 5 % CO_2 and 95 % humidity.

2.1.1 Isolation of MSCs from human adipose tissue

All used MSCs were of human origin and derived from adipose tissue of several donors (Table 2-1). Thus, the cells are called adipose tissue-derived MSCs (AT-MSCs). All cell batches were gathered with donor's consent at the University Hospital of Leipzig (Germany), approved by its Institutional Ethics Review Board.

Table 2-1: Human AT-MSC batches

Donor #	Batch #	Gender	Date of birth	Date of extraction
1	0312	m	1947	2012
2	0512	f	1986	2012
3	0612	f	1933	2012
4	0712	m	1978	2012
5	0812	f	1973	2012
6	0113	m	1954	2013
7	0213	m	1962	2013
8	0214	f	1965	2014

Table 2-2: Analyzed characteristics of AT-MSCs

Stem cell markers positive for: CD13, CD29, CD44, CD54, CD90, CD105, CD166
Hematopoietic markers negative for: CD11c, CD14, CD34, CD45, glycophorin-A, HLA-DR
Differentiation osteogenic, adipogenic, hepatogenic

Isolation and characterization of the AT-MSCs were carried out by the laboratory of Dr. B. Christ from the Applied Molecular Hepatology Laboratory, Department of Visceral, Transplantation, Thoracic and Vascular Surgery, University Hospital Leipzig (Germany). The protocol is based on a collagenase digestion of the adipose tissue, followed by filtration through a nylon mesh, and the separation of the different cell populations with a Percoll® gradient centrifugation. The mononucleated cells were harvested from the interphase, washed and seeded on uncoated plastic flasks. Due to the MSCs' characteristic of adhering to plastic surfaces, they remain in the flask while suspension cells can be washed away (Christ, Brückner, & Stock 2011). Purity and entity of the cells were verified using flow cytometry and *in vitro* differentiation into other lineages (Table 2-2) (Aurich et al. 2007; Christ & Pelz 2013). The used protocols were similar to the published ones for bone marrow-derived MSCs (BM-MSCs).

2.1.2 AT-MSC culture medium

The AT-MSCs were cultured with a special growth medium called EM6F, supplemented with 15 % (v/v) fetal calf serum (FCS). EM6F was provided by Prof. B. Christ from the Applied Molecular Hepatology Laboratory, Department of Visceral, Transplantation, Thoracic and Vascular Surgery, University Hospital Leipzig (Germany) and is composed of the ingredients listed in Table 2-3.

The resulting serum-containing full culture medium is termed in the following as 'EM6F15'.

Table 2-3: Composition of AT-MSC growth medium EM6F

Ingredient	Amount	Provider
DMEM	60 % (v/v)	Sigma
MCDB	40 % (v/v)	Sigma
apotransferrin	5 µg/ml	Sigma
selenous acid	5 ng/ml	Sigma
linoleic acid	5 µg/ml	Sigma
bovine insulin	5 µg/ml	Sigma
ascorbic acid 2-phosphate	100 µM	Sigma
dexamethasone	1 nM	Sigma
PDGF-BB	10 ng/ml	Sigma
EGF	10 ng/ml	Sigma
penicillin/streptomycin	100 U/ml / 100 µg/ml	Invitrogen

(Aurich et al. 2007)

2.1.3 Initial seeding of cryopreserved AT-MSCs

Prior to seeding, the culture flasks were coated with Dulbecco's Modified Eagle Medium (DMEM)/0.5 µg/ml fibronectin and left open under the sterile bench for 30-60 min to let the medium dry up in the flask. The cryopreserved AT-MSCs were rapidly thawed in a 37 °C water bath for a few seconds, transferred into 5 ml cold DMEM medium and centrifuged at 500 *g* for 5 min. Another washing step with cold DMEM was carried out to remove the dimethyl sulfoxide (DMSO). Finally, the cells were resuspended in EM6F15. Cells were seeded at a density of 400/cm².

2.1.4 AT-MSC maintenance

The culture medium was replaced every two to four days. One week after initial seeding, the cells were detached and seeded into designated dishes for the particular experiments. For that, the cells were washed twice with a warm phosphate-buffered saline (PBS) (Biochrom, cat. no. L 1825) and incubated with a warm 0.05 % trypsin-ethylenediaminetetraacetic acid (EDTA) (Gibco®, cat. no. 25300045) solution for 2 min. The detached cells were transferred into FCS-containing DMEM and centrifuged at 500 *g* for 5 min. After another washing and centrifugation step, the cells were resuspended in EM6F, counted with a cell counting chamber (Neubauer) and seeded for further purposes. Remaining and unused cells were split into new culture flasks.

All experiments were carried out with cells that were in culture no longer than one to three weeks (one to three passages). Cells for knockdown experiments (refer to paragraph 2.4.4, page 33) were in culture for three to four weeks due to the transduction protocols and expansion of the cells.

2.1.5 AT-MSC starvation

The AT-MSCs were starved before stimulation or migration experiments to synchronize cellular behaviors. Starvation was achieved by washing the cells twice with warm PBS and cultivating them in DMEM without additives for 24 h.

2.1.6 Hep3B cell line

The permanent cell line Hep3B derives from an eight-year-old patient with a correlation of hepatitis B virus (HBV) and primary HCC. It was established in the late 1970s, and although the HBV surface antigen is produced by the cell line, it yields no active virus particles, making it suitable for safety level 1. Hep3B cells grow in monolayers with an epithelial cell shape, resembling characteristics of liver parenchymal cells. When injected into severe combined immunodeficiency (SCID) mice, metastatic tumors arise (Aden et al. 1979; Knowles, Howe, & Aden 1980).

The Hep3B cell line was obtained from the Leibniz Institute DSMZ (German Collection of Microorganisms and Cell Cultures, cat. no. ACC93). The Hep3B cells were cultured in Roswell Park Memorial Institute medium (RPMI) 1640 (Biochrom, cat. no. FG1235) with 10 % (v/v) FCS (Biowest, cat. no. S1810) and 1 % (v/v) penicillin-streptomycin (final: 100 U/ml / 100 µg/ml) (Corning, cat. no. 30-002-CI), changing medium every two to three days. The cells adhere firmly to the flasks. Detaching them required washing with PBS and trypsin-EDTA, followed by 8-10 min incubation with fresh trypsin-EDTA.

The detached cells were transferred into FCS-containing RPMI and centrifuged at 500 *g* for 5 min. After another washing and centrifugation step, the cells were resuspended in RPMI, counted and seeded for further purposes.

2.2 Detection of PARs in AT-MSCs

2.2.1 mRNA expression analysis

2.2.1.1 RNA extraction

Total RNA was isolated from cells that covered a 3.5 cm dish with at least 60-80 % confluence. The procedure was carried out according to the manufacturer's protocol of the NucleoSpin® RNA kit (Macherney-Nagel, cat. no. 740955). The basic principle is a lysis buffer that inactivates RNases before they can degrade the released RNA. Via a tube-based ionic exchange column, nucleic acids are bound and cleansed from other cell compounds with a washing step. Incubation with DNase degrades all DNA, which is then washed away. Finally, RNA is eluted with water, which dislodges the RNA from the column.

The RNA was eluted in 50 µl double-distilled water (ddH_2O). The elution step was repeated by adding the eluate back on the column, in order to increase RNA yield. The RNA's concentration and purity were determined using a NanoDrop™ spectrophotometer (ND-1000, Peqlab) and following the manufacturer's instructions.

2.2.1.2 cDNA synthesis

The isolated RNA was transcribed into cDNA via the First Strand cDNA Synthesis Kit (Thermo Scientific, cat. no. K1612) on a Mastercycler® ep gradient (Eppendorf). For all experiments, Oligo(dT)$_{18}$ primers were used to ensure transcription of mRNA. The sample set up and used programs were as presented in Table 2-4.

The amounts of applied RNA were equal for all samples of their respective assays.

Table 2-4: Protocol for cDNA synthesis

Step 1:	
1 reaction = 11 µl	**[µl]**
RNA (500 ng) + H_2O	10
Oligo(dT)$_{18}$ Primer	1
	11
→ *65 °C, 5 min*	

Step 2:	
1 reaction = 9 µl	**[µl]**
5x Reaction Buffer	4
RiboLock RNase Inhibitor	1
dNTPs	2
M-MuLV Reverse Transcriptase	2
	9
→ *add 9 µl mix to every sample*	
→ *37 °C, 60 min*	
70 °C, 5 min	

2.2.1.3 Quantitative real-time PCR

With the help of the SYBR Green fluorescent dye-based technique of quantitative real-time PCR (qPCR) (Bustin et al. 2009), specific sequences of given cDNAs are amplified with specific primers, along with a real-time determination of present DNA. SYBR Green intercalates during each elongation step into double stranded DNA and emits light when excited. The signal intensity of SYBR Green is proportional to the amount of double-stranded DNA in the sample.

Analyses were conducted with the Maxima SYBR Green/ROX qPCR Master Mix (2x) (Thermo Scientific, cat. no. K0221) on a Mastercycler® ep realplex^4 (Eppendorf). Used primers, sample and program setups are shown in Table 2-5 and Table 2-6. Predesigned qPCR primers (KiCqStart® SYBR® Green Primers) were obtained from Sigma. PAR subtype primer sequences were obtained from PrimerBank (http://pga.mgh.harvard.edu/primerbank) or personally designed with the help of the Primer-BLAST tool from the homepage of the National Center for Biotechnology Information (NCBI) (http://www.ncbi.nlm.nih.gov/tools/primer-blast). The PAR subtype primer sequences were then synthesized by Sigma.

Table 2-5: List of used primers for qPCR

Gene/Target	Sequence [5' → 3']	T_A [°C]	Length of Amplicon	Species	Reference
Reference Gene					
GAPDH	F: ACCCACTCCTCCACCTTTGAC R: TCCACCACCCTGTTGCTGTAG	58	110	human	Sigma
PARs					
***F2R*/PAR$_1$**	F: GCCATCGTTGTGTTCATCCTG R: GCTGATCTTAAAGGGGAGCAC	58	114	human	PrimerBank ID: 166362739c2
***F2RL1*/PAR$_2$**	F: CTGTGGGTCTTTCTTTTCCGAA R: CAAGGGGAACCAGATGACAGA	58	102	human	PrimerBank ID: 216548424c2
***F2RL2*/PAR$_3$**	F: CCTGCCCAAGCACACCTATG R: GGTGGTGATGTCTGGCTGAA	58	124	human	personally designed
***F2RL3*/PAR$_4$**	F: CCTCTATGGTGCCTACGTGC R: GCACCTTGTCCCTGAACTCG	58	104	human	personally designed
Cytokines					
IL-8	F: TACTCCAAACCTTTCCACC R: CTCAGCCCTCTTCAAAAAC	55	174	human	Sigma
IL-6	F: GCAGAAAAAGGCAAAGAATC R: CTACATTTGCCGAAGAGC	55	178	human	Sigma
MCP-1	F: AGACTAACCCAGAAACATCC R: ATTGATTGCATCTGGCTG	53	143	human	Sigma

Table 2-6: Protocol for qPCR analyses

1 reaction = 12 µl	[µl]
Maxima SYBR Green/ROX qPCR Master Mix (2X)	6
ddH_2O	4.26
primer forward (10 µM)	0.37
primer reverse (10 µM)	0.37
cDNA	1
	12

qPCR profile		temp., duration
enzyme activation		95 °C, 10 min
40x	denaturation	95 °C, 15 s
	annealing	T_A, 30 s
	elongation	72 °C, 20 s
		60 °C, 15 s
T_M determination		60 → 99 °C, 10 min
		99 °C, 15s
end		20 °C, 2 min

Each analysis of a particular cDNA consisted of three technical replicates. Quantification cycle numbers (C_q) of each replicate were picked by applying the same threshold for the reference gene (GAPDH) and the genes of interest (GOI) in each experimental setup. The relative gene expression and fold changes were calculated with the presented equations on the right.

$$\Delta C_q = C_{q\,GOI} - C_{q\,GAPDH}$$

$$\Delta\Delta C_q = C_{q\,GOI,\ stimulated} - C_{q\,GOI,\ untreated}$$

$$relative\ expression\ towards\ GAPDH = 2^{-\Delta Ct}$$

$$fold\ change\ towards\ untreated\ GOI = 2^{-\Delta\Delta Ct}$$

Each replicate of $C_{q\,GOI}$ was paired with a replicate of $C_{q\,GAPDH}$. The mean value and standard deviation (SD) were calculated from the corresponding relative expression or fold change, respectively.

In order to compare the results for PAR subtype expressions, the applied primers were required to exert similar efficiencies in qPCRs. For analyzing the efficiencies of the PAR subtype primers, qPCRs

with series of dilutions (10^{-1}, 10^{-2}, 10^{-3} and 10^{-4}) from a mixture of cDNA were carried out for every pair of primers. The pooled cDNA of several different cell entities (AT-MSC, Hep3B, LX2, HEK293T, BV173, K562, Mv4-11 and Molm13) was provided in the efficiency analyses to counterbalance low expression and absence of expression of particular PAR subtypes.

The obtained C_q values were plotted against the logarithmic scale of the dilutions, and a linear regression was applied.

The qPCR's efficiencies were calculated from the regression line's properties:

$$amplification\ rate = 10^{-\frac{1}{slope}}$$

$$efficiency = (amplification\ rate - 1) \times 100$$

2.2.2 Ca^{2+} mobilization assay

PARs canonically trigger an increase in the cytoplasmic free Ca^{2+} concentration, which can be detected with Ca^{2+}-binding fluorophores like Fluo-4-acetoxymethyl ester (Fluo-4-AM) by laser scanning confocal microscopy. Hence, the functional presence of PARs in AT-MSCs can be verified by endogenous PAR-activating enzymes and artificial synthesized PAR subtype-specific activating peptides (PAR-APs).

AT-MSCs were seeded into 48-well plates (for overview images with 10x objective) or chambered cover glass slides with four wells (Nunc™, cat. no. 155383; for higher magnifications) in 500 µl EM6F15 medium and cultured up to approx. 80-90 % confluence. The subsequent steps involved the reagents listed in Table 2-7 and Table 2-8.

Table 2-7: Reagents for calcium assays

Reagent	Reagent/Amount	Amount	Provider (cat. no.)
Fluo-4-AM	Stock 1 g/l in DMSO	1:600	Molecular Probes (F-14201)
HEPES-buffer, pH 7.4	NaCl	145 mM	Roth (3957)
	KCl	5 mM	Roth (6781)
	$MgSO_4*7H_2O$	1 mM	Merck (5886)
	HEPES	10 mM	Applichem (A1069)
	Glucose	10 mM	Merck (1.08337)
	Na_2HPO_4	0.5 mM	Roth (K300.2)
$CaCl_2$-solution	$CaCl_2$ 1.5 mM	1.5 mM	Applichem (A4689)
HEPES/$CaCl_2$-buffer (H/Ca^{2+}-B)	*add freshly:* $CaCl_2$-Solution into HEPES-Buffer	1:1,000	-

Following a washing step with 500 µl 37 °C-warm 10 mM HEPES/1.5 µM $CaCl_2$-buffer (H/Ca^{2+}-B), the cells were incubated for 20 min with 1.5 µM Fluo-4-AM, which was diluted in H/Ca^{2+}-B. After washing twice, 200 µl of H/Ca^{2+}-B were loaded into the wells and kept at 37 °C prior to measurement.

Agents known or expected to elevate the intracellular free Ca^{2+} concentration were diluted in 100 µl of H/Ca^{2+}-B to reach the desired final concentration (Table 2-8) after adding it to the 200 µl in the chamber (1:3 dilution).

Further characterization of the agent-triggered increase in intracellular free Ca^{2+} concentrations was assayed with the PAR_1 antagonist Atopaxar and the Ca^{2+} chelating BAPTA-AM (1,2-Bis(2-aminophenoxy)ethane-N,N,N',N'-tetraacetic acid tetrakis (acetoxymethyl ester)). For relevant experiments, Atopaxar and BAPTA-AM were diluted into the buffers and were present during fluorescent dye staining and in the last remaining 200 µl of H/Ca^{2+}-B. Thus, the incubation time was approx. 40 min before each assay.

Table 2-8: Agents used for the investigation of PAR-mediated effects on intracellular calcium

Agent	Target	Stock	Final conc.	Specific Activity / Sequence	Provider (cat. no.)
human α-Thrombin	$PAR_{1,3,4}$	10 NIH-U/µl	0.5 - 2 NIH-U/ml	3045 ± 33 NIH U*/mg (mean of two batches)	Enzyme Research Laboratories (HT 1002a)
Trypsin	$PAR_{1,2,3,4}$	1 mM	10 nM	-	Sigma (T1426)
PAR_1-AP	PAR_1	10 mM	100 - 260 µM	TFLLRN-NH_2	Group of Dr. P. Henklein, Institute for Biochemistry (Charité), Berlin (Germany)
PAR_1-RP	-	10 mM	100 µM	RLLFT-NH_2	
PAR_2-AP	PAR_2	10 mM	10 µM	2-furoyl-LIGRLO-NH_2	
PAR_4-AP	PAR_4	10 mM	400 µM	AYPGKF-NH_2	
Atopaxar	PAR_1	1 mM	0.1 µM	-	Axon (2030)
Ionomycin	Ca^{2+} stores	1 mM	5 µM	-	Sigma (I9657)
BAPTA-AM	Ca^{2+}	10 mM	5 - 7.5 µM	-	Calbiochem (196419)
BIM-1	PKC	10 mM	1 - 10 nM	-	Merck Millipore (203290)

*1 NIH (National Institute of Health) unit (NIH-U) is approximately 1.1-1.3 international unit (Gaffney & Edgell 1995).

The AT-MSCs' intracellular free Ca^{2+} concentration was monitored and recorded with a confocal Axiovert 100M laser scanning microscope (Zeiss). The excitation by an argon ion laser at 488 nm wavelength caused Ca^{2+}-bound Fluo-4-AM to emit light at 516 nm. An increase in Fluo-4-AM-fluorescence was interpreted as an elevation of the intracellular free Ca^{2+} concentration. Every recording was concluded with a re-stimulation by Ionomycin in order to obtain a positive control. Ionomycin causes an elevation of intracellular free Ca^{2+} concentrations by stimulation of intracellular stores and translocation of extracellular Ca^{2+} (Morgan & Jacob 1994). For this purpose, 100 µl of an Ionomycin solution (10 µl of 1 mM Ionomycin diluted in 500 µl H/Ca^{2+}-B) were added to the wells.

2.2.3 Freeze-fracture replica immunolabeling assay of PAR_1

Freeze-fracture replica immunolabeling (FRIL) provides an elaborate technique to visualize cell structures and the distribution of proteins of interest. FRIL requires complex machines and qualified experimenters. Therefore, the detection of PAR_1 on the MSC plasma membrane (donor #7) was conducted by the team of Dr. Martin Westermann in the Center for Electron Microscopy of the University Hospital of Jena (Germany).

Small drops of resuspended MSCs were placed between two 0.1 mm thick copper carriers and rapidly frozen by plunging into a cup with liquid ethane/propane (1:1), which in turn was cooled by liquid nitrogen. The carrier sandwich was then mounted in the cooled (-150 °C, 10^{-6} Pa) freeze-fracture

machine (BAF400T, Balzers) and tensile fractured by the swift separation of both carriers from each other. The tensile fracturing causes the cells to split up, predominantly in the hydrophobic region of the membrane bilayer, thus generating an exoplasmic fracture face (EF) and a protoplasmic fracture face (PF). Afterward, the fracture faces were replicated by two electron beam guns that first vapor-deposited a 2 nm thin platinum/carbon layer in a 35° angle onto the surface. The angle is required to create 'shadows' on cellular structures and thereby making them visible on microscopic images. Secondly, this layer was stabilized by a 15 nm thick carbon layer that was vapor-deposited from above (90°). In the next step, the major proportion of the biological material was dissolved in a cleaning solution (2.5 % (w/s) SDS, 10 mM Tris-HCl pH 7.5, 30 mM saccharose) overnight, which leaves a thin layer of macromolecules attached to the replica. The replicas were washed three times with PBS-buffer for 10 min each (75 mM NaCl, 12.5 mM NaH_2PO_4, 67 mM $NaHPO_4$ pH 7.2) and blocked for 30 min with labeling buffer (1 % (w/v) BSA, 0.5 % (w/v) gelatin, 0.005 % (v/v) Tween in PBS). Remaining epitopes are suitable for detection by primary antibodies. For the assay, the PAR_1-specific mouse monoclonal antibody WEDE15 (Beckman Coulter, cat. no. IM2085) was diluted 1:10 in labeling buffer and incubated on the replicas overnight at 4 °C. The replicas were washed again three times with labeling buffer. The primary antibody was detected by a 10 nm gold particles-labeled secondary antibody (anti-mouse IgG, British Biocell International). The replicas were washed again with PBS-buffer and fixed with 0.5 % (v/v) glutaraldehyde for 10 min and finally washed in ddH_2O.

The replicas were mounted on copper grids and imaged in a transmission electron microscope (CEM 902.A, Zeiss). The gold particles scatter the electron beam and are visible as black dots on the images, thereby indicating the location of PAR_1. Further comprehensive details on freeze-fracture and FRIL are described in the reviews by Fujimoto and Severs (Fujimoto 1995; Severs 2007).

2.3 Cellular effects of PAR_1 activation on AT-MSCs

2.3.1 Proliferation assay

1,500 MSCs in 200 µl EM6F15 were seeded per well of micro-clear flat bottom 96-well plates (Greiner, cat. no. 655098) and incubated for 24 h, followed by washing twice with PBS and starvation in 100 µl DMEM for further 24 h. Afterward, the starvation medium was replaced with 100 µl of EM6F, including stimulating agents and particular concentrations of FCS. The plates were placed in an additional humid chamber in the incubator, to prevent evaporation at the rim of the plates, and incubated for up to three days.

20 µl of CellTiter-Blue® reagent (Promega, cat. no. G8080) were added to each well, gently shaken and further incubated for up to 4 h. The contained dye resazurin is converted by living cells into the fluorescent resorufin that was detected at $540_{exitation}$ nm/$610_{emission}$ nm wavelength with the Infinite®

F200 plate reader (Tecan). The recorded fluorescence is proportional to the number of living cells. All wells were seeded with the same number of cells at the start of the experiment. Therefore, fluorescence differences between particular stimulations are likely to represent a larger or smaller number of cells and were interpreted as higher or lower rate of proliferation. (Riss et al. 2004).

2.3.2 Migration assay

Migration assays were carried out in a Neuro Probe 48-well micro chemotaxis chamber with a migration area of 8 mm² per well and polycarbonate membranes with pores of 8 µm diameter (Neuro Probe, cat. no. AP48, PFB8).

The membranes were handled with sterile forceps and incubated overnight in a 0.35 % (w/v) collagen solution (Sigma, cat. no. C3867; diluted in PBS), followed by washing with PBS for three to five times under a sterile bench. After the last washing step, they were air-dried for approx. 5 min.

In the lower compartment, cell culture medium with attractants was added with a total volume of 27 µl. A dry collagen-coated membrane was placed carefully on top of the filled bottom wells, facing the reflective side up. The rubber gasket and the upper chamber part were placed on top and tightened with the nuts. 2,000 cells in 51 µl EM6F were seeded into each well.

At all times, the wells were checked for proper loading and that no air bubbles were trapped under the membrane. Moreover, loading of the upper chamber was done swiftly by getting close above the membrane without touching or poking it with the pipet tip and lifting the pipet while injecting the medium. In this way, air bubbles were less likely to be trapped in the upper chamber.

The fully loaded chamber was placed in the incubator for 10-30 min to let it warm up. Afterward, an objective slide was placed on the chamber to serve as a lid and prevent evaporation. The migration was carried out for 16 h overnight.

For analyzing the migration, the nuts were removed, and the upper chamber was lifted and turned upside down on a paper towel. Membrane and rubber gasket were stuck on the upper part. Hence, migrated cells were facing upside. The upper left corner of the membrane was cut off with scissors, and the whole membrane was placed into PBS and washed to remove remaining medium. Afterward, the membrane was fixed in -80 °C cold methanol for 1 h at room temperature. The reusable chamber components were immediately washed thoroughly with distilled water and tapped onto paper towels to remove excess water from the wells. They were placed into sterile plastic boxes and dried at 37 °C. Subsequently to fixation, the membranes were quickly air-dried in a few seconds, and placed into a 0.5 % (w/v) crystal violet (Serva Electrophoresis, cat. no. 27335) solution for 20 min. The membranes were washed carefully with ddH_2O until the rinsing water stayed clear from the violet dye. The wet membrane was placed, with migrated cells facing down, onto a 60 mm long cover slip. Non-migrated cells were wiped off with a wet cotton swab from the other side of the membrane. While leaving the

slide with the membrane to dry up, a few drops of immersion oil (Merck Millipore, cat. no. 1046990001) were placed onto an object slide. The dry membrane was removed from the cover slip and placed on the object slide, with migrated cells facing up. Another two to three drops of oil were added, and the cover slip was put on top. Air bubbles in between the layers were removed by gently squeezing them out with forceps. Excess oil was removed over a few hours by placing the object slides between paper towels and putting a light box on top for constant pressure.
The total number of migrated violet cells per well was counted manually under a light microscope.

Every three experiments, the acrylic chamber parts were boiled in a 1 % (w/v) Terg-a-zyme® (Sigma, cat. no. Z273287) solution for 3 h at 60 °C; the rubber gaskets were boiled at 100 °C for 30 min. All parts were washed with sterile distilled water, dried and stored as described above.

2.3.3 Immunoblotting

The stimulation of cells results in the activation of intracellular signaling pathways that lead to alterations in cellular behaviors. One key factor of cellular signaling is the phosphorylation of cascades of proteins. The phosphorylation status can be assayed by SDS-PAGE-separated protein lysates, which have been transferred to protein-binding membranes for analyses. The detection is achieved by specific primary antibodies and light-emitting secondary constructs.

2.3.3.1 Stimulation of AT-MSCs for immunoblot analyses

AT-MSCs were seeded into 6-well plates, grown up to 70 % confluence, washed twice with PBS and starved in 1.5 ml DMEM for 24 h. The plates were placed on a heating plate (37 °C) and respective stimulating agents, which were pre-diluted into 500 µl of DMEM, were added to the wells.

2.3.3.2 Protein determination assay

The AT-MSCs in the 6-well plates were washed with PBS and lysed in 150 µl cold lysis buffer (Table 2-9) on ice. The protein content was determined with the Micro BCA™ Protein Assay Kit (Thermo Scientific, cat. no. 23235). 2 µl of each sample were diluted in 200 µl ddH_2O, along with a lysis buffer and ddH_2O control. 200 µl of bovine serum albumin (BSA) standards (10, 20, 40, 80 µg/ml) served as positive controls. The bicinchoninic acid (BCA) reagent was prepared according to the manufacturer's instructions; 200 µl were added to each tube. After incubation at 37 °C for 2 h, each tube was distributed into two wells of a 96-well plate, and the absorption was measured at 570 nm.
The absolute protein concentration was calculated via comparison to the linear regression of the BSA standards.

Table 2-9: Lysis buffer composition

Ingredient	Amount	Provider (cat. no.)
HEPES	50 mM, pH 7.4	AppliChem (A1069)
NaCl	150 mM	Roth (3957)
EDTA	1 mM	Roth (8043)
EGTA	2 mM	AppliChem (A0878)
NP-40 alternative	1 % (v/v)	Merck (492016)
add freshly		
Sodium orthovanadate	1 mM, *reactivate for 5 min at 95 °C*	Sigma (S6508)
Aprotinin	16 µg/ml	Sigma (A6297)
Pefablock (AEBSF hydrochloride)	1 µg/ml	AppliChem (A1421)
Leupeptin hemisulfate	2 µg/ml	AppliChem (A2183)
Pepstatin A	2 µg/ml	AppliChem (A2205)
Phenylmethanesulfonyl fluoride (PMSF)	1 mM, *add prior to use*	Sigma (P7626)

2.3.3.3 SDS-PAGE

The protein lysates were separated on vertical sodium dodecyl sulfate-polyacrylamide gel electrophoresis (SDS-PAGE). The gels were prepared as listed in Table 2-10 and filled into Hoefer electrophoresis units equipped with 1 mm spacers.

Table 2-10: Buffers used for SDS-PAGE

	Ingredient	Amount	Provider (cat. no.)
Separation gel (10 %)	Acrylamide/bisacrylamide 30 %, Rotiphorese® Gel 30	33 % (v/v)	Roth (3029)
	Separation gel buffer (2 M Tris pH 8.8)	19 % (v/v)	AppliChem (A1086)
	SDS 20 %	0.5 % (v/v)	Applichem (A3942)
	Ammonium persulfate (APS) 20 %	0.4 % (v/v)	Serva Electrophoresis (13375)
	N,N,N',N'-Tetramethyl-ethylenediamine (TEMED)	0.08 % (v/v)	Serva Electrophoresis (35930)
Stacking gel (4 %)	Acrylamide/bisacrylamide 30 %, Rotiphorese® Gel 30	19.8 % (v/v)	Roth (3029)
	Stacking gel buffer (0.5 M Tris pH 6.8)	25 % (v/v)	AppliChem (A1086)
	SDS 20 %	0.5 % (v/v)	Applichem (A3942)
	APS 20 %	0.6 % (v/v)	Serva Electrophoresis (13375)
	N,N,N',N'-Tetramethyl-ethylenediamine (TEMED)	0.04 % (v/v)	Serva Electrophoresis (35930)
10x Running buffer pH 8.4	Glycin	1.92 M	Roth (3908)
	Tris	250 mM	AppliChem (A1086)
	SDS 20 %	1 % (v/v)	Applichem (A3942)
6x Loading buffer	Tris pH 6.8	62.5 mM	AppliChem (A1086)
	Glycerol	10 % (v/v)	Roth (3783)
	SDS 20 %	2 % (v/v)	Applichem (A3942)
	β-mercaptoethanol	5 % (v/v)	Roth (4227)
	Bromophenol blue	a pinch	Roth (A512)

500 µl of the separation gel were mixed with additional APS and TEMED and immediately pipetted into the gel unit to seal all borders. The sealing gel polymerized within few seconds and the remaining separation gel was added and sealed with isopropanol (Roth, cat. no. 6752) to achieve a smooth upper border. The stacking gel was added upon hardening of the separation gel and removal of remaining isopropanol; a comb was inserted to form the lanes. After polymerization of the stacking gel, the comb was removed, and the whole system was assembled, flushed and filled with 1x running buffer.

20 µg of total protein from each lysate were mixed with loading buffer, boiled for 5 min at 95 °C and loaded onto respective lanes, along with a molecular weight marker (PageRuler™ Prestained Protein Ladder, Thermo Scientific, cat. no. 26616). The separation was conducted at constant 120 V.

2.3.3.4 Immunoblotting

The separated proteins were further blotted onto polyvinylidene fluoride (PVDF) membranes with pore sizes of 0.45 µm (Merck Millipore, cat. no. IPVH00010) using a semidry technique.

Table 2-11: Buffers used for immunoblotting

	Ingredient	Amount	Provider (cat. no.)
Anode buffer	Tris	300 mM	AppliChem (A1086)
	Methanol	20 % (v/v)	Roth (3880)
Cathode buffer	Tris	25 mM	AppliChem (A1086)
	6-aminocapronic acid	40 mM	Roth (3113)
	Methanol	20 % (v/v)	Roth (3880)
	SDS (20 %)	0.05 % (v/v)	Applichem (A3942)
10x Tris-buffered saline/Tween (TBST)	Tris	200 mM, pH 7.4	AppliChem (A1086)
	NaCl	1.5 M	Roth (3957)
	Tween® 20	0.5 % (v/v)	Serva Electrophoresis (37470)
Ponceau solution	Ponceau S	0,25 % (w/v)	Sigma (P3504)
	Acetic acid	5 % (v/v)	Roth (3735)
Blocking solution	BSA in 1x TBST	5 % (w/v)	PAA Laboratories (K41-001)
Stripping buffer	Tris pH 6.7	62.5 mM	AppliChem (A1086)
	β-mercaptoethanol	100 mM	Roth (4227)
	SDS (20 %)	2 % (v/v)	Applichem (A3942)

Three layers of anode buffer-soaked Whatman® cellulose filter paper were placed on the anode of a Trans-Blot® SD Semi-Dry Transfer Cell (Bio-Rad). The PVDF membrane was activated for 10 s in methanol and placed on the papers. The polyacrylamide gel was calibrated for few minutes in cathode buffer and placed on top of the membrane, followed by three further layers of cathode buffer-soaked filter papers. The device was closed, and blotting was conducted at constant 2 mA/cm² for 1 h.

Subsequently, the membranes were rinsed with water and incubated in Ponceau S solution for 5 min, which turns proteins red. The protein bands were made visible by rinsing one to two times with water to remove excess dye. The membranes were cut according to the intended usage of primary antibodies and further rinsed with water until the red dye was completely gone. The destaining of the membranes required frequent rinsing with fresh water over 5-10 min.

The membranes were blocked with blocking solution at constant gentle shaking for 1 h.

Following three washing steps with TBST over 30 min, the membranes were incubated with primary antibodies at constant gentle shaking and 4 °C overnight. The antibodies were diluted in 1 % (w/v) BSA in TBST.

Table 2-12: Antibodies used for Immunoblotting

Antibody	Dilution	Provider (cat. no.)
primary		
ATAP2	1:1,000	Santa Cruz Biotechnology (sc-13503)
WEDE15	1:1,000	Beckman Coulter (IM2085)
pERK 1/2 (p44/p42) mouse monoclonal antibody	1:1,000	Cell Signaling (9107)
ERK 1 (K-23) rabbit polyclonal antibody	1:3,000	Santa Cruz Biotechnology (sc-94)
secondary		
goat anti-mouse IgG-HRP	1:500	Santa Cruz Biotechnology (sc-2005)
goat anti-rabbit IgG-HRP	1:2,000	Santa Cruz Biotechnology (sc-2004)

The following day, the membranes were washed again with TBST for three times over 30 min and were incubated with horseradish peroxidase (HRP)-labeled secondary antibody, diluted in 1 % (w/v) BSA in TBST, for 50 min at RT. After another washing procedure, the membranes were placed on a dry glass plate and covered with Western Lightning® Plus-Enhanced Chemiluminescence Substrate (Perkin Elmer, cat. no. NEL105001EA) for 1 min. Afterward, excess solution was drained off. The membranes were covered with a transparent film, and the emission of light was detected with an LAS-4000 (Fujifilm). The obtained images were converted into negatives for better display and visibility.

2.3.4 Proteome Profiler™ antibody array

To investigate the profile of secreted proteins of stimulated and unstimulated AT-MSCs, supernatants of growing AT-MSCs were applied on antibody-based proteome arrays from R&D Systems. The arrays consist of strips of nitrocellulose membranes with spotted duplicates of immobilized capture antibodies for specific sets of proteinases (cat. no. ARY021), cytokines (cat. no. ARY022) or proteins involved in angiogenesis (cat. no. ARY007).

AT-MSCs were seeded into 6-well plates and cultivated up to a confluence of 50-70 %, starved for 24 h, and fresh EM6F medium was left on the cells for another 24 h for conditioning. The supernatants were collected and centrifuged to sediment cell debris.

The following steps were conducted according to the manufacturer's protocol. In brief, the conditioned medium was mixed with a biotinylated detection antibody and incubated on the washed membranes overnight at 4 °C. The spotted antibodies on the membranes capture their respective target proteins in complex with the pre-bound biotinylated detection antibody. After washing, the membranes were incubated with a streptavidin-HRP-conjugate. Streptavidin binds to biotin, thus linking HRP to the detection antibody, which in turn is bound to the immobilized protein.

After a further washing step, the membranes were placed on a dry glass plate and 1 ml Chemi Reagent Mix was added onto each membrane. The reagent was drained, and a transparent film was placed on

the membrane to prevent desiccation. The HRP converts the substrate in the reagent into a chemiluminescent signal, which was photographed using an LAS-4000 (Fujifilm).

The resulting images were quantified using the Multi Gauge v3.0 software (Fujifilm). The calculated mean pixel densities of each particular protein were divided by the mean density of the positive controls from the respective membrane, to normalize possible differences between the membranes. On a subjective basis, the results were grouped according to their strength in respect to the positive controls (PC): "+++" of more than 75 % of PC; "++" of 25 to 75 % of PC; "+" of 5 to 25 % of PC; and "o" of 2 to 5 % of PC. Less than 2 % of PC were close to the background levels and considered as no secretion, "-."

2.3.5 Enzyme-linked immunosorbent assay

To further address the AT-MSCs' expression patterns as a response to PAR_1 stimulation, the targets of the mRNA expression analysis were subjected to enzyme-linked immunosorbent assays (ELISAs) for proving mRNA expression into functional secreted protein. Therefore, the AT-MSCs were prepared as described in paragraph 2.3.4, and the supernatant medium was collected and frozen at -80 °C.
RNA samples were gained and analyzed from the underlying cells according to paragraph 2.2.1 (page 18). Additional wells with cells were used for protein determination according to paragraph 2.3.3.2 (page 25).

ELISAs for the detection of IL-8 and IL-6 were purchased from ImmunoTools (cat. no. 31670089, 31670069) and conducted according to the manufacturer's protocols.
In brief, 96-well ELISA plates were coated with primary capture antibodies and incubated at 4 °C overnight. Excess medium was tapped out of the wells. The wells were blocked with blocking buffer for 2 h. Samples and a dilution series of a positive control were pipetted in duplicates into the wells. No washing steps were required between those steps. Incubation was carried out at 4 °C overnight.
The following steps required three to five thorough washing steps and tapping out of the excess buffer in between. Stepwise, secondary antibody, HRP-streptavidin conjugate and substrate solution (Table 2-13) were added and incubated. The HRP is turning a colorless substrate solution into a blue dye.
The substrate conversion was stopped with sulfuric acid, which changed the color of the dye from blue to yellow. The amount of each colorimetric development was quantified with an Anthos Reader HT3 (Anthos Mikrosysteme) at 450 nm wavelength.

Table 2-13: Substrate solution for ELISAs

	Ingredient	Amount	Provider (cat. no.)
Solution A	*prepare prior to experiment, store up*		
5 ml	*to few days at 4 °C:*		
	3,3',5,5'-Tetramethylbenzidine (TMB)	12 mg	Sigma (860336)
	Acetone	0.5 ml	Roth (KK40)
	Ethanol	4.5 ml	Roth (K928)
	H_2O_2 (30 %)	10 µl	Roth (9681)
Solution B	Citric acid	288 mg	Roth (6490)
50 ml	ddH_2O	50 ml	-
	Potassium hydroxide solution	*raise pH to 4.1*	solid NaOH, Roth (9356)
Substrate solution	*combine prior to use:*		
	Solution A	0.5 ml	-
	Solution B	10 ml	-

2.4 Interaction of AT-MSCs and Hep3B cells in an *in vivo* xenograft mouse model

The interaction of MSCs and tumor cells harbors a complex microenvironment with multiple components that may promote or inhibit tumor growth (Yagi & Kitagawa 2013). The interaction is presumably affected by surrounding and attracted cell types as well. In order to assess the potential interaction between MSCs and HCC cells, AT-MSCs were subcutaneously co-injected with cells from the HCC cell line Hep3B into the flank of mice from the CB17 SCID strain. Whether AT-MSCs' PAR_1 is contributing to tumor growth in the model was addressed using a stable PAR_1 knockdown in the AT-MSCs. The knockdown cells were then co-injected with Hep3B cells. Furthermore, the AT-MSCs' fate in the tumor model was assayed in a batch with green fluorescent protein (GFP)-labeled AT-MSCs.

2.4.1 CB17 SCID mouse strain

The CB17 severe combined immunodeficient (SCID) mouse strain is an albino mouse that lacks functioning B and T cells, thereby making it suitable for implantation of cells from other organisms without rejection of the xenograft. Macrophages, natural killer cells and granulocytes remain unaffected by the deficiency (Charles River 2015). The mice were originally purchased from Charles River (strain code 236) and bred in a pathogen-free environment at the Service Unit Small Animal, Research Center Lobeda (FZL), University Hospital of Jena (Germany) at a constant 12 h light/dark cycle, and freely access to food and water. Handling and experiments were approved by respective authorities and followed governmental animal care regulations. Male mice with similar age and weights were used for all experiments.

2.4.2 Preparation and injection of AT-MSCs and Hep3B cells into CB17 SCID mice

Before the mice experiments, all cells were cultured according to protocols mentioned earlier (paragraph 2.1, page 16). On the day of cell injection into the mice, the cells were detached from the flasks, washed with PBS and resuspended in small volumes of RPMI. 200 µl of RPMI were prepared with respective amounts of cells according to Table 2-14.

Table 2-14: Number of cells for Injection

Cell type	Number of cells
Hep3B	100,000
AT-MSCs	500,000
Hep3B + AT-MSCs	100,000 + 500,000

The cells were kept at 37 °C in 1.5 ml tubes and flicked frequently to prevent agglutination and sedimentation of the cells while the mice were prepared. The resuspended cells were drawn up into a syringe and injected subcutaneously into the flank of mice that were anesthetized with diethyl ether. The mice were placed back into the cages and observed for tumor formation over the following 11-24 days.

When tumor formation was sufficient, all mice were scanned with the X-ray computed tomography TomoScope® Synergy Twin (CT Imaging). For that, the mice were anesthetized by inhalation of 2 % (v/v) isoflurane in a closed plastic box and then placed into the tube of the tomograph with further isoflurane inhalation. The mice were scanned for 29 s at 65 kV between skull and tail to make sure to cover all possible locations of the tumors. Tumor formations were analyzed with the ImpactView software (CT Imaging). Deformations beneath the skin, the presumed tumors, were measured at their point of maximum height, length and width. Tumor volume was calculated as follows:

$$V_{tumor} = length \times width \times height \times \frac{\pi}{6}$$

3D reconstruction of the CT images was conducted by using Imalytics software (Philips). All CT measurements and analyses were carried out with the kind help of Y. Ozegowski from the Department of Radiology, University Hospital of Jena (Germany).

After scanning all mice, they were sacrificed by cervical dislocation. The part of the skin with the tumor was cut off from the respective mouse, and a photo was shot to document angiogenesis. After the tumor was cut loose from the skin, it was placed onto graph paper, and another photo was shot. For further histochemical analysis, the tumors were put into 5 % (v/v) formalin, pH 7, to fix and preserve them for further processing. Mice showing no perceptible tumors were skinned and carefully checked for possibly overlooked formations of tumors. Tumors with GFP-labeled AT-MSCs were cut in half and separated onto a tube of formalin or Tissue-Tek® (Sakura, cat. no. 4583), respectively.
All cell co-injections and removals of tumors were carried out with the kind help of Dr. B. Günther from the Service Unit Small Animal, Research Center Lobeda (FZL), University Hospital of Jena (Germany).

2.4.3 Histological tumor analysis

The fixed tumors were placed into gaskets and washed with tap water, to remove the formalin, for 2 h. After that, the tissue was dehydrated by increasing amounts of ethanol (2x 70 % ethanol, 2x 96 % ethanol, 3x 100 % ethanol), followed by soaking in xylene (1x xylene-ethanol mixture, 2x xylene) to remove ethanol and serving as a solvent for paraffin embedding. All twelve washing steps lasted for 1 h each, using the tissue processor TP1020 (Leica). Paraffin was heated up to 60 °C to turn it liquid. The tumors were thoroughly soaked in paraffin (2x) and cast into metal gaskets to form small paraffin blocks using the Embedding Center EG1160 (Leica).

After hardening and cooling down of the blocks, thin tumor containing slices of 3-4 µm diameter were cut off using a microtome (Microm) and N35 microtome blades (Feather) and placed on objective slides for further immunohistochemical treatment.

The prepared slides were stained with hematoxylin/eosin (HE) using the ST5020 Multistainer (Leica) for general staining of tumor tissue. Hematoxylin binds basophilic cellular structures, while eosine binds acidophilic structures (Chan 2014). The staining procedure comprised: washing in xylene (3x; 3/2/1 min), decreasing ethanol concentrations (100/96/70 %; 80 s each), ddH_2O (15 s), 2x hematoxylin (4 min each), rinsing water (5 min), eosin (4 min), increasing ethanol concentrations (70/96/2x 100 %; 80 s each) and xylene (3x; 2/1 min).

Furthermore, primary antibodies for detection of cytokeratins 5, 6, 8, 17 and 19 (Clone MNF116; Dako, cat. no. M0821), alpha-smooth muscle actin (α-SMA; Clone 1A4; Dako, cat. no M0851) and Ki-67 (Clone MIB-1, cat. no. M7240) were applied. The slides were prepared in the PT-Link (Dako) with preheated (84 °C) Target Retrieval Solution (Dako; high pH, cat. no. K8004, cytokeratin and α-SMA; low pH, cat. no. K8005, Ki-67) for 20 min at 97 °C and subsequently washed in Wash Buffer (Dako, cat. no K8007) for 5-10 min. The following steps were conducted by the Autostainer Link 48 (Dako) with the EnVision™FLEX, High pH (Link) kit (Dako, cat. no. K8000). Staining steps comprised: blocking of peroxidases (5 min), incubation with primary antibody (30 min), secondary antibody Mouse (LINKER) (Dako, cat. no. K8021), HRP (20 min), substrate working solution (10 min), hematoxylin (7 min), and final rinsing with ddH_2O. Wash Buffer was applied between every incubation step.

Finally, the slides were washed with ddH_2O (2x), ethanol (2x 70 %, 2x 96 %, 2x 100 %) and xylene (4x), and covered with mounting medium (Dako, cat. no. CS703) and cover slips.

The stained slides were scanned and digitally converted into virtual slides using the NanoZoomer 2.0-HT digital slide scanner (Hamamatsu) and its viewing platform NDP.view2.

All histological assays and evaluations were carried out with support from E. Oswald from the Department of General, Visceral and Vascular Surgery (Experimental Transplantation Surgery)

University Hospital of Jena (Germany) and Dr. K. Katenkamp from the Institute of Pathology, University Hospital of Jena (Germany).

2.4.4 Genetic modification of AT-MSCs

The fate of the AT-MSCs and the impact of PAR_1 in AT-MSCs on the tumor development in the AT-MSC-Hep3B SCID mouse model was addressed with genetically modified AT-MSCs. To that end, we labeled a batch of AT-MSCs with GFP to track them inside the tumor mass. In another batch, the stable knockdown of PAR_1 mRNA was achieved by post-transcriptional silencing of the PAR_1 gene *F2R* with short hairpin RNA (shRNA). The protocol was carried out with commercially available bacterial stocks from Sigma that contain plasmids with a particular shRNA sequence, which targets PAR_1 mRNA, and a puromycin resistance for the selection of successfully transduced cells (Table 2-15).

Table 2-15: F2R MISSION® shRNA bacterial glycerol stocks used for PAR_1 knockdown

Provider:	Sigma
Product type:	SHCLNG-NM_001992
Species:	human

#	TRC number	Clone ID	Sequence
1	TCRN0000352793	NM_001992.3-1247s21c1	CCGGCCCACAAACGTCCTCCTGATTCTCGAGAATCAGGAGGAC GTTTGTGGGTTTTTG
2	TCRN0000352674	NM_001992.3-1270s21c1	CCGGGCATTACTCATTCCTTTCTCACTCGAGTGAGAAAGGAAT GAGTAATGCTTTTTG
3	TCRN0000342351	NM_001992.3-384s21c1	CCGGCCCGGTCATTTCTTCTCAGGACTCGAGTCCTGAGAAGAA ATGACCGGGTTTTTG
4	TCRN0000342352	NM_001992.3-1068s21c1	CCGGCCTACTACTTCTCAGCCTTCTCTCGAGAGAAGGCTGAGA AGTAGTAGGTTTTTG
5	TCRN0000003688	NM_001992.x-2152s1c1	CCGGGACGGCAAGGTTTAAGTTATTCTCGAGAATAACTTAAAC CTTGCCGTCTTTTT

TRC = The RNAi Consortium

Table 2-16: Material for plasmid purification, transfection and transduction

	Ingredient	Amount	Provider (cat. no.)
LB agar	LB-medium	25 g/l	Roth (X968)
	Agar	15 g/l	Applichem (A0949)
	autoclave		
	cool down to 50 °C		
	ampicillin	100 µg/ml	Roth (K029)
LB medium	LB-medium	25 g/l	Roth (X968)
	autoclave, cool down		
	ampicillin	100 µg/ml	Roth (K029)
DNA plasmid purification	NucleoBond® Xtra Midi	-	Macherey Nagel (740410.10)
Polyethylenimine	Stock: 10 µg/µl	2.5 µg/µg DNA	Sigma (408727)
Polybrene (Hexadimethrine bromide)	Stock: 0.8 mg/ml	1:100	Sigma (107689)
Puromycin	Stock: 2 mg/ml	1:1000	Sigma (P-8833)

2.4.4.1 Breeding of E. coli stocks / amplification of plasmids

Ampicillin-containing LB agar plates were prepared by pouring the warm and liquid solution into sterile 10 cm bacterial dishes, leaving them aside to cool down and harden. After that, ampicillin resistant bacterial stocks were plated onto the LB agar by scratching some cells out of the frozen stock with a pipet tip, and carefully wiping the tip over the plate. The plates were incubated at 37 °C for 16 h/overnight.
The following day, a single colony was picked and transferred into 200 ml LB medium with ampicillin in a 500 ml conical flask. The flask was loosely closed with an aluminum cap and shaken at 37 °C and about 180 rpm for 16 h.

The purification of the plasmids from the *Escherichia colis* (*E. coli*) suspension was carried out following the protocol of the NucleoBond® Xtra Midi Kit (Macherey Nagel, cat. no. 740410). In short, the suspension was spun down in an Avanti™ J-20 XPI centrifuge (Beckman Coulter) and the cell pellet was resuspended in an RNase-containing buffer. Hence, possible interfering RNA is 'removed' from the purification. The suspended cells were lysed with an alkaline buffer containing denaturing SDS. Plasmid DNA was separated by a column filtration based on an ionic exchange resin that captures the negatively charged DNA. In the final step of this protocol, the plasmid DNA was eluted with ddH_2O. Afterward, the DNA was precipitated with ethanol and isopropanol, washed again, and resuspended in ddH_2O. The plasmid's concentration and purity was determined using a NanoDrop™ spectrophotometer (ND-1000, Peqlab) and following the manufacturer's instructions.

2.4.4.2 Transfection of HEK293T cells / lentivirus production

Following the preparation of a sufficient amount of plasmid, HEK293T cells were transfected with plasmids that encode viral particles and the shRNA for knockdown or non-targeting control, respectively. HEK293T cells serve as a host to produce lentiviruses that in turn are able to transduce target cells with high efficiency.
HEK293T cells derive from human embryogenic kidney (HEK) cells that were transformed with the simian virus 40 (SV40) large T antigen (Shein & Enders 1962), which drives continuous replication by primarily binding and inactivating the tumor suppressors retinoblastoma protein and p53 (Ali & DeCaprio 2001).
HEK293T cells were kindly provided by Dr. Carol Stocking-Harbor from the Heinrich-Pette-Institute in Hamburg (Germany). The culture medium was DMEM with 10 % (v/v) FCS and 1 % (v/v) penicillin/streptomycin (termed DMEM10).

A minimum of one T160 flask of HEK293T cells was required per one 6-well plate of target cells. In the beginning, 2.5 Mio HEK293T cells were seeded in 20 ml DMEM10 in a T160 flask and left to grow for one and a half days for proper attachment. On the day of transfection, the plasmids (Table 2-17) were prepared as listed in Table 2-18.

Table 2-17: Vectors used for transfection of HEK293T cells

	Product Name / Description	Provider
non-taget (nt) control	MISSION® pLKO.1-puro Non-Mammalian shRNA Control Plasmid DNA	Sigma (SHC002)
pMDL, pRSV, pVSV	Lentiviral Packaging Plasmids	provided by Dr. Carol Stocking-Harbor, Heinrich-Pette-Institute, Hamburg (Germany)
eGFP	LeGO-iG2	Lentigo Vectors

Table 2-18: Ratios of DNA for preparation of transfection

For one T160 flask		Tube 1	Tube 2
DMEM		0.5 ml	0.5 ml
Expression vector (nt/PAR$_1$KD/eGFP)		20 µg	-
Viruscapsule	pMDL	20 µg	-
	pRSV	10 µg	-
	pVSV	4 µg	-
Polyethylenimine (Sigma, cat. no. 40872) (PEI, 2.5 µg PEI per 1 µg DNA)		-	135 µg

Tube 1 and 2 (Table 2-18) were pipetted together, gently vortexed immediately and left at RT for 30 min.

Just before the end of the incubation time, the medium of the HEK293T cells was changed to FCS-free DMEM. HEK293T cells do not adhere firmly to the flask, and the transfection process reduces the adhesion additionally. Therefore, gentle conduction of all following steps was required to prevent loss of cells and diminished virus output. The mixture of plasmid DNA was added drop-wise to the medium in the flasks and incubated for another 6 h. Electrostatic attraction causes PEI and plasmid DNA to build up condensed particles with a cationic charge, which in turn bind to anionic surface molecules on the cells, thus favoring endocytosis of the particles. PEI alters the osmotic potential of the endosomes and swelling causes them to release the particles from the vesicles (Sonawane, Szoka, & Verkman 2003). Unused transfection material was washed away by replacing transfection medium with fresh DMEM10.

The following days, the virus-containing medium was harvested at 24, 48 and 72 h, and fresh DMEM10 was refilled into the flasks. The harvested medium was filtered through 0.2 µM syringe filters to remove cell debris. Filtered medium was frozen and stored at -80 °C. Prior to transduction, the virus-containing medium was concentrated by factor 50-100 with an Amicon Ultra-15 Centrifugal Filter Unit with Ultracel-30 membrane (Merck Millipore, cat. no. UFC903) at 4,000 *g*. In general, target cells were tried to be prepared in sync to virus production to avoid freezing of viruses.

2.4.4.3 Lentiviral transduction of AT-MSCs

About six days prior to transduction, 400 AT-MSCs/cm² were seeded into fibronectin-coated 6-well plates.

The concentrated virus-containing medium of one T160 flask was added to the amount of fresh EM6F15, which was required for one whole 6-well plate, along with the cationic polymer polybrene (Stock: 0.8 mg/ml → 1:100). Polybrene enhances the transduction rate by aggregation of viruses and adsorption to target cells by neutralizing negatively charged cell surfaces (Davis, Morgan, & Yarmush 2002; Davis et al. 2004). The AT-MSC culture medium was carefully replaced with the transduction medium mix. Afterward, the 6-well plates were placed in aerosol-tight trays of a swinging bucket rotor and centrifuged in a Heraeus Multifuge 1S (Thermo Scientific) at 500 *g* for 1 h. This procedure was carried out three times in a row with 8-16 h incubation in between (e.g. morning, evening, next morning).

After a minimum time of 48 h post-transduction, the culture medium was changed to selection medium, containing 2 µg/ml puromycin. Previous tests for the selection efficiency showed that all AT-MSCs detach within 48 h at puromycin concentrations of more than 1 µg/ml. At the end of the selection, surviving cells were washed properly and given fresh medium.

The cells were detached at confluences of approx. 50-70 %, and were passaged from initially a single well of a 6-well dish to a T75 flask and then further to one T160 flask. After a total duration of 3.5 to 4 weeks *in vitro*, with two passages, the AT-MSCs were ready for *in vivo* experiments. The PAR_1 knockdown efficiency was assessed with small proportions of cells that were split at passage two and grown in a 6-well plate dish prior to mRNA extraction. The GFP labeling was evaluated with a fluorescence microscope.

The co-injection tumor-assay set up for AT-MSC-nt, AT-MSC-PAR_1KD and AT-MSC-GFP was the same as the one for wild type AT-MSCs described in paragraph 2.4.2 (page 31).

2.5 Statistical analysis

All data were tested for statistical significance by independent two-sample student's t-tests assuming equal variances. Significances were indicated with stars (*) or circles (°) above the mean values with their respective standard deviation (SD) bars. Further details are given in the figure legends. Calculations were carried out in Microsoft Excel.

3 Results

Mesenchymal stem cells (MSCs) are of keen interest to current medical research to cure tissue diseases with chronic inflammation, fibrosis or impaired regenerative capacities. Cancerous diseases like hepatocellular carcinoma (HCC) may benefit from the ameliorative effects of MSCs, too. The progression of HCC has been shown to benefit from the activation of proteinase-activated receptors (PARs) in tumor cells as well as surrounding cell entities of the tumor microenvironment. However, the biological role of PARs in MSCs and the impact of MSCs on the HCC microenvironment are currently insufficiently understood. Therefore, we conducted *in vitro* assays to characterize PARs in MSCs and assessed their impact on biological features of MSCs. Subsequently, we analyzed the significance for surrounding HCC cells *in vivo* in a xenotransplantation HCC tumor model.

3.1 Characterization of PARs in AT-MSCs

PARs have not been of particular interest to stem cell research so far, and comprehensive analyses are still lacking. Hence, in order to understand the importance of the PAR family in MSCs, it was necessary to analyze their presence, functionality and distribution inside the cells.

3.1.1 PAR_1 is the predominantly expressed PAR family member in AT-MSCs

Addressing the presence and relative quantities of the PAR family in adipose tissue-derived (AT) MSCs required primer pairs of similar quality. Therefore, PAR subtype-specific primers were employed in qPCRs of a dilution series of a mixture of cDNA (1.5 µg/µl) from several cell types. The obtained

A **Primer efficiency test**

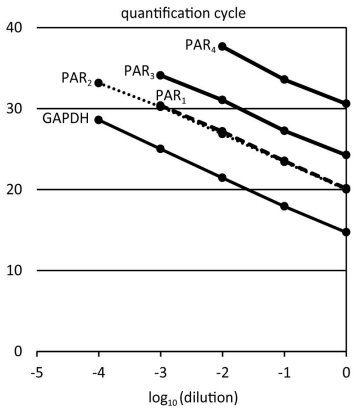

B **Attributes of linear regression** (desired value)

Primer Pair	R^2 (> 0.99)	Slope (-3.58 – -3.10)	Amplification rate (2)	Efficiency [%] (90 – 110 %)
GAPDH	0.9995	-3.4840	1.94	94
PAR_1	0.9994	-3.4350	1.95	96
PAR_2	0.9991	-3.3070	2.01	101
PAR_3	0.9978	-3.3325	2.00	100
PAR_4	0.9922	-3.5325	1.92	92

Figure 3-1: Efficiency of primers used for PAR expression analyses

(A) Primer efficiency test. Depiction of the quantification cycles (C_q) from qPCRs using dilutions of a cDNA mixture (1.5 µg/µl, pooled from various cell types) and PAR subtype-specific primers. Dots show the mean values of technical duplicates from one assay. (B) Attributes of the respective linear regressions from the primer efficiency test. GAPDH and PAR subtype primers fulfilled the efficiency requirements. R^2 = coefficient of determination

quantification cycles (C_q) for each dilution were fitted with a linear regression (Figure 3-1, A) and respective attributes were calculated (Figure 3-1, B) as described in paragraph 2.2.1.3 (page 20).
The present DNA in a PCR is duplicated every cycle if it runs with 100 % efficiency (amplification rate = 2). Hence, the desired values of a standard PCR can be calculated (Figure 3-1, B). Any primer pair should have an efficiency of 90 to 110 %, with respective values of the coefficient of determination (R^2) and slope. All of our applied primer pairs fulfilled the desired values for each attribute and demonstrated efficiencies between 92 and 101 % over the given range of concentrations of template cDNA. As further displayed in Figure 3-1 A, no amplification was monitored for PAR_1 and PAR_3 at cDNA concentrations below 1.5 ng/µl (10^{-3} dilution), and for PAR_4 below 15 ng/µl (10^{-2} dilution). In general, the PAR_4 gene transcript showed little presence in the pooled cDNA, since undiluted cDNA demonstrated C_q values above 30.

We employed the PAR subtype primers in qPCRs with cDNA from AT-MSCs from eight different patients (see Table 2-1, page 16). The expression was assessed as a percentage of GAPDH expression and showed a significant overall dominance of PAR_1 mRNA expression, compared to PAR_2, PAR_3 and PAR_4 (Figure 3-2, A). PAR_3 was expressed in larger amounts than PAR_2. PAR_4 was barely detected. The expression of PAR_1 varied strongly among the different donors. Hence, all single donor results were plotted again in relation to the PAR_1 expression (Figure 3-2, B). The expression pattern remained similar and displayed that PAR_1 was expressed in significantly larger amounts, of about five to ten times more, than PAR_2 PAR_3 and PAR_4.

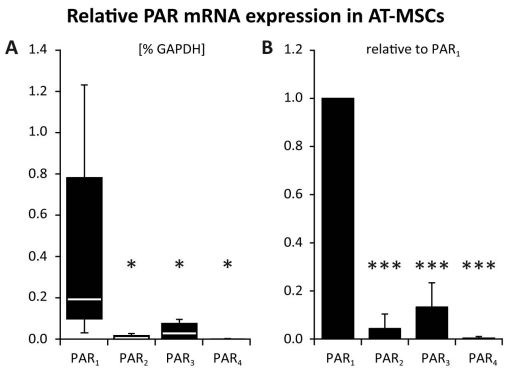

Figure 3-2: Expression levels of PARs in AT-MSCs

The mRNA expression of the four PARs in AT-MSCs was analyzed in one batch of AT-MSC cDNA per donor. Bars represent mean values ± SD of technical qPCR triplicates, eight donors in total. (A) Box plot of relative expression levels as percentage of GAPDH expression. (B) Results of single donors relative to PAR_1 expression.

PAR_1 was the predominantly expressed PAR subtype in the analyzed AT-MSCs. ***p-value ≤ 0.001; *p-value ≤ 0.05

3.1.2 PAR activation causes an increase in $[Ca^{2+}]_i$ in AT-MSCs

PARs are capable of eliciting a distinct increase in the intracellular free Ca^{2+} concentration ($[Ca^{2+}]_i$) upon stimulation. The expression analyses of the PAR subtypes in AT-MSCs revealed the expression of PAR_1, PAR_2 and PAR_3 while PAR_4 was barely detected. Thus, the activation by canonical activating proteinases and PAR subtype-specific activating peptides (APs) provided additional feedback on presence and functionality of the particular PARs.
The images displayed in Figure 3-3 show that stimulation of AT-MSCs with thrombin (Figure 3-3, B) and the PAR_1-AP (Figure 3-3, E) resulted in a strong temporary increase in $[Ca^{2+}]_i$, comparable to the

response that was induced by Ionomycin, which triggers Ca^{2+} mobilization from intracellular stores and Ca^{2+} intake from surrounding buffer. The caused Ca^{2+} peak was triggered immediately after addition of the agents and went steadily down to the initial state within 70-100 s. Ionomycin's effects were permanent and caused disruption of cellular integrity in the applied range of concentration since the Ca^{2+} peaks were usually constant, and leakage of cytoplasm into the buffer was occasionally observed.

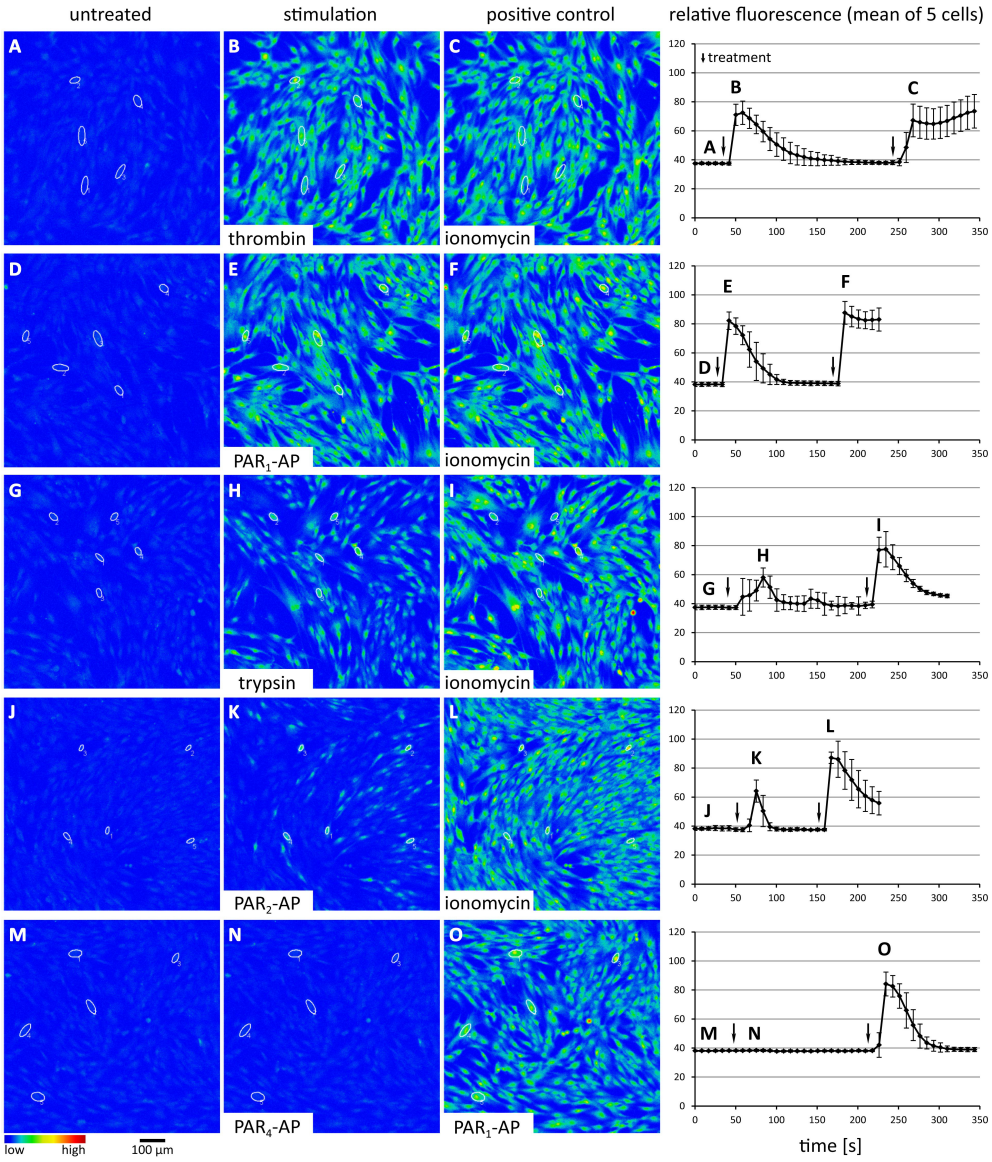

Figure 3-3: Intracellular Ca^{2+} response to stimulation of PARs in AT-MSCs

AT-MSCs (donor #6) were cultured in 48-well dishes and labeled with the Ca^{2+}-binding dye Fluo-4-AM. The treatments with agonists resulted in an increase in $[Ca^{2+}]_i$, which was seen as an increase in Fluo-4-AM-fluorescence and recorded by an inverted confocal laser scanning microscope. Each row represents the time course of a single well with representative images. The mean fluorescence ± SD of five representative cells (white circles) is depicted in the respective graph on the right, with marked time points of images (A-O) and treatments (labeled in white bars in pictures; time points marked with arrows in graphs). The displayed images are representative for one additional separate assay with donor #8.

Stimulation of AT-MSCs with thrombin (1 NIH U/ml; A-C) and PAR_1-AP (260 µM; D-F) resulted in a strong increase in $[Ca^{2+}]_i$, comparable to the positive control Ionomycin (5 µM). Trypsin (10 nM; G-I) and PAR_2-AP (10 µM; J-L) triggered less, PAR_4-AP (400 µM; M-O) triggered no signal.

Trypsin (Figure 3-3, H) caused a weaker Ca^{2+} response than thrombin, PAR_1-AP or Ionomycin and cells did not react at once but rather kept flashing up after each other distributed over a long time. However, the main peak appeared within the first 50 s after stimulation. The PAR_2-AP (Figure 3-3, K) activated single AT-MSCs. The Ca^{2+} response was about 40 s short and less strong than thrombin, PAR_1-AP or Ionomycin. The intensity was similar to trypsin, but, all affected cells reacted at once. The PAR_4-AP (Figure 3-3, N) was unable to induce an intracellular free Ca^{2+} signal in the AT-MSCs. Therefore, we subsequently applied the PAR_1-AP as a positive control, in order to verify the ability of the cells to respond with a membrane receptor-mediated Ca^{2+} signal.

Due to the lack of specific tools for the analysis of PAR_3, only PAR_1, PAR_2 and PAR_4 were portrayed in further assays. PAR_3-derived activating peptides were found to activate PAR_1 and PAR_2, and currently, no subtype-specific PAR_3-AP is known (Hansen, Saifeddine, & Hollenberg 2004; Zhao, Metcalf, & Bunnett 2014).

Thrombin and PAR_1-AP caused an increase in $[Ca^{2+}]_i$ in AT-MSCs. However, thrombin canonically cleaves and activates PAR_1, PAR_3 and PAR_4. Therefore, in the next experimental step both agents were sequentially combined in order to (1) deplete the amount of PAR_1 on the plasma membrane by activation with PAR_1-AP, and (2) to see if an additional stimulation via PAR_3 or PAR_4 is possible in a follow-up stimulation with thrombin (Figure 3-4). Moreover, Experiments with the reverse PAR_1-peptide RLLFT (PAR_1-RP), validated as a negative control for PAR_1-AP (Kaufmann & Hollenberg 2012), were performed.

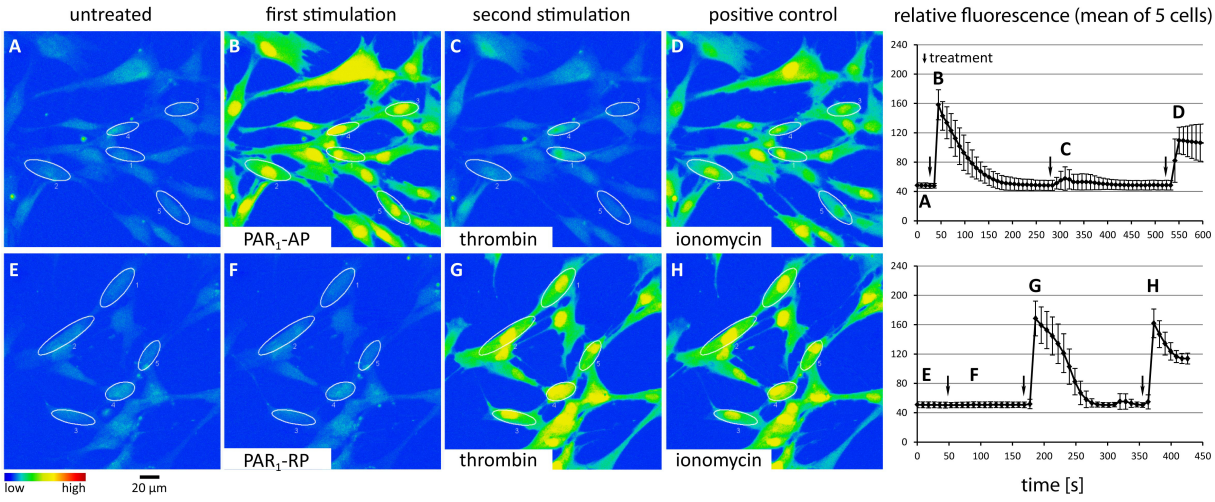

Figure 3-4: Subsequent stimulation of AT-MSCs with PAR_1-AP and thrombin

AT-MSCs (donor #1) were cultured in 48-well dishes and labeled with the Ca^{2+}-binding dye Fluo-4-AM. The treatments with agonists resulted in an increase in $[Ca^{2+}]_i$, which was seen as an increase in Fluo-4-AM-fluorescence and recorded by an inverted confocal laser scanning microscope. Each row represents the time course of a single well from one assay with representative images. The mean fluorescence ± SD of five representative cells (white circles) is depicted in the respective graph on the right, with marked time points of images (A-H) and treatments (labeled in white bars in pictures; time points marked with arrows in graphs).

(A-D) Stimulation of AT-MSCs with PAR_1-AP (100 µM) resulted in a strong increase in $[Ca^{2+}]_i$, comparable to the positive control Ionomycin (5 µM) while subsequent treatment with thrombin (1 NIH U/ml) had almost no effect. (E-H) The stimulation of AT-MSCs with the reverse peptide PAR_1-RP (100 µM), which served as negative control, showed no effect on the cells while the subsequent treatment with thrombin (1 NIH U/ml) resulted in a strong increase in $[Ca^{2+}]_i$, comparable to the positive control Ionomycin.

As shown in Figure 3-4, PAR_1-AP led to an increase in $[Ca^{2+}]_i$ in AT-MSCs, comparable to Ionomycin (D), while PAR_1-RP had no effect (B + F). Subsequent treatment with thrombin showed that if PAR_1 was already stimulated with PAR_1-AP, no further stimulation was induced by thrombin in the cells (C). Following the PAR_1-RP application, thrombin was able to cause a strong Ca^{2+} signal (G). These results indicated that PAR_1 might be the sole PAR subtype in AT-MSCs to respond to thrombin via Ca^{2+} signals.

3.1.3 PAR_1 antagonist Atopaxar inhibits PAR_1-mediated $[Ca^{2+}]_i$ increase in AT-MSCs

Additional Ca^{2+} assays were carried out with the PAR_1 antagonist Atopaxar, in order to test its efficacy and to verify that the observed Ca^{2+} mobilization by PAR_1 agonists was specific to the PAR_1 stimulation. As shown in Figure 3-5, thrombin and PAR_1-AP were able to increase rapidly the $[Ca^{2+}]_i$, comparable to Ionomycin. Preceded incubation of the AT-MSCs with the PAR_1 antagonist Atopaxar caused a concentration-dependent reduction of the thrombin or PAR_1-AP-triggered $[Ca^{2+}]_i$ increase. The concentration of 0.1 and 0.5 µM Atopaxar sufficiently inhibited thrombin's actions on a majority or almost all of the AT-MSCs. The results for the stimulation with PAR_1-AP were similar. Hence, the other thrombin receptors PAR_3 and PAR_4 did not seem to contribute to the Ca^{2+} elevation that was triggered by thrombin.

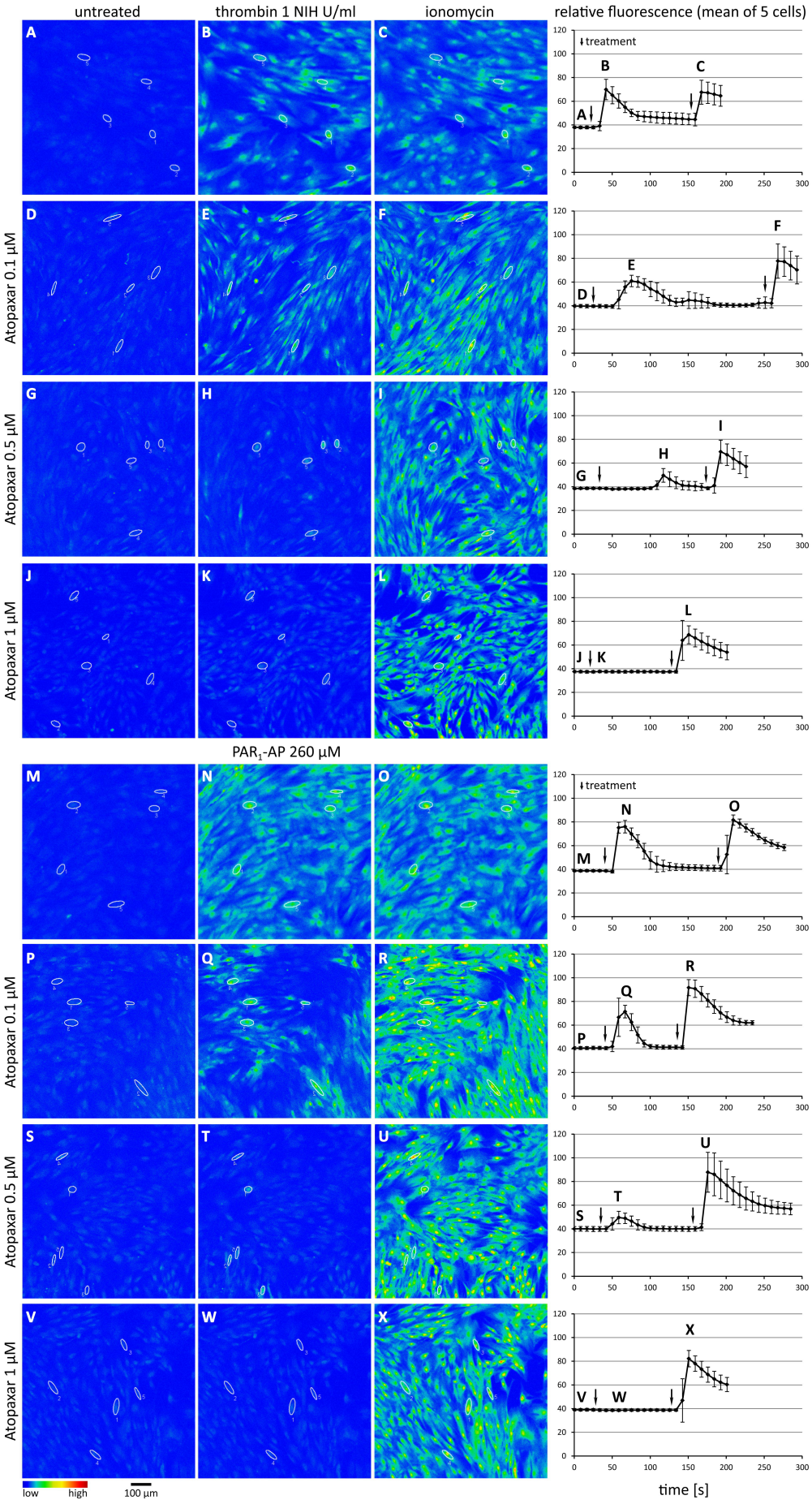
untreated
thrombin 1 NIH U/ml
ionomycin
relative fluorescence (mean of 5 cells)
Atopaxar 0.1 µM
Atopaxar 0.5 µM
Atopaxar 1 µM
PAR1-AP 260 µM
treatment
time [s]
low
high
100 µm

Figure 3-5: PAR_1 antagonist Atopaxar reduces Ca^{2+} mobilization in AT-MSCs upon PAR_1 activation with thrombin or PAR_1-AP

AT-MSCs (donor #8) were cultured in 48-well dishes and labeled with the Ca^{2+}-binding dye Fluo-4-AM. Treatments with thrombin (time point marked with arrows in diagrams) resulted in an increase in $[Ca^{2+}]_i$, visualized by an inverted confocal laser scanning microscope as an increase in Fluo-4-AM fluorescence. Each row represents a single well with the mean ± SD time course of five representative cells (white circles) depicted in each diagram, along with marked time points of pictures for the measured areas (A-X). Images of two representative assays are shown.

The pre-treatment of AT-MSCs with increasing concentrations of Atopaxar resulted in a concentration-dependent blocking of the thrombin- (A-L) and PAR_1-AP-induced (M-X) Ca^{2+} increase in AT-MSCs.

3.1.4 Effect of the Ca^{2+} chelator BAPTA-AM on AT-MSCs

PAR_1 was shown to exert a strong increase in the free cytosolic Ca^{2+} concentration in AT-MSCs upon stimulation with thrombin and PAR_1-AP (see Figure 3-3, Figure 3-4 and Figure 3-5). The Ca^{2+} signal may result in further downstream signaling and biologic effects on the cells. In order to intercept the Ca^{2+} signal, we depleted the intracellular free Ca^{2+} with the selective Ca^{2+}-chelating agent BAPTA-AM (1,2-Bis(2-aminophenoxy)ethane-N,N,N',N'-tetraacetic acid tetrakis(acetoxymethyl ester)). In the following initial assays, we assessed its efficacy on depleting intracellular free Ca^{2+}.

3.1.4.1 Ca^{2+} chelator BAPTA-AM reduces PAR_1-triggered $[Ca^{2+}]_i$ increase in AT-MSCs

As shown in Figure 3-6, thrombin and PAR_1-AP were able to trigger a rapid increase in $[Ca^{2+}]_i$, comparable to Ionomycin. In the presence of the Ca^{2+} chelator BAPTA-AM, the Ca^{2+} response in the AT-MSCs was reduced for both thrombin and PAR_1-AP stimulation. At a concentration of 2.5 µM BAPTA-AM the response was already diminished by approximately half, and at 5 µM almost no remaining reaction was visible. BAPTA-AM also attenuated the increase in $[Ca^{2+}]_i$ triggered by Ionomycin. However, the Ca^{2+} influx seemed to saturate the chelator at the employed concentrations, and the maximum fluorescence was still achieved after approx. 100-150 s.

These results show that BAPTA-AM is able to reduce and even abrogate the effects of PAR_1 activation on intracellular free Ca^{2+} elevation.

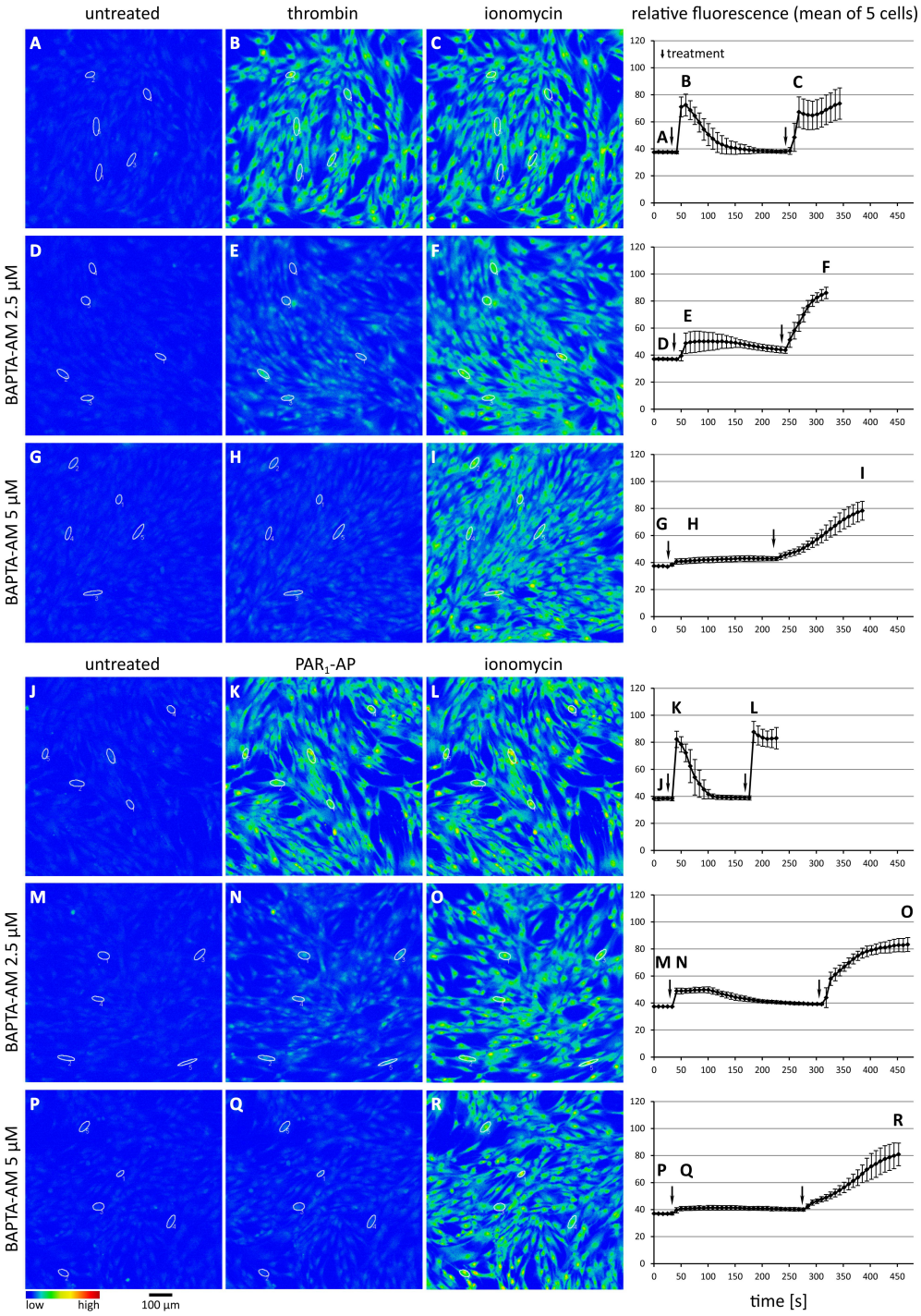

Figure 3-6: Intracellular Ca^{2+} response to PAR stimulation in AT-MSCs in presence of the Ca^{2+} chelator BAPTA-AM

AT-MSCs (donor #6) were cultured in 48-well dishes and labeled with the Ca^{2+}-binding dye Fluo-4-AM. Treatments with thrombin and PAR_1-AP (time point marked with arrows in diagrams) resulted in an increase in $[Ca^{2+}]_i$, visualized by an inverted confocal laser scanning microscope as an increase in Fluo-4-AM fluorescence. Each row represents a single well from one assay with the mean ± SD time course of five representative cells (white circles) depicted in each diagram, along with marked time points of pictures for the measured areas (A-R).

Stimulation of AT-MSCs with thrombin (1 NIH U/ml) and PAR_1-AP (260 µM) resulted in a strong $[Ca^{2+}]_i$ increase, comparable to positive control Ionomycin (5 µM). Pre-treatment of AT-MSCs with increasing concentrations of the Ca^{2+} chelator BAPTA-AM resulted in a concentration-dependent suppression of (A-I) thrombin- and (J-R) PAR_1-AP-induced Ca^{2+} increase in MSCs. The influence of BAPTA-AM caused Ionomycin to require more time to raise the $[Ca^{2+}]_i$ to levels as without BAPTA-AM.

3.1.4.2 AT-MSCs remain viable in prolonged presence of BAPTA-AM

The abrogation of the PAR_1-mediated $[Ca^{2+}]_i$ elevation by BAPTA-AM was shown in paragraph 3.1.4.1. However, incubation times of 24 h were intended for upcoming assays, and the strong impact of BAPTA-AM might exert negative effects on general Ca^{2+} homeostasis and AT-MSC viability over longer periods. Therefore, AT-MSCs were treated with several concentrations of BAPTA-AM and incubated for 24 h.

As shown in Figure 3-7, a BAPTA-AM concentration of 10 µM altered the morphology of multiple AT-MSCs. We observed structural changes that resembled a multitude of internal compartments or vacuoles. The application of trypan blue revealed that these altered cells remained viable by showing no uptake of the dye. Dead cells would take up the dye and appear dark blue. The assayed cells appeared transparent and similar to the background, hence remaining viable. At lower BAPTA-AM concentrations, only a few single altered cells were found. Therefore, 2.5-7.5 µM BAPTA-AM were considered suitable for the application in long-term assays.

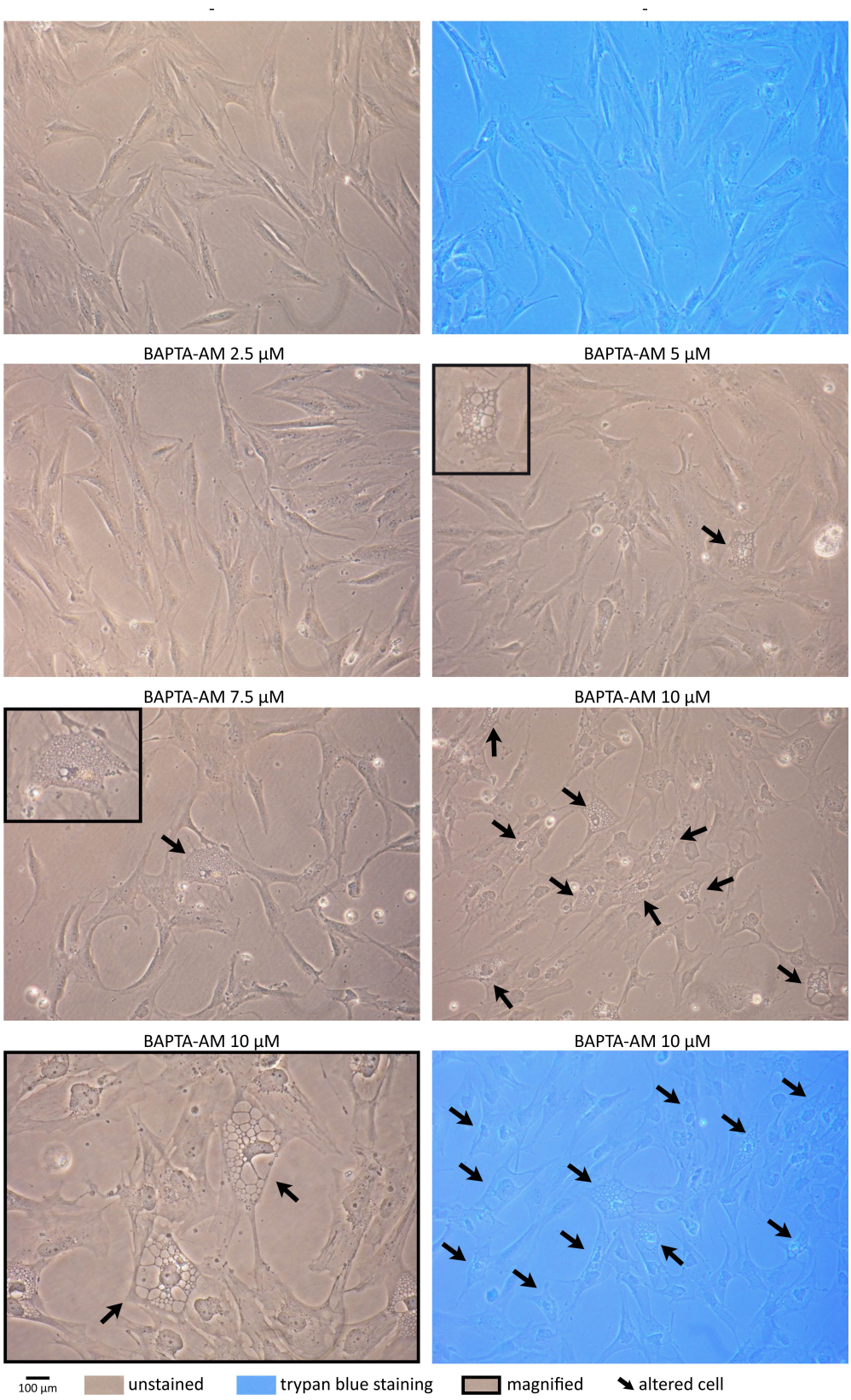

Figure 3-7: Ca^{2+} chelator BAPTA-AM causes multiple internal changes in AT-MSCs' morphology at a concentration of 10 µM

AT-MSCs (donor #6) were cultured in 6-well plates and incubated with increasing concentrations of the Ca^{2+} chelator BAPTA-AM for 24 h. Cell viability was determined by trypan blue staining. Dead cells accumulate the dark blue stain (not present in the pictures) while living cells appear transparent and similar to the background as is the case in the displayed pictures. The figure displays representative images of one assay.

AT-MSCs showed morphological changes after incubation with 10 µM BAPTA-AM while staying viable. The alterations resembled vacuoles (indicated by black arrows, highlighted in black boxes). Between 2.5 and 7.5 µM BAPTA-AM only single altered AT-MSCs were found.

3.1.5 PAR_1 is located on the plasma membrane of AT-MSCs

The expression analyses of paragraph 3.1.1 revealed that PAR_1 was the predominantly expressed PAR subtype in the analyzed AT-MSCs. Furthermore, the PAR_1-activating agonists thrombin and PAR_1-AP exerted a strong Ca^{2+} elevation inside the cells as pointed out in paragraph 3.1.2. Therefore, we focused further PAR analysis in AT-MSCs on PAR_1.

The presence of PAR_1 in AT-MSCs on protein level was verified by immunoblotting and electron-microscopic images of immunolabeled freeze-fracture replicas using PAR_1-specific antibodies.
We employed two different PAR_1-specific antibodies on AT-MSC lysates, ATAP2 (Santa Cruz Biotechnology) and WEDE15 (Beckman Coulter). PAR_1 has a molecular weight of 47 kDa or 66 kDa, respectively, depending on its degree of glycosylation. The glycosylation alters movement behavior during SDS-PAGE and may cause smear bands if heavily glycosylated. As shown in Figure 3-8, ATAP2 highlighted multiple bands, including a faint one at approx. 47 kDa and three stronger bands at approx. 37, 43 and 66 kDa. WEDE15 highlighted bands at the same molecular weights, but the ones at 43 and 47 kDa appeared more prominent in respect to the other faint bands. Therefore, WEDE15 marked PAR_1 at expected molecular weights more prominently and with less strong bands at unexpected weights than ATAP2. WEDE15 is also able to detect both cleaved and the intact receptor and has been used extensively by other researchers over the past two decades. Hence, we used WEDE15 for the detection of PAR_1 on AT-MSC plasma membranes.

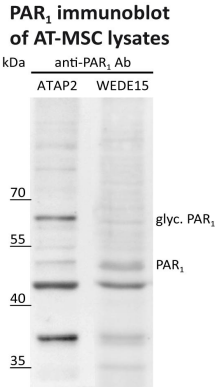

Figure 3-8: Test of PAR_1-specific antibodies ATAP2 and WEDE15 on AT-MSC lysates

AT-MSCs (donor #1) were seeded into 6-well-plates, grown to approx. 70 % confluence and then lysed. 20 µg of AT-MSC protein lysates were separated by SDS-PAGE and blotted onto protein-binding PVDF membranes. PAR_1 was detected with the specific primary antibodies ATAP2 (Santa Cruz Biotechnology) or WEDE15 (Beckman Coulter), HRP-labeled secondary antibody and a chemiluminescent detection. The immunoblots (negative images shown) depict PAR_1 immunoblots of AT-MSC lysates from one assay.

The PAR_1 antibodies ATAP2 and WEDE15 detected several bands on immunoblots of AT-MSC lysates (donor #1). Unglycosylated PAR_1 has a molecular weight of about 47 kDa. Glycosylated (glyc.) PAR_1 has a molecular weight of about 66 kDa. Note that ATAP2 seemed to recognize less PAR_1 at 47 kDa than WEDE15, while WEDE15 detected less glyc. PAR_1 at 66 kDa than ATAP2 (negative images shown), both in relation to respective co-appearing bands.

The distribution of PAR_1 on AT-MSC plasma membranes was visualized on freeze-fracture replicas of AT-MSCs. This technique provides cross sections of frozen cells, which primarily fracture between bilipid membranes. Replicas of the protoplasmic and exoplasmic facing membrane structures are recreated to strengthen the biologic material for cell structure visualization. Membrane proteins may then be detected by the application of primary antibodies and gold particle-labeled secondary antibodies. The gold particles cause black dots on electron microscopic images of the replicas (detailed information in paragraph 2.2.3, page 22).

We applied the PAR_1-specific antibody WEDE15 on AT-MSC freeze-fracture replicas. As presented in Figure 3-9, multiple black dots were found on the exoplasmic fracture face of AT-MSC replicas, which were treated with WEDE15 and a gold-labeled secondary antibody (A), while no black dots were found on negative control replicas, which were treated with the same secondary antibody, but without WEDE15 (B). Therefore, the black dots represented the distribution of presumed PAR_1 on the plasma membrane of AT-MSCs. Note that single as well as closely co-localized dots were found on the images.

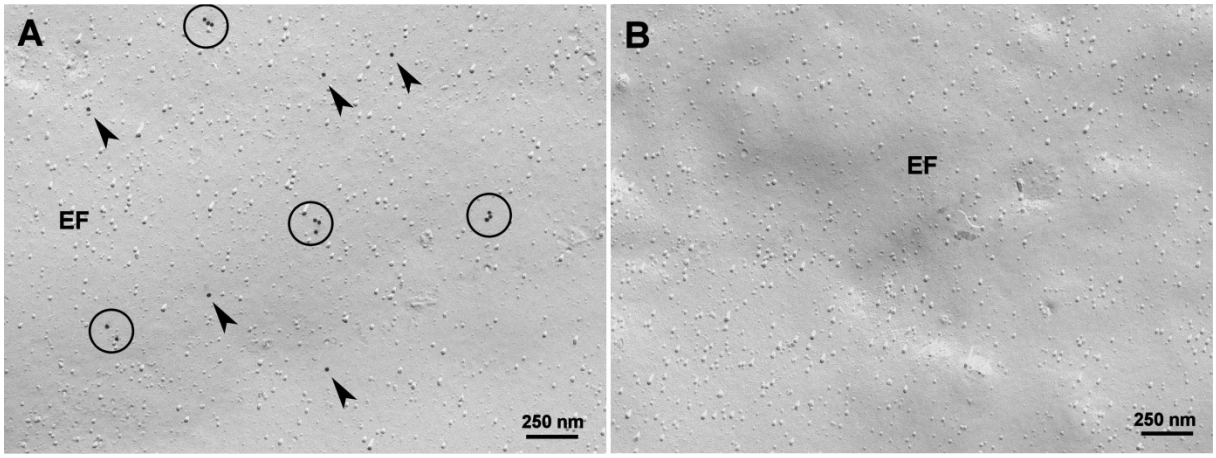

Figure 3-9: PAR_1-immunolabeled freeze-fracture replica of the exoplasmic fracture face (EF) of AT-MSCs

Localization of PAR_1 on AT-MSCs (donor #7) was visualized by electron microscopic images of freeze-fracture replicas on the exoplasmic fracture face (EF). Replicas were treated with the PAR_1-specific antibody WEDE15 (Beckman Coulter) and a gold-labeled secondary antibody, which were detected as black dots on the images. Intramembrane proteins are visible as small particulate structures. Shown are representative images of one assay. (A) PAR_1 was labeled on the AT-MSC plasma membrane as single particles (arrows) and clusters (circles). (B) Negative Control. Representative image of replicas treated without primary antibody WEDE15.

3.2 PAR_1 signaling in MSCs – AT-MSCs show high basal ERK phosphorylation

PAR_1 was detected on the plasma membrane of AT-MSCs. Moreover, it was found to be presumably the major expressed PAR family member that will respond to activation in AT-MSCs. In order to unravel PAR_1 downstream effectors and possible signaling pathways, we conducted immunoblot assays and focused on the extracellular-signal-regulated kinase (ERK) due to strong initial signals.

The mitogen-activated protein kinase (MAPK) pathway was addressed by the analysis of the ERK phosphorylation status in immunoblot-based assays with stimulation by thrombin or PAR_1-AP of starved AT-MSCs. Though multiple experiments were carried out with two batches of AT-MSCs (donors #1 and 6) with attempts to optimize conditions for stimulation, including time, concentration, HEPES-buffering of medium and the use of heated plates during stimulation, no consistent pattern and correlation of the strong ERK signal with the stimulation could be obtained. The immunoblots in Figure 3-10 display representative results of different experiments for the ERK phosphorylation status in AT-MSCs from donor #6.

Though a strong ERK phosphorylation in cells stimulated with thrombin or PAR_1-AP was observed in frequent cases, negative controls frequently presented the same amount of ERK phosphorylation. This raised the question if the examined AT-MSCs possessed a high basal ERK phosphorylation or if they were particularly sensitive to stimuli from the outside, which might have caused the observed inconsistency.

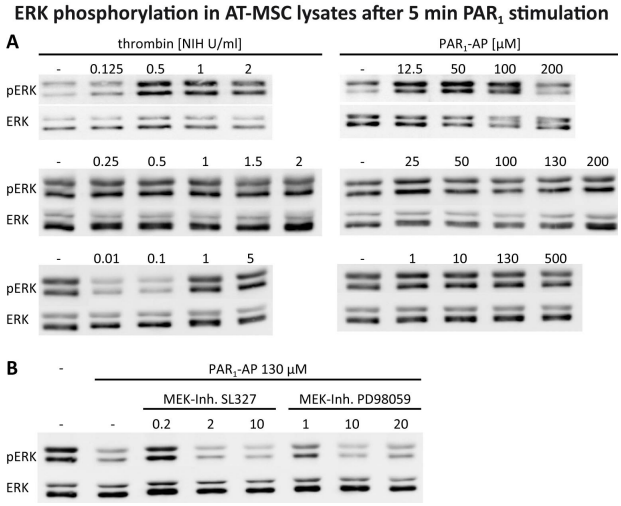

Figure 3-10: AT-MSCs show inconsistent ERK phosphorylation upon PAR_1 stimulation, probably due to high basal pERK levels

The immunoblots (negative images shown) depict ERK-immunoblots of AT-MSC lysates from three representative assays (A) or one assay (B), respectively. AT-MSCs (donor #6) were seeded into 6-well plates, grown to approx. 70 % confluence, starved for 24 h, and stimulated with several concentrations of thrombin and PAR_1-AP. Inhibitors were incubated for 1 h prior to stimulation. 20 µg of AT-MSC protein lysates were separated by SDS-PAGE and blotted onto protein-binding PVDF membranes. ERK and pERK were detected with specific primary antibodies, horseradish peroxidase (HRP)-labeled secondary antibodies and a chemiluminescent detection technique.

No clear correlation between stimulation with several concentrations of thrombin and PAR_1-AP, and the level of ERK phosphorylation was observed. Note that untreated controls vary between a low and high phosphorylation status of ERK. Hence, making it unclear whether the PAR_1 stimulation caused the observed pERK levels in stimulated samples (A+B). The pre-treatment with two different agents to inhibit upstream-located MEK decreased pERK levels in presence of PAR_1-AP. Therefore, the influence of PAR_1-AP did not seem to purposely affect pERK levels.

In another approach, the AT-MSCs were pre-incubated with two different inhibitors of the upstream-located MAPK/ERK kinase (MEK). As seen in Figure 3-10 B, the MEK-inhibitors were able to attenuate the pERK level in comparison to unstimulated control, even though PAR_1-AP was present. At the same time, the pERK level in the PAR_1-AP stimulated positive control was relatively low and with the lowest concentration of the inhibitors even somewhat higher.

Taken together, the AT-MSCs may possess elevated pERK levels in general, with seemingly unstable consistency. Although the involvement of the MAPK signaling in mediating the biologic effects of PAR_1 activation seems likely, we could not conclusively resolve the effect of PAR_1 stimulation on ERK activation.

3.3 Biological effects of PAR_1 activation on AT-MSCs

The general ability of PAR_1 to activate multiple intracellular effectors and influence other pathways via cross-activation of other signaling pathways may have a significant influence on MSC growth and migration. In addition, PAR_1 signaling comprises actin rearrangements via coupling to $G\alpha_{12/13}$, which

might directly affect the MSCs' ability to migrate (Ramachandran et al. 2012; Siehler 2009). Therefore, we investigated the impact of PAR_1 stimulation on MSC proliferation and migration.

3.3.1 PAR_1 mediates reduced migration of AT-MSCs

MSCs have been shown to exert impressive capacities of migrating to tumors and other inflamed tissues (Bayo et al. 2013). Those pathologic microenvironments are enriched with thrombin and other PAR-activating proteinases (ten Cate & Falanga 2008). Therefore, it was of great interest to assess the migration of MSCs under the presence of PAR_1-activating thrombin and PAR_1-AP.

The migration assays were carried out in a Neuroprobe chemotaxis system. 2,000 starved AT-MSCs were seeded into small wells that were separated from the bottom wells by a collagen-coated polycarbonate membrane with 8 µm-sized pores. The bottom wells contained culture medium with fetal calf serum (FCS), thrombin or PAR_1-AP. As seen in Figure 3-11 A, about one-fourth of initially seeded cells were migrating across the membrane in control culture medium. FCS enhanced the number of migrated cells by a large amount and reached the limit of proper single cell counting. In the presence of thrombin and PAR_1-AP, the number of migrated cells decreased. However, the number of migrating cells differed between each assay. Hence, data were plotted again with every single assay with respect to control (Figure 3-11 B) and showed a significant reduction of the relative migration rates of thrombin and PAR_1-AP stimulated AT-MSCs of approx. 20-40 %.

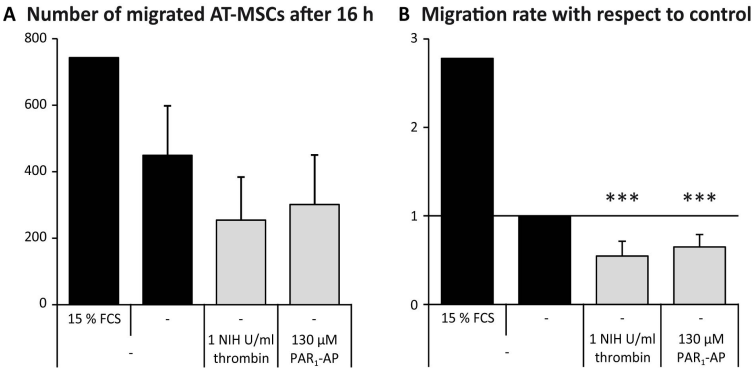

Figure 3-11: Stimulation of PAR_1 reduces the migration rate of AT-MSCs

The migration assay was carried out in a Neuroprobe 48-well micro chemotaxis chamber using collagen-coated polycarbonate membranes with 8 µM-sized pores. 2,000 starved AT-MSCs (donor #6) were seeded into each well. After 16 h of migration in EM6F medium, non-migrated cells were wiped off the membrane and remaining cells were stained with crystal violet and counted. Bars show mean values ± SD of five separate assays.

The presence of thrombin or PAR_1-AP significantly reduced the rate of migration of AT-MSCs. Positive control with FCS was carried out only once due to massive migration compared to control without FCS. (A) Absolute number of migrated cells; (B) combined single assays relative to their respective control. ***p-value ≤ 0.001 versus untreated control.

3.3.2 PAR_1 mediates no significant enhancement of AT-MSCs' proliferation

The analysis of MSC proliferation was approached with viability assays in 96-well microtiter plates. Viable cells are able to convert the non-fluorescent substrate resazurin into the fluorescent dye resorufin, which can be detected by plate readers. The higher the fluorescence, the more cells are present per well, which can be interpreted as presumed higher rate of proliferation.

PAR_1's impact on the AT-MSCs' proliferation was approached with multiple different experimental setups. Figure 3-12 displays a representative assay with a time- and FCS-dependent assessment of AT-MSCs' proliferation rate in the presence of thrombin or PAR_1-AP.

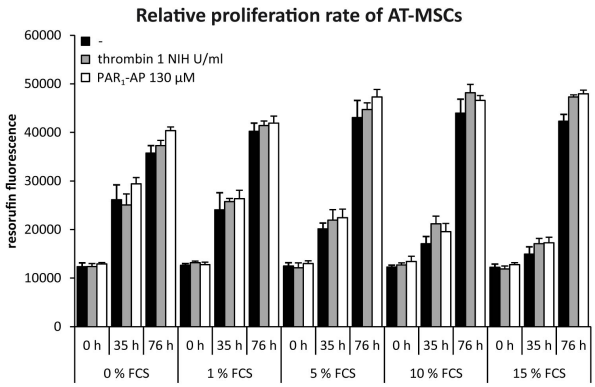

Figure 3-12: PAR_1 stimulation has no significant effect on AT-MSC proliferation

1,500 AT-MSCs (donor #6) were seeded into 96-well plates, leaving them 24 h to attach, followed by starvation in DMEM for 24 h. The medium was replaced with EM6F containing PAR_1 agonists and various FCS concentrations. After 0, 35 and 76 h, the cell viability was measured by applying the Promega CellTiter-Blue® Cell Viability Assay. Viable cells convert the dye resazurin into fluorescent resorufin and thereby giving feedback on cell proliferation. The graph shows data of one experiment with mean values ± SD of technical quadruplicates. This experiment was representative for five in total.

Stimulation of AT-MSCs with thrombin or PAR_1-AP over up to 76 h, along with the presence of increasing concentrations of FCS, showed no significant enhancement of AT-MSC proliferation at any given conditions.

Three 96-well microtiter plates were initially seeded with equal amounts of AT-MSCs and were incubated for up to 76 h post-stimulation. As seen in the figure, a similar resorufin fluorescence was recorded for all wells of the first plate measured at 0 h, representing that the AT-MSCs were seeded uniformly over the whole plate. The second plate, which was analyzed 35 h post-stimulation, showed approximately twice as much fluorescence as at 0 h for cells without FCS. This amount seemed to reduce in a concentration-dependent manner with increasing concentrations of FCS. AT-MSCs growing in the presence of 15 % FCS showed a minor increase in fluorescence, compared to respective wells on the '0 h plate'. The third plate, which was analyzed 76 h post-stimulation, showed a minor increase in fluorescence for cells without FCS and an apparently concentration-dependent major increase in fluorescence for AT-MSCs in the presence of increasing concentrations of FCS, compared to respective wells on the '35 h plate'. Overall, there was no or only a minor impact of thrombin or PAR_1-AP on the fluorescence, especially with 15 % FCS after 76 h. Otherwise, the standard deviations of the PAR_1-stimulation quadruplicates were greater than the difference of the enhanced fluorescence in respect to controls. The other experiments (not shown) included thrombin concentrations up to 5 NIH U/ml and PAR_1-AP concentrations up to 500 µM, but with no significant enhancement of the AT-MSCs' proliferation.

3.4 Protein secretion activity of AT-MSCs and impact of PAR_1

Current trends in medical therapy deem MSCs as potential mediators to cure chronic wounds, by the limitation of inflammation and the promotion of regeneration and self-renewal. While differentiation and incorporation into diseased tissue provides one aspect of their potential, the literature stresses their paracrine activity by secreting a plethora of immunomodulatory proteins and growth factors. This cocktail of active paracrine agents might have unforeseeable effects on especially cancerous diseases.

Since the literature is pointing out a tumor-inhibiting as well as a tumor-promoting impact of MSCs, the assessment of their influence on the designated disease, tissue entity and involved cell types becomes an essential key component of basic research, in order to understand and limit potential side effects. (Maxson et al. 2012; Zhang & Wang 2013).

Therefore, the following sections were dedicated to identifying the secreted proteins of the applied AT-MSCs with proteome arrays. Furthermore, if MSCs would be inoculated into diseased tissues, they would presumably encounter several potential PAR_1-activating proteinases. Hence, in the subsequent step, our goal was to verify the proteins that were influenced by PAR_1 activation as detected by the array analyses, via enzyme-linked immunosorbent assays (ELISAs) and mRNA expression analyses.

3.4.1 General overview of proteins secreted by AT-MSCs

The analysis of proteins that were secreted by AT-MSCs was carried out by conditioning basic culture medium by starved AT-MSCs for 24 h. The conditioned medium was then employed in three different proteome arrays, which comprised the detection of sets of cytokines, proteinases and angiogenesis-related proteins. This profiling approach delivered a broad overview of proteins that were secreted by AT-MSCs under serum-free standard growth conditions over 24 h. The arrays consisted of specific protein-capturing antibodies that were spotted in duplicates on membranes. The capture antibody-protein complex was in turn recognized by HRP-labeled detection antibodies. The final signal was quantified and ranked according to their signal intensity with respect to positive controls. Although the signal intensity is dependent on the quality of each single antibody population, the results were also grouped into strong (+++), medium (++), few (+) and weak (o) secretion, which covered signals that were distinct from insignificant/background levels (-).

Two separate batches of conditioned medium from AT-MSCs (donor #7) were analyzed. One was employed on the angiogenesis-related proteins array, the other batch on the proteinases and cytokines arrays. The total results are presented in Table 3-1, and prominent secreted proteins are shown in Figure 3-13. Altogether, the arrays are capable of analyzing more than 160 proteins and approx. one-third of them were secreted by AT-MSCs in noteworthy amounts of more than 5 % of the mean positive controls. In general, a variety of extracellular matrix-related proteins (tissue inhibitor of matrix metalloproteinases (TIMPs), thrombospondin 1 (TSP-1), Serpin E1) and proteinases (matrix metalloproteinases (MMPs), cathepsins) were secreted along with a set of growth factors (angiogenin (Ang), angiopoietins (Ang-1), hepatocyte growth factor (HGF)) and immunoregulatory proteins (pentraxin 3, interleukin 8 (IL-8), IL-6, monocyte chemotactic protein (MCP-1)).

Table 3-1: Proteins secreted by AT-MSCs into supernatant growth medium over 24 h

Angiogenesis-related proteins (Proteome Profiler™ Human Angiogenesis Array)	
+++	IGFBP-3, Pentraxin 3, Serpin E1, TIMP-1, TSP-1
++	Serpin F1
+	Activin A, Angiogenin, Angiopoietin-1, Angiopoietin-2, EG-VEGF, Endostatin/Collagen XVIII, Endothelin-1, IGFBP-1, MMP-9, Platelet factor 4 (PF4), TIMP-4, uPA, VEGF
o	ADAMTS-1, Angiostatin/Plasminogen, Artemin, Coagulation Factor III, CXCL16, Endoglin, FGF acidic, FGF basic, FGF-7, GM-CSF, HB-EGF, HGF, IGFBP-2, IL-8, LAP (TGF-beta1), MCP-1, MIP-1alpha, MMP-8, NRG1-beta1, PD-ECGF, PDGF-AA, Persephin, PIGF, Prolactin, Serpin B5, TSP-2
-	Amphiregulin, DPPIV, EGF, FGF-4, GDNF, IL-1beta, Leptin, PDGF-bb, Vasohibin, VEGF-C
Proteinases (Proteome Profiler™ Human Protease Array Kit)	
+++	-
++	Cathepsin B, Cathepsin X/Z/P, MMP-1, MMP-2, MMP-3
+	ADAMTS1, Cathepsin A, Cathepsin C, Cathepsin D, Cathepsin V, DPPIV/CD26, MMP-13, Proprotein, Convertase 9
o	ADAMTS13, Cathepsin L, Cathepsin S, Kallikrein 3/PSA, Kallikrein 7, Kallikrein 10, Kallikrein 13, MMP-7, MMP-8, MMP-9, Neprilysin/CD10, Presenilin-1, uPA/Urokinase
-	ADAM8, ADAM9, Cathepsin E, Kallikrein 5, Kallikrein 6, Kallikrein 11, MMP-12, Proteinase 3
Cytokines (Proteome Profiler™ Human XL Cytokine Array Kit)	
+++	Serpin E1
++	Chitinase 3-like 1, DKK-1, ENA-78, MCP-1, Pentraxin-3
+	Angiogenin, Angiopoietin-1, Complement Factor D, EMMPRIN, Endoglin, FGF-19, GDF-15, HGF, IGFBP-3, IL-11, IL17A, IL-6, IL-8, MIF, Osteopontin, SDF-1alpha, TSP-1, uPAR, VEGF
o	Adiponectin, Aggrecan, Angiopoietin-2, BDNF, CD14, CD30, CD40 Ligand, C-reactive Protein, Cystatin C, EGF, FGF basic, FGF-7, Flt-3 Ligand, GM-CSF, GRO-alpha, ICAM-1, IFN-gamma, IL-1alpha, IL-1beta, IL-2, IL-3, IL-10, IL-12 p70, IL-22, IL-24, IL-27, IL-32alpha/beta/gamma, I-TAC, Kallikrein 3, Lipocalin-2, M-CSF, MMP-9, Myeloperoxidase, PDGF-AA, RANTES, RBP4, Relaxin-2, Resistin, SHBG, TARC, TFF3, Vitamin D BP
-	BAFF, C5/C5a, Cripto-1, DPPIV, FAS Ligand, G-CSF, GH, IGFBP-2, IL-1ra, IL-4, IL-5, IL-13, IL-15, IL-16, IL-18 Bpa, IL-19, IL-23, IL-31, IL-33, IL-34, IP-10, Leptin, LIF, MCP-3, MIG, MIP 1alpha/MIP-1beta, MIP-3alpha, MIP-3beta, PDGF-AB/BB, PF4, RAGE, ST2, TfR, TGF-alpha, TNF-alpha

"+++" > 75 % of positive control (PC); "++" 25-75 % of PC; "+" 5-25 % of PC; "o" 2-5 % of PC; "-" < 2 % of PC/background

Due to the large number of identified proteins, only a few were investigated more thoroughly in further experiments.

3.4.2 PAR_1 activation affects protein secretion by AT-MSCs

We detected a plethora of different cytokines, chemokines, proteinases and other proteins in the supernatant of conditioned growth medium of AT-MSCs (Table 3-1, Figure 3-13). For the purpose of identifying the secreted proteins that might be affected by stimulation of PAR_1, we additionally characterized conditioned growth medium of thrombin- or PAR_1-AP-stimulated AT-MSCs. As presented in Figure 3-14, the arrays showed duplicates of signals for detected protein targets (Figure 3-14, A), which were quantified and assessed for the impact of PAR_1 stimulation (Figure 3-14 B). We focused our efforts on the proteins that were described in the literature to exert crucial impacts on angiogenesis, proliferation and immunoregulation, and might, therefore, be of paramount clinical relevance of the MSC-mediated treatment of HCC.

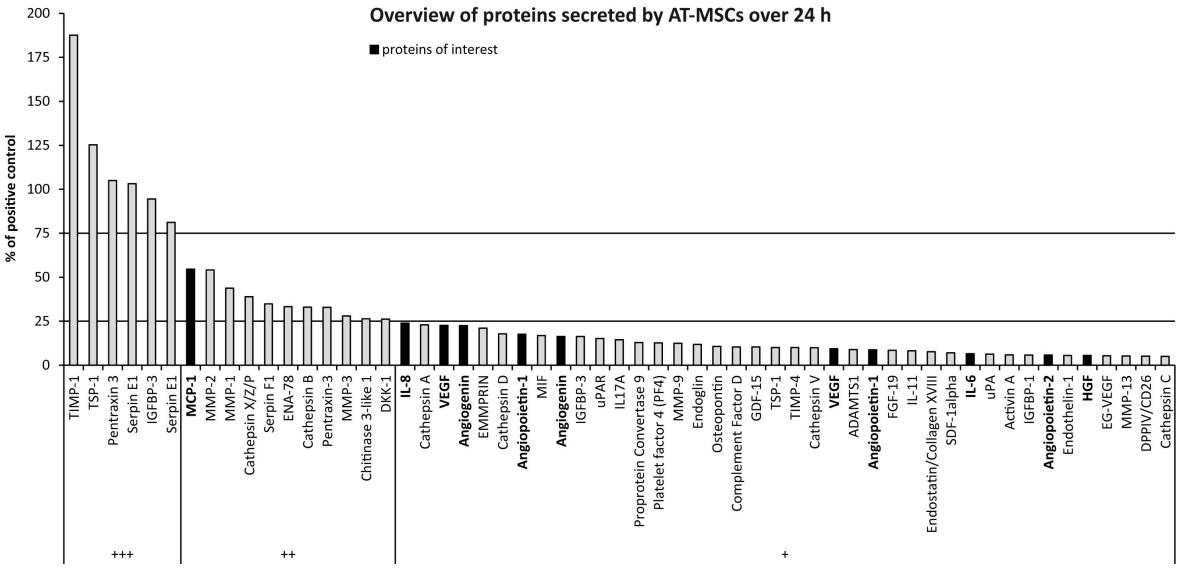

Figure 3-13: AT-MSCs secrete various proteins with potential effects on tumor microenvironments

AT-MSCs (donor #6) were seeded into 6-well plates, grown to a confluence of approx. 50 %, starved for 24 h, and fresh FCS-free medium was conditioned for the following 24 h. The medium was applied on Proteome Profiler™ Arrays for the analysis of angiogenesis-related proteins, proteases and cytokines. The duplicate spots for each detection of the immunoblot-based arrays were quantified, and the obtained mean pixel densities were plotted with respect to positive controls in order of decreasing intensity. Some proteins were present on two of the three arrays, but were listed separately. The chart displays the major secreted proteins detected in two separate conditioned medium preparations from one donor. The results were grouped according to the signal intensity with respect to positive control (PC): "+++" more than 75 % of PC; "++" 25 till 75 % of PC; "+" 5 till 25 % of PC; proteins with lower secretion not shown. Highlighted in black bars are proteins of further interest, which are potential tumor promoters and partially showed influences by PAR_1 stimulation (shown in Figure 3-14).

The analyzed AT-MSCs secreted a variety of extracellular matrix proteins, proteases, growth factors and immunoregulatory proteins, in general, a set of proteins that can potentially promote tumor environments by enhanced angiogenesis and growth. Among the proteins that were present on two of the three arrays (e.g. serpin E1, VEGF, angiogenin), quantitative rather than qualitative differences were observed between the two batches of conditioned medium from one donor.

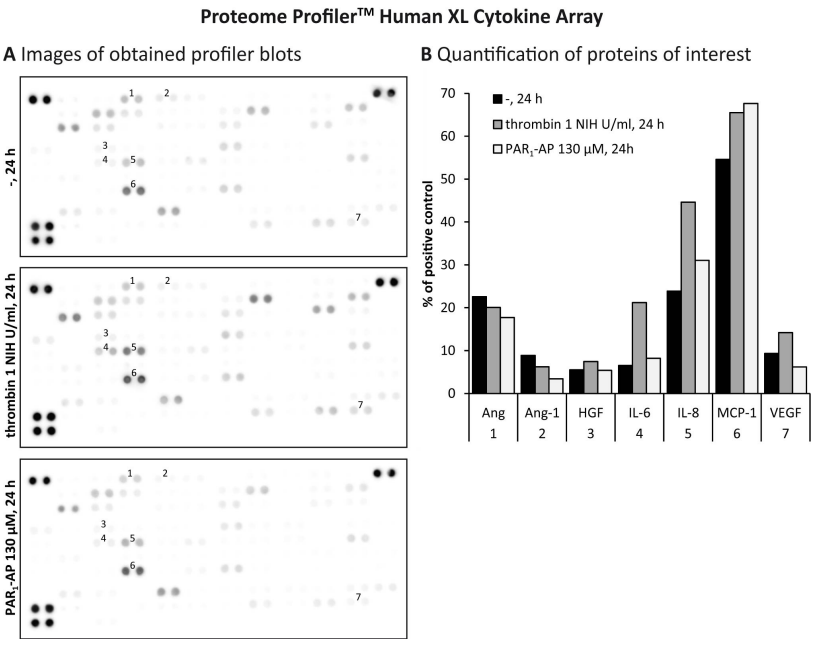

Figure 3-14: Overview of cytokines and growth factors secreted by AT-MSCs under the influence of PAR_1 activation over 24 h

AT-MSCs were seeded (donor #6) into 6-well plates, grown to a confluence of approx. 50 %, starved for 24 h, and fresh FCS-free medium was conditioned over the following 24 h. The medium was applied on a Proteome Profiler™ Human XL Cytokine Array. The immunoblot-based array (A, negative images shown) was quantified, and obtained pixel densities were plotted in respect to positive controls (B). The chart displays one assay with mean values of technical duplicates from selected proteins (1-7) in conditioned medium from AT-MSCs of one donor.

The AT-MSCs secreted a variety of cytokines that showed influences by the presence of thrombin and PAR_1-AP. We focused on the ones with potential tumor-promoting features. Especially, the secretion of IL-6, IL-8 and MCP-1 seemed to be influenced by PAR_1-stimulation.

Among those presented proteins in Figure 3-14, the spots for the detection of IL-6, IL-8 and MCP-1 caused stronger signals when incubated with supernatants from PAR_1-stimulated AT-MSCs than with conditioned medium from untreated AT-MSCs. Therefore, the impact of PAR_1 on the secretion of these cytokines by AT-MSCs was further verified by qPCRs and ELISAs.

3.4.3 PAR_1 mediates increase in IL-8, IL-6 and MCP-1 expression in AT-MSCs

The activation of PAR_1 in AT-MSCs indicated the enhancement of the basal secretion of IL-6, IL-8 and MCP-1 (Figure 3-14). These events might be due to the upregulation of the expression of their respective mRNAs. Therefore, we performed mRNA expression analyses of IL-6, IL-8 and MCP-1 mRNA in AT-MSCs, which were treated with increasing concentrations of thrombin and PAR_1-AP for 24 h. Furthermore, we assessed the impact of the PAR_1 antagonist Atopaxar on their mRNA expression. The cells were pre-incubated with Atopaxar for 40 min, and it was present throughout the 24 h of stimulation. The results are presented in Figure 3-15.

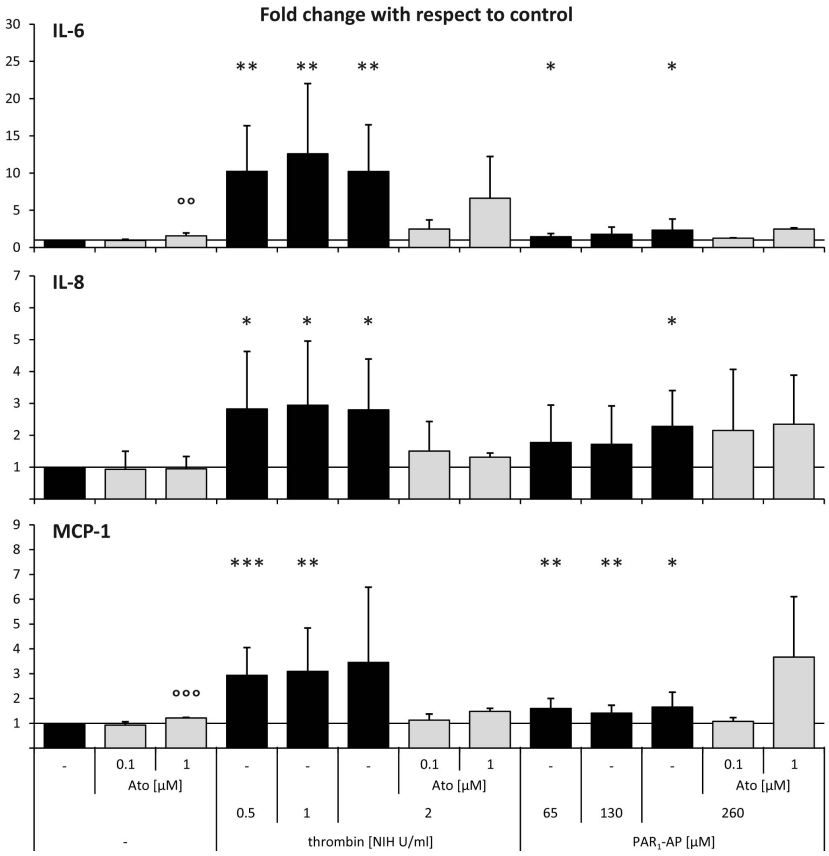

Figure 3-15: Effect of 24 h PAR_1 activation on the fold change of IL-6, IL-8 and MCP-1 mRNA expression in AT-MSCs

AT-MSCs (donors #3 and 7) were stimulated with thrombin and PAR_1-AP for 24 h, followed by qPCR of IL-6, IL-8 and MCP-1 mRNA. Bars depict mean values ± SD of technical qPCR triplicates from two to seven separate experiments.

Stimulation of PAR_1 with thrombin or PAR_1-AP in AT-MSCs caused a significant upregulation of IL-6, IL-8 and MCP-1 gene expression. Pre-treatment with the PAR_1 antagonist Atopaxar seemed to prevent the observed mRNA upregulation in frequent cases, especially for 0.1 µM Atopaxar. ***/°°°p-value ≤ 0.001, **/°°p-value ≤ 0.01, *p-value ≤ 0.05 versus untreated control (stars) or respective samples without antagonist (circles).

The treatment with thrombin caused a significant upregulation of IL-6, IL-8 and MCP-1 mRNA, with no apparent dose-dependence for the used concentration range. IL-6 mRNA expression was enhanced up to 20-fold, IL-8 mRNA up to five-fold, and MCP-1 mRNA up to seven-fold. No increase in expression by treatment with 2 NIH U/ml thrombin was observed with prior Atopaxar incubation.

In some cases, PAR_1-AP stimulated a significant two- to threefold increase in the IL-6, IL-8 and MCP-1 mRNA expression. No increase in expression was observed for MCP-1 and IL-6 mRNA for the stimulation with 260 µM PAR_1-AP and prior treatment of 0.1 µM Atopaxar. However, in the cases of pre-treatment with 0.1 µM Atopaxar for IL-8, and pre-treatment with 1 µM Atopaxar for MCP-1 and IL-8, a mean upregulation of mRNA expression was observed. This might hint at off-target effects at

higher Atopaxar concentrations. Since 0.1 µM Atopaxar was consistently abrogating the effect of both PAR_1 agonists, this concentration was used for further analyses.

3.4.4 AT-MSCs secrete IL-6 and IL-8

Given the stimulation of mRNA expression of IL-6, IL-8 and MCP-1 by PAR_1 stimulation in AT-MSCs (Figure 3-15), it appeared plausible that this should also lead to enhanced protein synthesis, and thus the secretion of these cytokines into the surrounding culture medium. This was already indicated by the preliminary analysis with the proteome arrays (Figure 3-14). Therefore, we followed up the analysis using commercially available ELISA systems that allow a multitude of assays at a reasonable price. Such ELISA systems were only readily available for IL-6 and IL-8, and therefore, the analyses were limited to these cytokines.

The AT-MSCs for the following assays were cultured in 6-well plates, starved for 24 h, and conditioned in the presence of thrombin or PAR_1-AP over the following 24 h. Inhibitors and antagonists were pre-incubated prior to conditioning.

3.4.4.1 AT-MSCs secrete IL-6 and IL-8 in larger amounts than Hep3B cells

In order to grasp the basal amount of secreted IL-6 and IL-8 by AT-MSCs, we examined the secretion of these cytokines via specific ELISA arrays and referred them to the amount of total cell protein that was present during the time of secretion.

The AT-MSCs of two analyzed donors secreted approx. 1.5 pg IL-6/µg protein, and 2 pg IL-8/µg protein over 24 h (Figure 3-16). Since MSCs are under investigation for targeted cellular therapy of various diseases including malformations of the liver, cells from the HCC cell line Hep3B served as a reference in order to comprehend the secreted amounts of IL-6 and IL-8. As further seen in Figure 3-16, the Hep3B cells hardly secreted any IL-6 and approx. only one-third of the amount of IL-8 as the AT-MSCs. As a consequence, MSCs would presumably contribute larger amounts of IL-6 and IL-8 to an HCC microenvironment than Hep3B cells themselves.

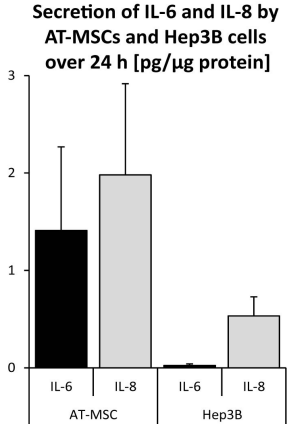

Figure 3-16: Absolute secretion of IL-6 and IL-8 by AT-MSC and Hep3B cells over 24 h

AT-MSCs (donors #6 and 8) and Hep3B cells were cultured in 6-well plates and grown up to approx. 50 % confluence, followed by 24 h starvation. Medium was replaced with fresh, FCS-free culture medium and left on the cells for 24 h. The concentrations of IL-6 and IL-8 in the supernatant were analyzed by specific ELISAs and the cell protein concentrations of respective wells were determined. Bars depict mean values ± SD of technical duplicates from two to four separate experiments, showing absolute secretion of IL-6 and IL-8 per amount of total cell protein.

AT-MSCs secreted larger amounts of IL-6 and IL-8, compared to Hep3B cells.

3.4.4.2 PAR_1 mediates increase in IL-6 and IL-8 secretion by AT-MSCs

Our experiments showed that PAR_1 activation led to an increase in mRNA expression of IL-6 and IL-8 in AT-MSCs (Figure 3-15). Furthermore, we showed that AT-MSCs actually secreted those cytokines and that PAR_1 stimulation in AT-MSCs possibly affected their secretion (Figure 3-14 and Figure 3-16). Building up on these data, we performed further assays to verify the initial secretion data.

The AT-MSCs were cultured in the presence of increasing concentrations of thrombin and PAR_1-AP. In addition, we included increasing concentrations of the PAR_1 antagonist Atopaxar. Initial data was collected for IL-6 only since PAR_1 stimulation in AT-MSCs led to a strong upregulation of its mRNA up to 25-fold. Hence, we assumed a stronger impact of PAR_1-stimulation on IL-6 secretion than on IL-8, thereby making it presumably a better system to assess agonists and antagonist concentrations in initial experiments. As seen in Figure 3-17, thrombin and PAR_1-AP enhanced the secretion of IL-6 in a concentration-dependent manner, while pre-treatment with Atopaxar seemed to hamper this effect in frequent cases. Considering the results of Figure 3-15 and Figure 3-17 together, a thrombin activity of 1 NIH U/ml and a PAR_1-AP concentration of 260 µM were assumed most effective for these experiments and were applied in further assays. Additionally, 0.01 µM Atopaxar seemed to antagonize the PAR_1-mediated increase in IL-6 secretion sufficiently. 1 µM Atopaxar exerted adverse effects in more frequent cases in the assays.

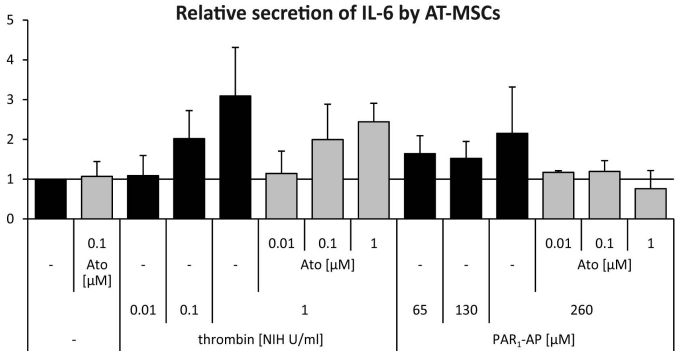

Figure 3-17: Influence of Atopaxar on the relative secretion of IL-6 by AT-MSCs upon PAR_1 activation

AT-MSCs (donors #3, 6 and 8) were cultured in 6-well plates and grown up to approx. 50 % confluence, followed by 24 h starvation. Medium was replaced with fresh EM6F and left on the cells for 24 h. 40 min of incubation with several concentrations of Atopaxar (Ato) were carried out prior to stimulation with different concentrations of thrombin and PAR_1-AP. IL-6 content of supernatant was measured with specific ELISAs and plotted in relation to control samples of each experiment. Bars depict mean values ± SD of technical duplicates from two to five separate experiments.

Stimulation of AT-MSCs with thrombin and PAR_1-AP caused increased concentrations of secreted IL-6 in AT-MSC supernatants (black bars). Pre-treatment with PAR_1 antagonist Atopaxar seemed to prevent observed enhanced secretion in frequent cases (gray bars).

The stimulation of PAR_1 with thrombin or PAR_1-AP in AT-MSCs was shown to stimulate mRNA expression and secretion of IL-6 and IL-8 (Figure 3-15, Figure 3-17). Moreover, these agonists triggered a PAR_1-mediated increase in $[Ca^{2+}]_i$ (Figure 3-3, Figure 3-4). In order to assess the importance of the PAR_1-stimulated Ca^{2+} pathway on the cytokine secretion by AT-MSCs, we treated the cells with the PAR_1 antagonist Atopaxar and the Ca^{2+} chelator BAPTA-AM prior to conditioning of the culture medium, which have been shown to attenuate PAR_1-triggered Ca^{2+} release in AT-MSCs in our Ca^{2+}

assays (Figure 3-5, Figure 3-6). Moreover, Ca^{2+} affects the central Ca^{2+}-dependent downstream effector protein kinase C (PKC), which is involved in the regulation of expression and secretion (Hilfiker & Augustine 1999; Kang 2014). PKC was inhibited by prior treatment with BIM-1. The results are presented in Figure 3-18.

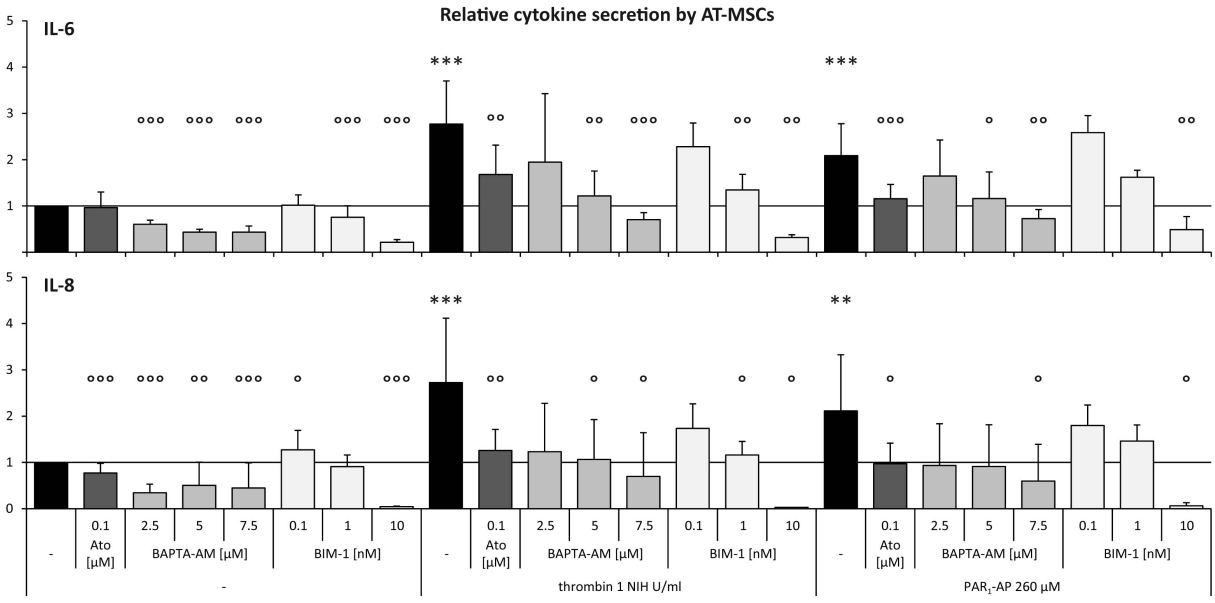

Figure 3-18: Influence of Atopaxar, BAPTA-AM and BIM-1 on the relative secretion of IL-6 or IL-8 by AT-MSCs upon PAR_1 activation

AT-MSCs (donors #3, 6 and 8) were cultured in 6-well plates and grown up to approx. 50 % confluence, followed by starvation for 24 h. Subsequently, the culture medium was replaced with fresh EM6F. Prior to stimulation with thrombin or PAR_1-AP, 40 min of incubation with Atopaxar (Ato) and several concentrations of BAPTA-AM and BIM-1 were carried out. The conditioned medium was collected after 24 h. The IL-6 and IL-8 content of the supernatant were measured with specific ELISAs. Bars depict mean values ± SD of technical duplicates of two to eleven assays in relation to unstimulated control of respective assays. ***/°°°p-value ≤ 0.001, °°p-value ≤ 0.01, °p-value ≤ 0.05 versus untreated control (stars) or respective stimulations without antagonist (circles).

Stimulation of AT-MSCs with thrombin and PAR_1-AP caused a significant enhancement of IL-6 and IL-8 concentrations in AT-MSC supernatants versus unstimulated control (black bars). Pre-treatment with PAR_1 antagonist Atopaxar, Ca^{2+} chelator BAPTA-AM and PKC inhibitor BIM-1 attenuated the observed enhanced secretion in a concentration-dependent manner.

The stimulation of AT-MSCs with thrombin or PAR_1-AP led to a significant enhancement of IL-6 secretion by up to 1.5- till 3.5-fold. While the PAR_1 antagonist Atopaxar showed no effect on basal secretion rate, it significantly attenuated the stimulation by both activating agents.

The Ca^{2+}-chelating agent BAPTA-AM and the PKC inhibitor BIM-1 reduced basal IL-6 secretion as well as the elevated IL-6 secretion in response to the PAR_1 agonists in a concentration-dependent manner. The secretion pattern of IL-8 was found to be quite similar to the one of IL-6. While thrombin and PAR_1-AP generated an up to a four-fold enhancement of IL-8 secretion compared to basal levels, this effect was completely abolished by Atopaxar. BAPTA-AM as well as BIM-1 caused a concentration-dependent attenuation of PAR_1-stimulated secretion of IL-8.

Although the impact of PAR_1-stimulation on the mRNA expression of IL-6 and IL-8 in AT-MSCs was already assessed in paragraph 3.4.3 (page 56), we conducted further expression analyses to correlate

directly the secretion data shown in Figure 3-18 with the expression of the respective cytokines in AT-MSCs. Figure 3-19 shows the mRNA expression analyses of samples from the ELISA analyses in Figure 3-18.

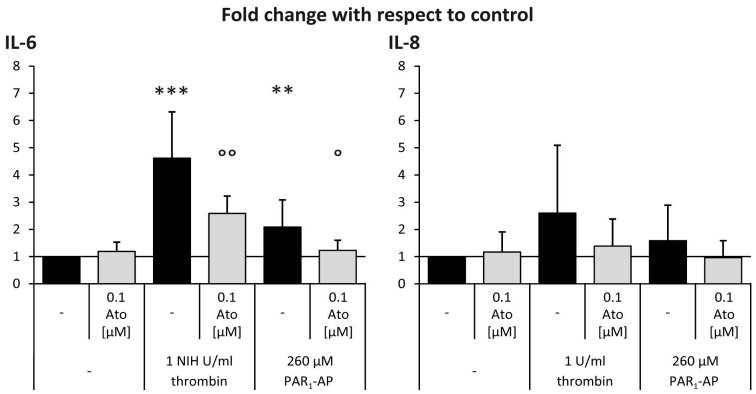

Figure 3-19: Effect of PAR_1 activation on IL-6 and IL-8 mRNA levels in AT-MSCs

The AT-MSCs (donors #6 and 8) from the ELISAs (Figure 3-18) were analyzed for fold changes in IL-6 and IL-8 mRNA expression using qPCR. Bars depict mean values ± SD of technical triplicates of eight assays in relation to unstimulated control of respective assays. ***p-value ≤ 0.001, **/°°p-value ≤ 0.01, °p-value ≤ 0.05 versus untreated control (stars) or respective stimulations without antagonist (circles).

Stimulation with thrombin or PAR_1-AP caused a significantly increased expression of IL-6 mRNA in AT-MSCs, while pre-treatment with Atopaxar attenuated this effect significantly. No significant change was observed for the IL-8 expression. However, the trend was similar to IL-6.

As seen in Figure 3-19, PAR_1 stimulation with thrombin or PAR_1-AP significantly increased the IL-6 mRNA expression, which in turn was significantly attenuated by Atopaxar. However, thrombin exerted an increase in expression of up to six-fold, while PAR_1-AP exerted an increase of up to three-fold only. The data for IL-8 were rather inconsistent and not significant for the analyzed number of samples, but the trend appeared to be similar to IL-6.

3.5 Assessment of the interaction of AT-MSCs and Hep3B cells at *in vivo* conditions and impact of PAR_1

MSCs provide a valuable source for a cell-based therapy of damaged and cirrhosis-affected liver parenchyma. Though MSCs tend to support the curation of liver failure and cirrhotic liver through their paracrine activity, which favors limitation of inflammation and support of self-renewal and proliferation (Zhang & Wang 2013), their impact on cancerous cells remains unclear. Our experiments pointed out a biological relevance of PAR_1 activation for biologic features of AT-MSCs, including the enhanced expression and secretion of regulatory cytokines. This paracrine activity could potentially support tumor progression. Hence, we employed a murine *in vivo* xenotransplantation model in order to assess the impact of AT-MSCs on cells from the HCC cell line Hep3B. Moreover, we generated a PAR_1 knockdown in AT-MSCs to analyze PAR_1's impact on the xenograft tumor growth.

3.5.1 Generation of a PAR_1 gene knockdown in AT-MSCs

For additional assessment of PAR_1's relevance for the biological features of AT-MSCs, we applied shRNA technology to deplete the cells of PAR_1. Since we used primary MSCs, it was an open question

if the required lentiviral delivery of shRNA and selection of depleted cell pools would be possible with the concomitant maintenance of MSC properties.

The knockdown protocol was carried out according to paragraph 2.4.4 (page 33), including the treatment with PAR_1-shRNA mounted lentiviruses and following the selection of successfully transduced AT-MSCs with puromycin over 48 h. Figure 3-20 A shows the effects of five out of nine available PAR_1-shRNA clones provided by Sigma that were tested for their PAR_1 knockdown efficiency in AT-MSCs. Compared to non-target shRNA, clone number 5 (Clone ID: NM_001992.x-2152s1c1) yielded the best knockdown levels, with a remaining PAR_1 expression of 17 %.

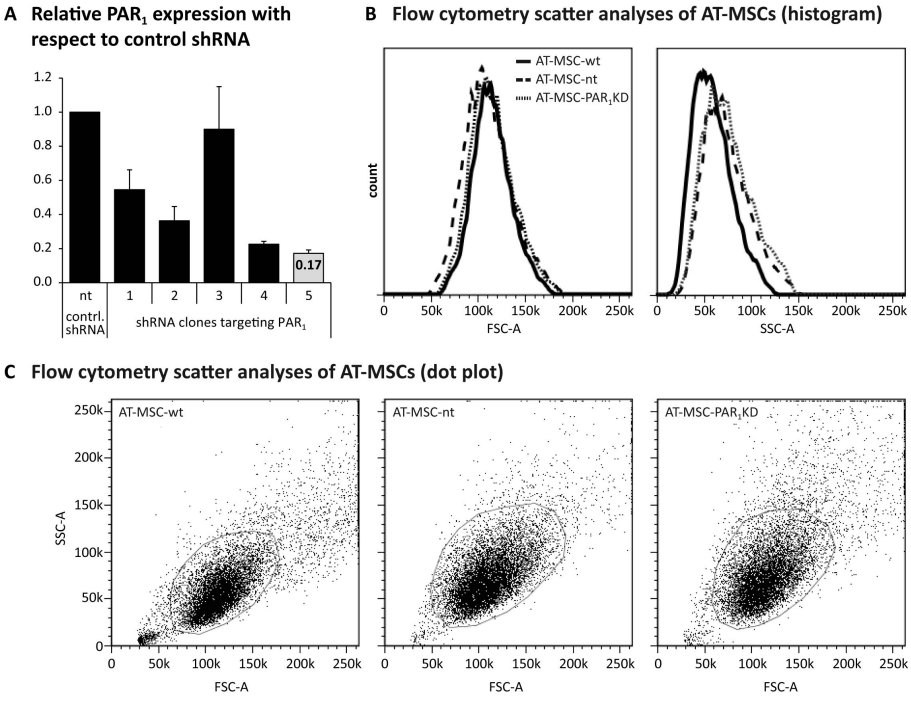

Figure 3-20: mRNA and flow cytometry scatter analyses of genetically modified AT-MSC-nt and AT-MSC-PAR_1KD

A: AT-MSCs were lentivirally transduced with different plasmids containing shRNA to knockdown PAR_1. Remaining PAR_1 levels were quantified with qPCR and compared to AT-MSCs that were transduced with control shRNA (non-target, nt). The bars represent mean values ± SD of technical triplicates from one assay. The knockdown for clone #5 is representative for two separate assays.

The best stable knockdown of PAR_1 in AT-MSCs was achieved with Sigma's PAR_1 shRNA clone number 5 (clone ID: NM_001992.x-2152s1c1).

B: Suspended AT-MSCs were analyzed with flow cytometry to acquire scatter data that correlate with relative-size (forward scatter, FSC) and cell complexity (side scatter, SSC) of the cells. Data for AT-MSC-wild type (wt), AT-MSC-non-target (nt) and AT-MSC-PAR_1knockdown (KD) were plotted as histograms (B) and dot plots (C).

The FSC of AT-MSC-nt and AT-MSC-PAR_1KD did not change during the transduction protocol compared to AT-MSC-wt, thus showing no apparent change in cell volume/size. However, SSC, which hints on granularity, showed increases compared to AT-MSC-wt.

The lentivirus-mediated transduction had no apparent negative effect on the AT-MSCs. Furthermore, approx. 50-80 % of the cells survived the selection with puromycin, thus being successfully transduced. In the following period of culture expansion, the AT-MSC proliferation occurred slower than before the selection process. In addition, the general cell size of adherent AT-MSC-nt and AT-MSC-PAR_1KD was larger than AT-MSC-wt (not shown). Therefore, a proportion of the cells was analyzed with flow

cytometry analyses before they were employed for the *in vivo* xenotransplantation studies (paragraph 3.5.2).

The flow cytometry technique is based on suspended cells that pass through a laser beam. The beam gets refracted by passing cells, which causes light diffusion at small and large angles. The magnitude of diffused light depends on cell properties and is detected and grouped as forward scatter (FSC, small angle scatter) and side scatter (SSC, large angle scatter). SSC hints on complex structures inside the cells, like granules. The FSC is a sign for the relative size of the cells. Both are proportional to the particular cell characteristics (Picot et al. 2012). Figure 3-20 B clarifies that the FSC remained unchanged for the transduced AT-MSCs, but the whole cell populations of the modified cells showed slightly increased SSCs, compared to wild type AT-MSCs. Therefore, the size of the modified cells, in terms of volume, was apparently not changed. Moreover, the overall cell distributions in the scatter plots showed a similar pattern for all three AT-MSC-entities (Figure 3-20 C).

3.5.2 Co-injection of AT-MSCs and Hep3B cells enhances tumor formation in a subcutaneous xenograft SCID mouse model – PAR_1 gene knockdown in AT-MSCs has no significant effect on tumor formation

The treatment of cirrhosis- or HCC-affected patients comprises various techniques with good prognosis at early tumor stages and poor prognosis at late stages. MSCs may provide an alternative tool to cure completely late-stage liver diseases like cirrhosis. But, the development of HCC might occur simultaneously and beneath the limits of detection. Moreover, the impact of MSCs on tumor cells is uncertain and cancer-inhibiting as well as cancer-promoting effects through the paracrine activity of MSCs were described.

Our goal was to assess the interaction of AT-MSCs and cells from the HCC cell line Hep3B under *in vivo* conditions. Since we found the enhanced paracrine activity of AT-MSCs after PAR_1 stimulation, the second question was whether PAR_1 in AT-MSCs contributes to the stimulation of Hep3B cell proliferation.

The HCC cell line Hep3B readily generates tumors upon xenotransplantation into severe combined immunodeficiency (SCID) mice. To test the effect of potential MSC-HCC cell interactions, Hep3B cells were subcutaneously co-injected with AT-MSCs into SCID mice, and the tumor formation was monitored. Genetically modified AT-MSCs bearing the PAR_1 knockdown, as described in paragraph 2.4.4 (page 33), were also included to assay the possible influence of PAR_1.

Figure 3-21 presents all the *in vivo* results of tumor growth experiments done in SCID mice. The display comprises (1) the effect of AT-MSCs on Hep3B tumor growth in general, (2) the fate of the AT-MSCs during the onset of tumor formation, and (3) the influence of a PAR_1KD in AT-MSC on Hep3B cell tumor

growth compared to a non-target (nt) control. The adjacent graphs show the mean volumes of each experimental group, which were calculated on the basis of obtained computed tomography (CT)-scans.

(1) As seen in the tumor overview (Figure 3-21, A-D), Hep3B cells were occasionally able to generate tumors under the chosen conditions. Four out of nine injections of Hep3B cells caused the formation of tumors, which remained small, less than 10 mm^3, and did not grow to a much larger size even when left longer inside the mice.
The injection of AT-MSCs alone caused no formation of visible aberrant tissue.
The co-injection of both cell types together resulted in each of the 13 cases in tumor growth. The tumor sizes did not seem to correlate with the duration of the experiment. After 16 days, the experiment B yielded the largest tumors of up to 150 mm^3, while experiment D yielded tumors of comparable sizes, but after 24 days.

Hep3B cells and AT-MSCs together caused large tumors. Even genetically modified AT-MSCs that had been treated with the transduction/knockdown protocol and were cultured *in vitro* for a total duration of four weeks were able to cause similar Hep3B cell tumor formations:

(2) AT-MSCs labeled with a green fluorescent protein (GFP) vector resulted in all three cases in a tumor of similar size compared to tumors induced by injection of Hep3B cells and AT-MSC-wt cells (Figure 3-21, D).

(3) The co-injection of Hep3B cells with AT-MSCs-nt caused tumor formation in eight out of twelve assayed mice, while Hep3B cells with AT-MSCs-PAR_1KD caused tumor formation in nine out of twelve mice (Figure 3-21, C-E). Both co-injections caused small tumors as well as large tumors of similar sizes like the co-injections of Hep3B cells and AT-MSC-wt. Hence, the PAR_1 knockdown in AT-MSCs had no significant impact on the caused tumor volume, compared to non-target control.

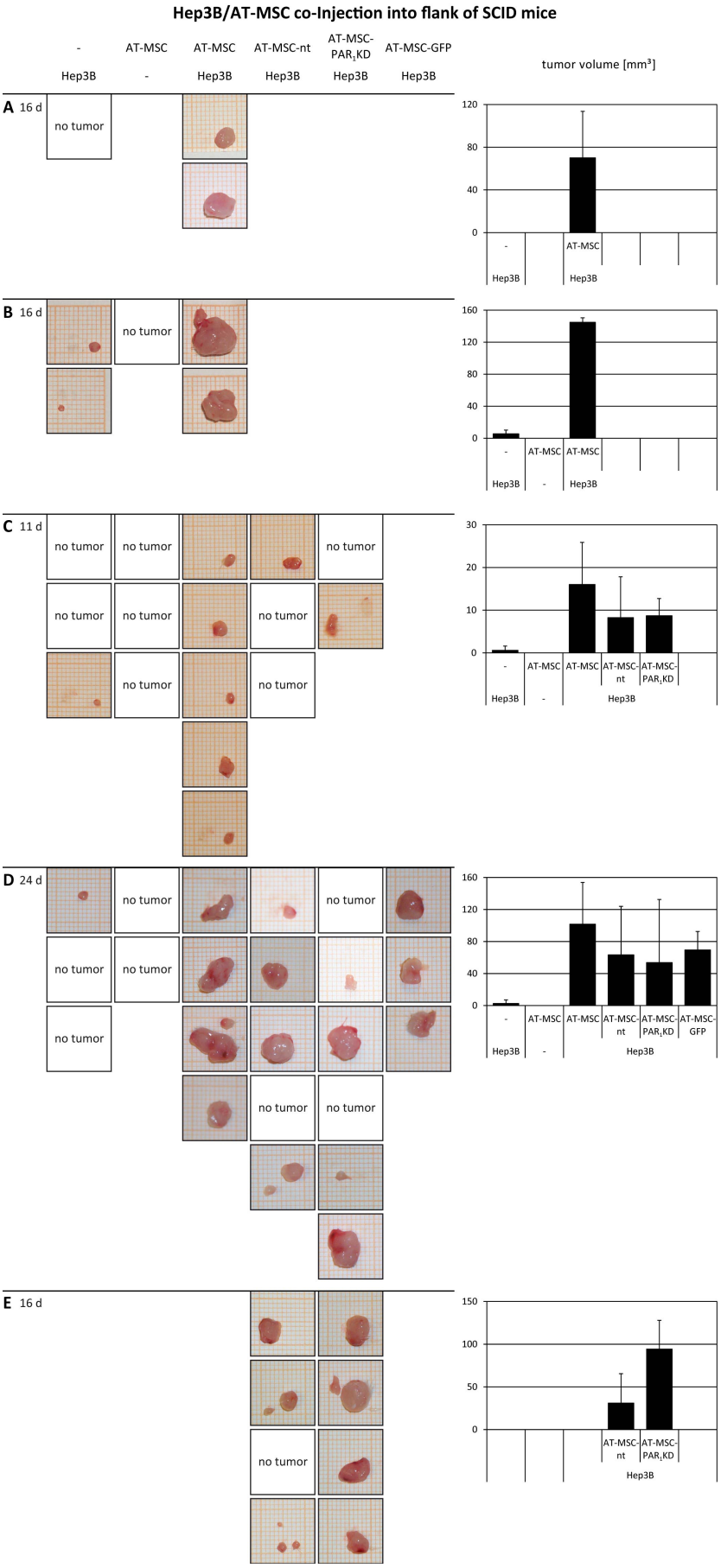

Figure 3-21: Overview of all obtained tumors after subcutaneous injection of Hep3B cells and AT-MSCs into SCID mice

100,000 Hep3B cells or/and 500,000 AT-MSCs (donors #1, 6 and 7) were subcutaneously (co-)injected into the flank of male SCID mice. After 11-24 days (d) the tumor formation was stopped and evaluated. White squares represent mice with no tumor formation. The charts on the right display the mean tumor volumes ± SD of the single groups of each experiment.

The injection of Hep3B cells under the skin of SCID mice caused occasional small tumors in approx. half of the cases, otherwise no tumors. AT-MSCs alone caused no tumors. Both cell types together caused large tumors in all cases. The co-injection of Hep3B cells with modified AT-MSCs caused in frequent cases tumors of comparable sizes like the ones with wild type AT-MSCs. However, not all injected mice grew tumors. The PAR_1-KD did not seem to affect the tumor formation or progression, compared to non-target control.

The caused tumors of the Hep3B and AT-MSC xenotransplantation were further characterized by histologic analyses. The tumors were fixed and embedded in paraffin, sliced and analyzed with hematoxylin/eosin stain and specific antibodies for cytokeratins, alpha-smooth muscle actin (α-SMA) and Ki-67. The slides were digitalized and evaluated.

The following panels show representative images of representative tumors for the groups (1) Hep3B and Hep3B + AT-MSC (Figure 3-22), (2) Hep3B + AT-MSC-GFP (Figure 3-23), and (3) Hep3B + AT-MSC-nt and Hep3B + AT-MSC-PAR$_1$KD (Figure 3-24). In general, all of the obtained tumors showed similar patterns for all assayed stainings. Moreover, the tumors displayed typical features of the HCC.

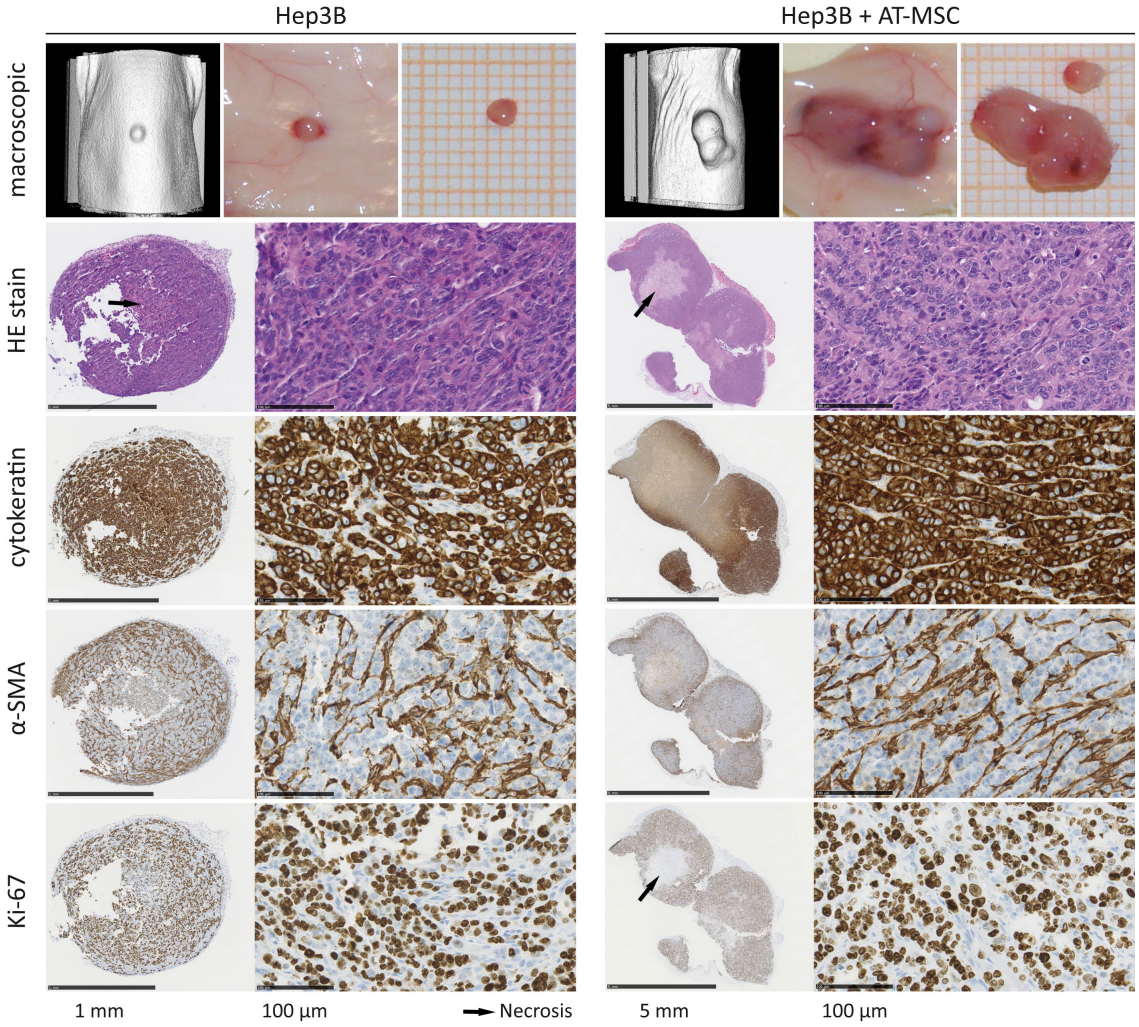

Figure 3-22: Tumor formation 24 days after subcutaneous injection of Hep3B cells or Hep3B cells + AT-MSCs into the flank of SCID mice

100,000 Hep3B cells and 500,000 AT-MSCs were injected under the skin of SCID mice alone or in combination. After 24 days, the formed tumors were imaged with a CT scan, the affected skin was removed, and the tumors were isolated (top row of each panel, left to right). Afterward, they were sliced and histologically stained with HE stain, and primary antibodies for detection of cytokeratin, α-SMA and Ki-67 (cross sections and magnified areas). Representative tumors and images are shown.

Hep3B cells occasionally caused small tumors. AT-MSCs caused no tumors (not shown). The co-injection of Hep3B cells and AT-MSCs caused tumors in all cases. All tumors resembled HCC tissue with vesicular tumor cells in a macro-trabecular arrangement (HE). The cells were of epithelial origin (cytokeratin), showed mitotic activity (Ki-67) and intense vascularization (macroscopic and α-SMA). Note the formation of typical intratumoral necrosis (black arrows).

(1) , (2) and (3) Before the tumors were removed from the murine skin, the angiogenesis was evaluated. Almost all of the tumors showed major angiogenic activity. As seen on the macroscopic pictures of Figure 3-22, Figure 3-23 and Figure 3-24, the tumors were surrounded by one to three clearly visible vessels. The unaffected murine skin was of pale reddish-white color with no highlighted red vessels.

The HE stainings showed tumor cells that were arranged in a macro-trabecular structure. In the normal liver, hepatocytes form single-cell-thick plates/trabeculas, which are separated by fenestrated capillaries (sinusoids). HCC forms characteristic micro- and macro-trabecula with two to ten and more cell layers. The trabecular pattern is more clearly visible in the cytokeratin staining images. Further HCC characteristics that were frequently found in the tumors comprised large vesicular nuclei and accented nucleoli, a general pathologic nucleus-plasma ratio, basophilic tumor plasma, and mitotic figures. These features indicate open phase nuclei with prominent DNA synthesis and gene expression that are characteristic for highly proliferative cells. (Bavle 2014; Paradis 2013; Pathpedia e-Atlas 2015).

Especially the larger tumors and some of the smaller ones showed central necrotic areas with infiltrated granulocytes and cell debris.

The staining with a cytokeratin-targeted antibody resulted in strong stainings throughout the tumor. Cytokeratins are expressed by hepatocytes, like all other epithelial cells (Karantza 2011), thus proving the epithelial origin of the tumor cells and highlighting the macro-trabecula. The observed staining differences of the large tumors on the right of Figure 3-22 and Figure 3-24 resulted from uneven stainings. The brighter areas still showed positive cytokeratin staining.

A-SMA is a marker for myoepithelial cells, smooth muscle cells and myofibroblasts and is used for the detection of vessels (Skalli et al. 1989). Although MSCs express α-SMA at low levels and only in the minority of cells in an MSC population (Hung et al. 2006; Tamama, Sen, & Wells 2008), our stainings were strongly α-SMA-positive throughout the tumors. Therefore, it implies a network of cells with a strong α-SMA expression that originate from surrounding tissue, since the tumor margins show stronger stainings, hence showing the presence of a multitude of capillary vessels throughout the tumor tissue.

Ki-67 is a protein that is specifically found in mitotic cells and is a validated marker for proliferative cells (Scholzen & Gerdes 2000). All obtained tumors showed positive Ki-67 stainings throughout the viable tumor tissue. Note that the necrotic areas showed no staining with this marker.

(2) As already mentioned, all tumors were highly proliferative and resembled HCC tissue by showing characteristic HCC-like features and epithelial origin (Figure 3-23). In order to determine the fate of the co-injected AT-MSCs, we performed co-injections of Hep3B cells with GFP-labeled AT-MSCs. Though tumor formation and histological stainings were similar to the other tumors with wild type AT-MSCs, essentially, no GFP-labeled AT-MSCs were found in the tumor tissues after 24 days (not shown). This implies that the GFP-labeled AT-MSCs were no longer present in the formed tumor tissue. Therefore, the underlying growing cells were presumably cells of the HCC cell line Hep3B.

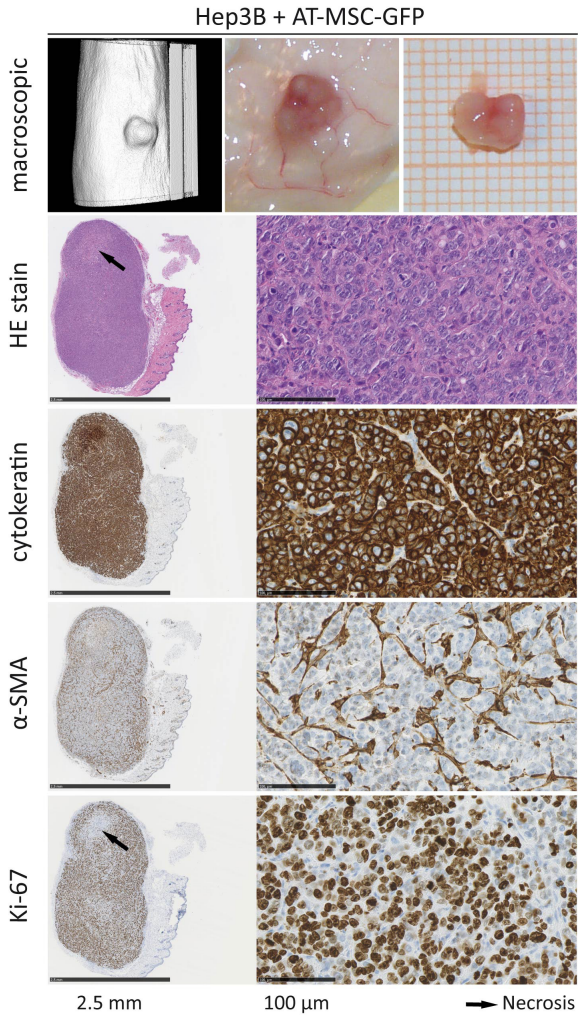

Figure 3-23: Tumor formation 24 days after subcutaneous injection of Hep3B cells + AT-MSC-GFP into flank of SCID mice

AT-MSCs were transduced with GFP (AT-MSC-GFP). 100,000 Hep3B cells and 500,000 AT-MSC-GFP were injected under the skin of SCID mice and caused formation of tumors. After 24 days, the formed tumors were imaged with a CT scan, the affected skin was removed and the tumors were isolated (top row of each panel, left to right). Afterward, they were sliced and histologically stained with HE stain, and primary antibodies for detection of cytokeratin, α-SMA and Ki-67 (cross sections and magnified areas). Representative tumors and images are shown.

The co-injection of Hep3B cells with AT-MSC-GFP caused tumors that resembled HCC tissue with vesicular tumor cells in a macro-trabecular arrangement (HE). The cells were of epithelial origin (cytokeratin), showed mitotic activity (Ki-67) and intense vascularization (macroscopic and α-SMA). Note the formation of typical intra-tumoral necrosis (black arrows).

(3) The co-injection of Hep3B cells with either AT-MSC-nt or AT-MSC-PAR$_1$KD led to frequent formations of tumors with no apparent impact of the PAR$_1$ knockdown in AT-MSCs on the tumor volume. The histological stainings showed similar features and staining patterns throughout the tumor tissues for Hep3B + AT-MSC-nt and Hep3B + AT-MSC-PAR$_1$KD and were similar to Hep3B and Hep3B + AT-MSC-wt tumors (Figure 3-24). As described before, all stainings resembled HCC-like features. Thus, there was presumably no impact of AT-MSC's PAR$_1$ on the overall Hep3B tumor formation on neither tumor volume nor histological features.

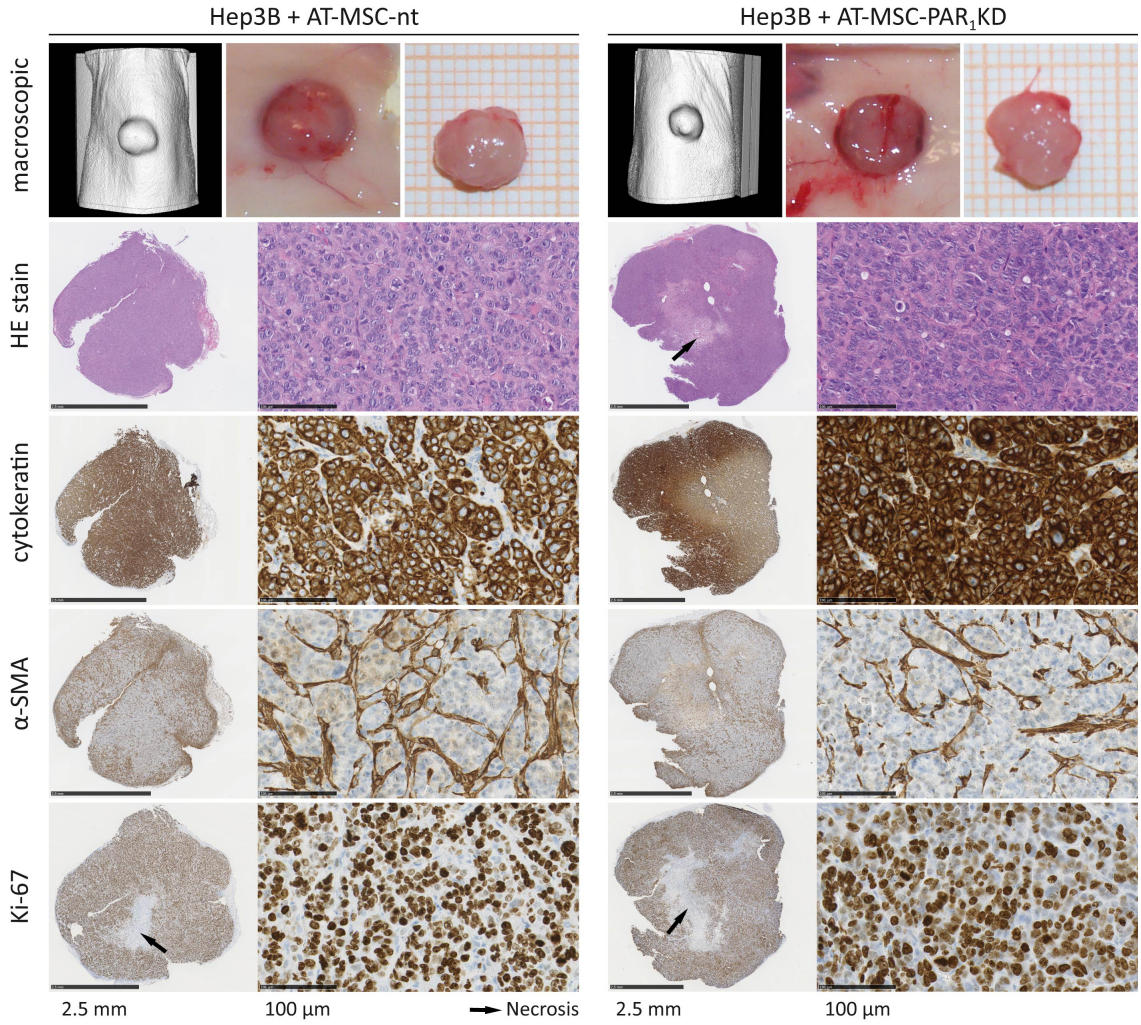

Figure 3-24: Tumor formation 24 days after subcutaneous co-injection of Hep3B cells + AT-MSC-nt or Hep3B cells + AT-MSC-PAR$_1$KD into the flank of SCID mice

AT-MSCs were transduced with a non-targeting control (AT-MSC-nt) or PAR$_1$ knockdown shRNA (AT-MSC-PAR$_1$KD). 100,000 Hep3B cells and 500,000 AT-MSCs of either transduction were injected under the skin of SCID mice and caused tumors in frequent cases. After 24 days, the formed tumors were imaged with a CT scan, the affected skin was removed and the tumors were isolated (top row of each panel, left to right). Afterward, they were sliced and histologically stained with HE stain, and primary antibodies for detection of cytokeratin, α-SMA and Ki-67 (cross sections and magnified areas). Representative tumors and images are shown.

The co-injection of Hep3B cells with AT-MSC-nt or AT-MSC-PAR$_1$KD caused tumors in frequent cases, but with rather inconsistent sizes among each group. All tumors resembled HCC tissue with vesicular tumor cells in a macro-trabecular arrangement (HE). The cells were of epithelial origin (cytokeratin), showed mitotic activity (Ki-67) and intense vascularization (macroscopic and α-SMA). Note the formation of typical intra-tumoral necrosis (black arrows). No correlation of the PAR$_1$ knockdown in AT-MSCs with tumor formation was observed in the applied co-injection mouse model.

4 Discussion

Mesenchymal stem cells (MSCs) secrete a variety of growth factors, angiogenic and immunoregulatory proteins that make them potentially suitable for the curative treatment of tissue diseases. Clinical research includes liver diseases as one target for MSC-guided cellular therapy, but liver diseases like hepatitis or cirrhosis may potentially lead to the formation of hepatocellular carcinoma (HCC). The progression of HCC has been shown to be promoted by proteinase-activated receptors (PARs) (Kaufmann et al. 2007, 2009; Mußbach et al. 2014). Moreover, liver diseases like cholangiocarcinoma and liver fibrosis were shown to be promoted by PARs, too (refer to paragraph 1.3.3, page 14). In conclusion, PARs might exert impacts on other liver cell entities as well, like liver stem cells and exogenously inoculated MSCs. MSCs as means of therapy would add a locally large amount of exogenous cells to diseased microenvironments harboring a variety of PAR-activating proteinases from various sources (Mason & Joyce 2011). However, the expression of PARs in MSCs and the influence of PAR activation on the biological features of MSCs and paracrine effects on surrounding cell entities, especially tumor cells, have not been characterized yet and were of keen interest to our research.

4.1 PAR_1 is the predominantly expressed PAR subtype in human AT-MSCs

The expression of PARs in MSCs has not been part of detailed investigations in the literature so far. Rasmussen et al. showed in a semiquantitative analysis the expression of PAR_2 in adipose tissue-derived MSCs (AT-MSCs) of three different donors and its localization on the plasma membrane using immune fluorescence (Rasmussen et al. 2012). Chen et al. demonstrated PAR_1 and less PAR_2 expression in bone marrow-derived MSCs (BM-MSCs) from two donors using semiquantitative PCR, while PAR_3 and PAR_4 were not detected (Chen et al. 2014b).

Using AT-MSCs of eight different donors, we could show in qPCR-based analyses that PAR_1 was predominantly expressed while PAR_2 was expressed at lower levels (Figure 3-2 A, page 38). Though the PAR_3 expression was low, it was apparently still higher than the expression of PAR_2. PAR_4 was only detected in marginal amounts. The PAR_1 levels seemed to vary among the analyzed donors over a wide range, but there were no obvious correlations between these variations and age or gender. Nevertheless, further analyses of additional donors are necessary to assess correlations of PAR_1 levels with donor gender and age.

Although PAR_1's expression seemed to vary among the analyzed donors, the expression ratio of the receptor subtypes remained constant for each donor, when plotted in relation to respective controls (Figure 3-2 B, page 38). To exclude that this ratio was simply based on unequal efficiencies of the applied subtype-specific primer pairs, they were verified in qPCRs of a dilution series of cDNA that was

pooled from several cell entities. The used primers performed with sufficient linear efficiencies of more than 90 % (Figure 3-1, page 37).

The differential PAR subtypes expression was further assessed by Ca^{2+} assays. The stimulation of PARs causes an increase in the intracellular free Ca^{2+} concentration, hence giving feedback on their presence and functionality in the cells. The PAR subtypes were stimulated with their canonical activating proteinases thrombin (PAR_1, PAR_3 and PAR_4) and trypsin (PAR_2). Subtype-specific activating peptides (APs) were employed to distinguish between the particular receptors.

As presented in Figure 3-3 (page 39), thrombin exerted an activation of the AT-MSCs resulting in a strong Ca^{2+} release inside the cells, seen as an increase in Ca^{2+}-binding fluorophore Fluo-4-AM. The PAR_1-AP resulted in a similar Ca^{2+} signal over time. The PAR_4-AP was unable to trigger a Ca^{2+} effect in the cells, consistent with the very low expression detected by qPCR. No additional PAR_3 experiments were carried out since available PAR_3 subtype-specific activating peptides cross-activate PAR_1 and PAR_2 (Hansen, Saifeddine, & Hollenberg 2004). Since our expression data showed that PAR_4 was minimally expressed by AT-MSCs and PAR_1 was expressed in significantly larger amounts than PAR_3, thrombin presumably exerted the majority of its impact via PAR_1.

Trypsin as a major PAR_2 activator exerted a weaker Ca^{2+} effect than thrombin, and the cells were not responding at once but rather in short peaks, distributed over a long time until all cells responded. The PAR_2-AP peptide also triggered a short increase in the intracellular free Ca^{2+} concentration, but only in a few cells, while the majority did not respond at all. The weak Ca^{2+} signals caused by stimulation with trypsin and PAR_2-AP might be due to PAR_2's low expression, which we described above. However, trypsin triggered a weak but overall stronger effect than the PAR_2-AP. This effect might be due to trypsin's potential to act via PAR_1 as well. PAR_1 can be activated by pancreatic trypsin isoforms at low rates (Grishina et al. 2005; Knecht et al. 2007; Salameh & Radisky 2013). The applied trypsin in our experiments derived from bovine pancreas (Sigma, cat. no. T1426) and resembled a cocktail of trypsin isoforms.

In order to distinguish thrombin's actions more thoroughly, we conducted further Ca^{2+} analyses and applied subsequent PAR activations and the PAR_1-specific antagonist Atopaxar. The subsequent stimulation makes use of that PARs get internalized after their activation (Ramachandran & Hollenberg 2008; Soh et al. 2010). Therefore, subtype-specific PAR_1 activation would deplete the plasma membrane of PAR_1 and thus leaving behind the other subtypes.

As seen in Figure 3-4 (page, 40) PAR_1-AP was able to cause a Ca^{2+} signal in AT-MSCs. The subsequent stimulation with thrombin was unable to cause another major Ca^{2+} signal. In other words, the stimulation with PAR_1-AP caused a depletion of PAR_1 on the plasma membrane of the AT-MSCs. The

subsequent stimulation with thrombin had almost no effect, supporting the data of the absence or low expression of other thrombin targets.

These findings were supported by assays including the pre-treatment with Atopaxar (Figure 3-5, page 42). Atopaxar was able to abolish obtained Ca^{2+} mobilizations for PAR_1-AP and thrombin in a concentration-dependent manner. Under the premise of Atopaxar's specificity for PAR_1, this would underscore PAR_1's sole responsibility for Ca^{2+} mobilization upon activation by thrombin in AT-MSCs. Currently, general extensive *in vitro* research on Atopaxar is lacking, and it was reported that it exerts minor off-target effects by weakly inhibiting ADP- and collagen-induced platelet activation (Serebruany et al. 2009). Hence, Atopaxar might not exclusively target PAR_1. However, Atopaxar showed strong abolishing effects on PAR_1-AP's actions, and thus provides a valuable antagonist for characterizing PAR_1's actions *in vitro*.

Taken together, our expression and functional analyses of the PAR subtypes indicate that PAR_1 is the predominantly expressed PAR subtype in AT-MSCs and that it is the major subtype to cause an intracellular Ca^{2+} signal in AT-MSCs upon treatment with thrombin.

In order to verify PAR_1's presence on the protein level, we performed immunoblots and the freeze-fracture replica immunolabeling technology with the PAR_1-specific primary antibodies WEDE15 (Beckman Coulter) and ATAP2 (Santa Cruz Biotechnology).

The application of the PAR_1 antibody WEDE15 was described in several publications by the Trejo group (Lin & Trejo 2013; Soto et al. 2015) and revealed a molecular weight of glycosylated PAR_1 at approx. 70 kDa, and 38 kDa for deglycosylated PAR_1 (Soto & Trejo 2010). Their immunoblots were obtained from PAR_1-enriched eluates of lysates of cells overexpressing PAR_1. We employed whole cell lysates of AT-MSCs and detected bands with molecular weights at approx. 38, 48 (and 60) kDa on the immunoblots (Figure 3-8, page 48). The life science companies Santa Cruz Biotechnology and Cell Signaling Technology claim a molecular weight of 47 kDa for unglycosylated PAR_1 (Phosphosite.org 2015) and 66 kDa for glycosylated PAR_1. Our PAR_1 immunoblots highlighted major bands at approx. 48 kDa. Therefore, it is possible that the detected AT-MSC's PAR_1 has a lesser state of glycosylation as the model in the publications by the Trejo group. Intriguingly, their experiments with a PAR_1 mutant, which lacked glycosylation at the extracellular loop two, showed a molecular weight of approx. 48 kDa. This mutant also exhibited increased $G\alpha_q$-signaling compared to wild type/highly glycosylated PAR_1. These findings might hint on an increased PAR_1 signaling via the $G\alpha_q$ pathway and lesser signaling via $G\alpha_{12/13}$ in AT-MSCs.

The ATAP2 antibody decorated more unexpected bands on PAR_1 immunoblots and the expected one at 47 kDa was less pronounced compared to the other bands. Also, the WEDE15 antibody recognizes the WEDE sequence in the PAR_1 N-terminal region, as depicted by Brass et al. (Brass et al. 1994), and is unaffected by receptor cleavage. Hence, we chose the WEDE15 antibody for detection of PAR_1 on freeze-fracture replicas of AT-MSCs.

The obtained electron microscopic images (Figure 3-9, page 49) of WEDE15-labeled freeze-fracture replicas of AT-MSCs showed single and grouped black dots on the exoplasmic face. The black dots were caused by gold particles, which obstruct the electron beam of the electron microscope. The gold particles were bound to secondary antibodies, which in turn detected the WEDE15 antibody. The control without WEDE15 caused no black dots. Therefore, the black dots are likely to represent the location of PAR_1 on the AT-MSCs' plasma membrane. The multiple dots might imply PAR_1 homodimers as PAR_1 is able to form receptor homodimers (Lin et al. 2013b).

Our group has earlier shown PAR_1 localization on the plasma membrane of HCC cells using the freeze-fracture immunolabeling technique (Kaufmann et al. 2007). Moreover, PAR_1's plasma membrane localization and trafficking upon stimulation have been shown by fluorescence imaging by the Trejo group (Lin & Trejo 2013).

4.2 PAR_1 signaling in MSCs – AT-MSCs show high basal ERK phosphorylation

As discussed above, our data clearly indicated that PAR_1 is presumably the major PAR subtype in AT-MSCs to respond to the activation by proteinases. In general, PAR_1 is described to signal mainly through $G\alpha_q$ and $G\alpha_{12/13}$, and thus acts via Ca^{2+} signals and the activation of various kinases like extracellular-signal regulated kinase (ERK), Akt or Ras homolog gene family member A (RhoA) kinase (McLaughlin et al. 2005; Zhao, Metcalf, & Bunnett 2014). In order to characterize PAR_1's signaling in AT-MSCs, we conducted measurements of intracellular free Ca^{2+} elevation and immunoblot assays for activation of signaling proteins.

As discussed in paragraph 4.1 (page 70), PAR_1 agonists thrombin and PAR_1-AP were able to enhance intracellular free Ca^{2+} levels, which was abolished by pre-treatment with the PAR_1 antagonist Atopaxar. The PAR_1-specific immediate and strong elevation of the intracellular free Ca^{2+} concentration could activate the MAPK pathway, which is a central signaling pathway for proliferation, apoptosis, differentiation and migration (Dhillon et al. 2007). Also, it could be demonstrated that PAR_1 activation led to the activation of ERK via the $G\alpha_q$ protein subunit, which causes an increase in intracellular free Ca^{2+} levels and formation of diacylglycerol (DAG). Subsequent DAG and/or Ca^{2+}-dependent protein kinase C (PKC)-mediated activation of rapidly accelerated fibrosarcoma kinase (Raf), proline-rich tyrosine kinase 2 (Pyk2) or transactivation of receptor tyrosine kinases like epidermal growth factor

receptor (EGFR) may ultimately lead to ERK activation (Gieseler et al. 2013; Wang & Reiser 2003; Wang et al. 2002).

Therefore, we approached this complex issue by performing initial immunoblot assays of phosphorylated ERK (pERK). These experiments showed a strong phosphorylation of ERK upon PAR_1 activation with thrombin or PAR_1-AP. However, repetitions of the assays revealed that the pERK signals in unstimulated controls were rather inconsistent in intensity by ranging from low to medium and frequently high pERK levels (Figure 3-10, page 50). Even though we attempted to optimize the experimental setup as much as possible, e.g. by usage of HEPES-buffered starvation/activation medium, the addition of stimulating agents in a larger volume to minimize stirring stress, and usage of a heating plate during the stimulation, the basal pERK level did not stabilize and seemed not to correlate with any of these factors. Even unstimulated controls from the same experiment differed without any obvious correlation while just standing on the heating plate for 1/5/10/20 min (not shown).

There is one publication that described high basal ERK phosphorylation levels in human embryonal stem cells (ESC) and that high levels of pERK were important for keeping self-renewing characteristics. Moreover, this seemed to contrast with features of murine ESCs, which possessed low basal pERK levels (Li et al. 2007). According to our findings, it may be possible that the ERK signaling status is similarly high in human AT-MSCs as described for human ESCs. However, Chen et al. reported strong activation of ERK in human BM-MSCs upon stimulation with thrombin and mentioned no technical issues as encountered in the current study (Chen et al. 2014b).

Hence, we cannot draw a firm conclusion on the ERK phosphorylation caused by PAR_1 stimulation in the AT-MSCs.

4.3 PAR_1 mediates reduced migration rate of AT-MSCs but has no impact on their proliferation

We showed that the activation of PAR_1 in AT-MSCs exerted a strong transient elevation of intracellular free Ca^{2+} levels. Though we faced technical problems in addressing the PAR_1 signaling in more detail (discussed in paragraph 4.2, page 72), the PAR_1 activation was likely to result in biological responses of the AT-MSCs, eventually. Two major effects, which are of relevance for the MSC-guided cellular treatment of diseases, include migration and proliferation. MSCs were described to migrate towards inflamed tissues and cancers. Furthermore, when reaching the proximity of a diseased microenvironment, they might get stimulated to proliferate in order to repopulate the tissue.

PAR_1 activation was described to cause rearrangements of the cytoskeleton via the $G_{\alpha 12/13}$ pathway (Siehler 2009; Soh et al. 2010), and our group was able to demonstrate that PAR_1 activation caused a

promotion of migration of colon carcinoma and HCC cells (Heider et al. 2004; Mußbach et al. 2014). Since we found PAR_1 to be predominantly expressed in AT-MSCs, PAR_1 might also affect the migratory behavior of AT-MSCs. In general, systemically administered MSCs seem to possess a high potential for homing to inflamed tissue sites like wounds and cancers along gradients of inflammatory mediators (Reagan & Kaplan 2011; Rustad & Gurtner 2012). Cancers are a source of activated coagulation proteins, and might, therefore, affect the PARs of MSCs and thus their local migration (ten Cate & Falanga 2008).

To address the migration of AT-MSCs in response to PAR_1-stimulating agents, the cells were seeded into reusable migration chambers and were allowed to migrate for 16 h. After that, they were fixed and counted. Our experiments affirmed the strong general ability of MSCs to migrate. As shown in Figure 3-11 (page 51), up to 30 % of initially seeded AT-MSCs were migrating through a polycarbonate membrane at serum-free control conditions. In comparison, only 0.1 % of a population of the HCC cell line Hep3B were migrating in a similar set up as previously published by our group (Mußbach et al. 2014). As further shown in Figure 3-11, the stimulation of PAR_1 in AT-MSCs led to a significantly reduced migration rate of AT-MSCs towards both thrombin and PAR_1-AP. These findings might add to the understanding of MSC's homing to cancer tissues. When MSCs approach tumors, they might get activated via PAR_1. Chen et al. showed that PAR_1 activation caused an increase in expression and secretion of fibronectin and enhanced the MSC's adhesion *in vitro* (Chen et al. 2014b). The enhanced adhesion might explain the reduced rate of migration that we observed. These PAR_1-mediated effects might limit the migration of MSCs towards various factors, which were shown to attract and activate MSCs and to stimulate their settlement at tumor sites. (Sun, Wang, & Zhao 2014).

Unfortunately, we were not able to verify the reduction of migration by stimulation of PAR_1 with AT-MSCs from another donor. The AT-MSCs' basal rate of migration (not shown) differed between the donors, thus making it difficult to apply the protocol on another batch without prior extensive adjustment and optimization of seeded cell counts. Furthermore, the amount of migrated cells of one donor differed between the single assays. These issues might be resolved by further verification of the observed reduced migration via other versions of the Neuroprobe chamber or scratch/barrier assays.

The proliferation rate of AT-MSCs upon stimulation with PAR_1-activating compounds was assessed with a variety of experimental conditions. Control experiments ensured that alterations in proliferation could be reliably detected by the used assays. However, no or only a minor enhancement of the AT-MSCs' proliferation rate was observed when several concentrations of thrombin and PAR_1-AP were applied (Figure 3-12, page 52). The authors of a recent publication (in Chinese) claimed in their English abstract that thrombin enhanced the proliferation of BM-MSCs *in vitro*, especially at higher thrombin

concentrations with a maximum at 8 U/ml. They observed an enhanced proliferation at a minimum of 0.5 U/ml (Chen et al. 2014a). We, however, applied concentrations of 1 NIH U/ml and also a maximum of 5 NIH U/ml (not shown), but no significant effects of PAR_1 activation on AT-MSCs were observed. Although Chen et al.'s and our employed proliferation assays were both based on the metabolic activity of viable cells, a repetition with more sensitive proliferation assays measuring DNA synthesis may verify these findings.

4.4 PAR_1 activation in AT-MSCs stimulates the secretion of pro-angiogenic factors

Apart from their multipotent character, MSCs possess the pre-eminent property to secrete a plethora of proteins with substantial effects on surrounding tissues. The secretion of various growth factors, immunoregulatory proteins, extracellular matrix-related proteins and proteinases, and angiogenesis-related proteins make MSCs and other stem cell entities potentially a valuable resource for therapeutic purposes. However, the amount and variety of secreted proteins may differ between stem cells from different origins and different interacting tissue microenvironments, which they may encounter by means of migration or direct injection at the site of interest. (Hass & Otte 2012; Laird, von Andrian, & Wagers 2008; Liang et al. 2014).

Therefore, we assessed the secretion properties of the AT-MSCs from our experiments and further characterized the impact of PAR_1 on the expression and secretion of AT-MSC-derived proteins.

To get an overview of the proteins and factors that were secreted by primary human AT-MSCs, immunoblot-based arrays were performed using culture supernatant of AT-MSCs. One-third of the potentially array-traceable proteins was detected in 24 h-conditioned media (Table 3-1, page 54). Among others, multiple proteins that are known for their direct or indirect angiogenic, mitogenic or migration-promoting properties were detected: angiogenin, angiopoietin 1, angiopoietin 2, hepatocyte growth factor (HGF), Interleukin 6 (IL-6), IL-8, monocyte chemotactic protein 1 (MCP-1) and vascular endothelial growth factor (VEGF).

Though we were able to analyze only one batch of cells for the complete panel of proteins detectable by the array, our data supports previously published data from other groups, which used human BM-MSCs from several donors. Park et al. showed in a similar approach that IL-6, IL-8, MCP-1 and VEGF were secreted in larger amounts, also tracing tissue inhibitor of matrix metalloproteinases 1 (TIMP-1) and HGF. However, they did not mention the timespan of medium conditioning (Park et al. 2009). Schinköthe and colleagues did not detect IL-6, but also showed the presence of angiopoietin 2, MCP-1, IL-8, HGF, TIMP-1 and VEGF. Their protocol included a conditioning over three days (Schinköthe, Bloch, & Schmidt 2008). Hsiao et al. compared BM-MSCs with AT-MSCs and also found IL-6, IL-8, MCP-1,

angiogenin and VEGF in the media with no distinct differences for those proteins among the two entities. However, they also conditioned the culture media over three days and additionally concentrated the media by 50-fold (Hsiao et al. 2012).
Apart from the protocols of conditioning, the covered proteins, and the MSCs' origin, these data collectively show that AT-MSCs are a source of IL-6, IL-8, MCP-1, VEGF, HGF and probably angiopoietins. However, our data and the published data from the mentioned groups were quantifications of immunoblot-based methods. The comparison of the resulting intensities with each other implies that certain proteins were secreted in larger proportions than others. But, the specificities and detection sensitivity of underlying primary antibodies for over hundreds of proteins are most likely not similar, and data from Table 3-1 (page 54) and discussed literature should only serve as an incentive for further detailed analyses.

It was beyond the scope of this dissertation to discuss the possible biological relevance of all the detected proteins, which were secreted by AT-MSCs. However, a few, which caused particularly strong signals on the proteome arrays, implying extensive secretion by the AT-MSCs, shall be highlighted. These include Serpin E1, matrix metalloproteinase 2 (MMP-2) and MMP-1. These proteins could serve as interesting targets in further MSC/tumor research since they were described to favor thrombosis, intravasation, and metastasis of tumors. Serpin E1 (also known as plasminogen activator inhibitor 1, PAI-1) is an inhibitor of fibrinolysis and promotes thrombosis and scarring (Ghosh & Vaughan 2012). MMP-2 degrades basement membranes and provides a basis for angiogenesis, and has been shown to be elevated in various cancers leading to poor prognosis (Bauvois 2012; Nussenbaum et al. 2010). MMP-1 is involved in extracellular matrix degradation and is an activator of PAR_1, which might support PAR_1's actions on MSCs and promote tumor metastasis (Arakaki, Marques, & Santos 2009; Juncker-Jensen et al. 2013).
In the following sections, we will focus on proteins whose secretion was affected by PAR_1 stimulation.

Among those detected proteins we sought to identify the ones that are affected by stimulation of PAR_1. To this end, we stimulated AT-MSCs with thrombin and PAR_1-AP over 24 h. The conditioned supernatant was then compared to medium from untreated AT-MSCs. As displayed in Figure 3-14 (page 55), especially IL-6, IL-8 and MCP-1 showed a putative influence of PAR_1 activation on their secretion since they were secreted in larger amounts by AT-MSCs in the presence of thrombin and PAR_1.
As a consequence, our first goal was to analyze the impact of PAR_1 activation on the mRNA expression of IL-6, IL-8 and MCP-1, which would presumably result in their enhanced secretion. Hence, we performed qPCRs of multiple AT-MSC batches that were cultured in the presence of thrombin or

PAR_1-AP for 24 h. The mRNA expression analyses revealed that IL-6, IL-8 and MCP-1 were indeed strongly influenced by PAR_1 activation (Figure 3-15, page 56). In general, thrombin significantly elevated their expression by up to five to 20-fold. PAR_1-AP enhanced the mRNA expression of IL-6, IL-8 and MCP-1 by 1.5- to 4-fold. The pre-treatment with PAR_1 antagonist Atopaxar caused an attenuation of PAR_1-mediated elevation of mRNA expression. Though PAR_1 activation seemed to cause constantly the elevation of mRNA expression for these proteins, we obtained, however, quite large standard deviations. In some assays, responses to PAR_1 activation were only weak, which might have been caused by too late time points of analysis for the particular cell batch, and therefore perhaps already declined PAR_1 effects. The kinetics of the PAR_1-mediated stimulation of IL-6, IL-8 and MCP-1 mRNA expression needs further characterization in future research.

A link between PAR_1 activation and the upregulation of cytokine expression was previously reported for several other cell entities by other researchers. The results for IL-6 and IL-8 will be discussed in the subsequent paragraphs. An increased expression of MCP-1 upon thrombin and PAR_1-AP stimulation was shown for monocytes, vascular smooth muscle cells and human umbilical vein epithelial cells (Brandes et al. 2001; Colotta et al. 1994; Marin et al. 2001). Kawawani et al. showed an increased MCP-1 secretion and the involvement of RhoA kinase in this response, thus implying a $G\alpha_{12/13}$-dependent thrombin-PAR_1 signaling (Kawanami et al. 2011). Furthermore, MCP-1 was found to increase the migration of murine and human BM-MSCs (Boomsma & Geenen 2012; Dwyer et al. 2007). Taken together, our results suggest that the thrombin-PAR_1 axis might play an important role for AT-MSCs in thrombotic microenvironments, by triggering enhanced MCP-1 expression and presumably enhanced secretion. MCP-1, in turn, could lure even more MSCs and other monocytes to the affected tissue.

PAR_1 mediates the elevation of IL-6 and IL-8 protein amounts in AT-MSC supernatants

Prompted by the results of the antibody arrays and the mRNA expression assays, we performed further experiments to assess the production and secretion of IL-6 and IL-8 with specific ELISAs. Unfortunately, we were not able to include MCP-1 in further analyses, since there were no suitable ELISAs available at this time.

As already discussed above, the stimulation of PAR_1 in AT-MSCs caused an enhanced expression of IL-6 and IL-8 mRNA. The upregulation of cytokine expression was expected to result in an increased secretion, thus causing elevated concentrations in AT-MSC supernatants. Indeed, the stimulation of AT-MSCs with thrombin or PAR_1-AP for 24 h led to elevated concentrations of IL-6 and IL-8 in their supernatant growth medium (Figure 3-17, page 58; Figure 3-18, page 59). As seen in Figure 3-18, thrombin exerted a significant up to four-fold and PAR_1-AP a significant up to three-fold increase in the

IL-6 or IL-8 concentration in the supernatant growth medium of AT-MSCs after 24 h. For both cytokines, the elevation was attenuated by PAR_1 antagonist Atopaxar, the Ca^{2+} chelator BAPTA-AM and the PKC inhibitor BIM-1. Therefore, our data suggest a major impact of PAR_1 on the secretion of IL-6 and IL-8 by AT-MSCs. Furthermore, intracellular free Ca^{2+} and Ca^{2+}-dependent PKC seem to be involved in conveying PAR_1's signals onto elevated secretory actions.

As will be discussed in the following paragraphs, recent publications described multiple PAR_1 downstream effectors of several signaling pathways that were found to contribute to the PAR_1-mediated IL-6 and IL-8 expression and secretion events. We applied MAPK/ERK kinase (MEK), phosphatidylinositide 3-kinase (PI_3K), EGFR and platelet-derived growth factor receptor (PDGFR) inhibitors (not shown), but with no obvious correlations on cytokine secretion after two assays. As the results tended to vary between every assay, additional experiments might point out contributions of these proteins for the underlying signaling.

Furthermore, we analyzed the IL-6 and IL-8 expression in the underlying AT-MSCs of these ELISAs, in order to draw conclusions about the correlation of the secretion data and mRNA expression. As seen in Figure 3-19 (page 60), IL-6 showed a significant enhancement of expression of about six-fold for thrombin and three-fold for PAR_1-AP mediated PAR_1 activation. In the presence of Atopaxar, these effects were significantly attenuated. Though the expression data for IL-8 were not significant, the PAR_1 stimulation caused an enhanced IL-8 expression in most of the cases with a change of up to six-fold for thrombin or three-fold for PAR_1-AP, and again Atopaxar attenuated the expression elevation. Hence, these data imply that the PAR_1 activation-caused enhanced expression and presumably *de novo* synthesis of IL-6 and IL-8 contributes to the elevated concentrations in the culture supernatant.

Regarding the literature, it is known that thrombin and PAR_1-APs upregulate the expression and secretion of IL-8 in macrophages, fibroblasts and epithelial cell lines in a concentration-dependent manner. Involved are PKC, RhoA and PI_3K pathways to activate nuclear factor kappa-light-chain-enhancer of activated B cells (NF-κB)- and activator protein (AP-1)-mediated transcription of IL-8 (Lin et al. 2013a; Ludwicka-Bradley et al. 2000; Scholz et al. 2004; Zheng & Martins-Green 2007). Studies with MSCs reported the secretion of IL-8 by human umbilical cord-derived MSCs and AT-MSCs with an autocrine enhancement of proliferation and IL-8 secretion (Jeon et al. 2013), and a paracrine promotion of IL-8 secretion and migration and metastasis of breast cancer cells (Ma et al. 2015). In addition, Hou et al. have shown the autocrine stimulation of VEGF secretion by IL-8 in BM-MSCs (Hou et al. 2014).

Similar results were published for IL-6. Thrombin, and if applied, PAR_1-APs too, triggered increased IL-6 expression and secretion in MSCs (De Luca et al. 2012; Ma et al. 2015), fibroblasts (Shin et al. 1999; Tanaka et al. 2004), epithelial cells (Marin et al. 2001; Scholz et al. 2004), vascular smooth muscle cells

(Tokunou et al. 2001), osteoblasts (Kozawa et al. 1997), mast cells (Gordon et al. 2000) and T cells (Li & He 2006). Some of these studies identified mediating signaling molecules including PKC, p38, ERK, RhoA, PI_3K, NF-κB, cAMP response element-binding protein (CREB) and the transactivation of EGFR as downstream effectors of thrombin-induced activation (Kozawa et al. 1997; Scholz et al. 2004; Shin et al. 1999; Tanaka et al. 2004; Tokunou et al. 2001). In addition, these studies revealed that IL-6 was elevated in co-cultures of MSCs and cancer cell lines (So et al. 2015), IL-6 exerted a promotion of migration and metastasis of breast cancer cells (Ma et al. 2015), and IL-6 enhanced VEGF secretion by BM-MSCs (Herrmann et al. 2011).

Tanaka et al. pointed out that the enhanced secretion of IL-6 upon PAR_1 activation seems rather due to enhanced *de novo* synthesis than the initial release of internally stored IL-6. They also claimed that BAPTA-AM had no effect on the secretion profile of IL-6 after 24 h, which stands in contrast to our assays. However, they removed the BAPTA-AM-containing medium after pre-treatment for 1 h, while it was present throughout the whole assay in our cases. BAPTA-AM is able to permeate into the cells, and one could imagine that present BAPTA-AM molecules are saturated after the initial thrombin-induced activation and might not attenuate the Ca^{2+} signal over longer time. Another group that analyzed the involvement of PKC and Ca^{2+} were Kozawa et al. They reported that TMB-8, a PKC inhibitor and Ca^{2+} antagonist, was able to reduce secreted IL-6 upon thrombin stimulation (Kozawa et al. 1997). These observations imply a general Ca^{2+} dependency and thus PAR_1's actions via $G\alpha_q$. Our Ca^{2+} assays displayed almost no elevation of the intracellular free Ca^{2+} concentration upon PAR_1 activation at the highest applied concentration of BAPTA-AM (Figure 3-6, page 45), but a minor enhancement of cytokine secretion was still achieved in the ELISAs (Figure 3-18, page 59). As shown by McLaughlin et al., abrogation of intracellular Ca^{2+} signaling by BAPTA-AM was not affecting PAR_1's actions via $G\alpha_{12/13}$ (McLaughlin et al. 2005). Therefore, a minor contribution via $G\alpha_{12/13}$ to the PAR_1-stimulated cytokine secretion may be possible.

All these observations point out an autocrine and paracrine activity of MSCs via IL-6 and IL-8, which are likely to contribute to favorable conditions for cancer cells. The treatment of diseased tissues with MSCs would bring the stem cells in proximity of active inflammation, coagulation and tissue remodeling, thus presumably causing PAR_1 activation in MSCs. As discussed above, this would cause enhanced expression and secretion of IL-6 and IL-8 by MSCs. The impact of these potent cytokines might cause beneficial or adverse effects on selected cell populations and processes and might favor curing diseased tissue. Cancerous cells that might occur in the liver during the progression of hepatitis, alcoholic liver diseases, cirrhosis and others can lead to the formation of HCC. Adding MSCs to these aberrant microenvironments would contribute an additional source of IL-6 and IL-8, and might cause unforeseeable effects on the HCC cells and the affected microenvironments.

In order to fathom the amounts of secreted cytokines that originate from MSCs, we correlated the concentrations of IL-6 and IL-8 from AT-MSC supernatants with the amount of total cellular protein, which was present during the conditioning of the medium, and compared the results to the values of cells from the HCC line Hep3B. As displayed in Figure 3-16 (page 57), we could show that AT-MSCs secreted a basal amount of about 1-2 pg IL-6 or IL-8 per µg of cells. Hep3B cells themselves hardly secreted IL-6 and approx. one-third of the IL-8 as the same amount of AT-MSCs.
So what would this larger amount of cytokines deriving from MSCs mean for Hep3B cells? Effects of IL-8 and IL-6 on Hep3B cells and other HCC cell lines were reported in several publications. Both cytokines have been shown to decrease sensitivity to potent anti-cancer drugs like doxorubicin. The expression of IL-8 and its receptor in HCC cells was shown to be increased by those drugs. Also, the knockdown of IL-8 showed a reduced proliferation *in vitro* and *in vivo*, as well as reduced expression and secretion of VEGF, EGF and HGF. Conditioned media of HCC cells with an IL-8 knockdown also exerted reduced potency to cause angiogenesis of human umbilical vein endothelial cells. (Choi et al. 2014; Liu et al. 2010; Park et al. 2009).

In conclusion, HCC cell lines are already generating self-stimulating microenvironments to favor their proliferation and survival, also by supporting surrounding angiogenesis. Adding MSCs into this context might increase the pool of angiogenic and anti-apoptotic cytokines that in turn will be promoted by the present coagulate microenvironment.

4.5 AT-MSCs promote Hep3B cell tumor formation at initial stages without the involvement of PAR_1 in a subcutaneous xenotransplantation SCID mouse model

The characterization of PAR_1 in AT-MSCs revealed that the stimulation of PAR_1 had a strong impact on the expression and secretion of IL-8 and especially IL-6. MCP-1 and other regulatory proteins might also be affected, although this has not been further investigated apart from initial overview analyses with antibody arrays. As discussed in paragraph 4.4 (page 78), IL-8 and IL-6 were reported to exert crucial impacts on HCC cell lines by favoring survival through pro-angiogenic and anti-apoptotic processes. Since clinicians intend to use MSCs as means of cellular therapy of e.g. diseased liver tissue, a direct or indirect interaction of MSCs and HCC cells may occur. Basal and stimulated secretion of a plethora of proteins by MSCs may provide complex stimuli and promote tumor growth. Hence, we assessed this complex issue with a xenograft tumor model in severe combined immunodeficiency (SCID) mice.

Immunodeficient mice were injected with the HCC cell line Hep3B or AT-MSCs alone, or with both cell types together. The cells were subcutaneously injected into the flank of the mice and tumor growth was analyzed after 11-26 days. The assays (Figure 3-21, page 64) revealed (I) a weak potency of 100,000 Hep3B cells to occasionally form tumors, (II) no potency of 500,000 AT-MSCs to form tumors, and that (III) the co-injection of Hep3B cells and AT-MSCs caused a strong formation of tumors in all assayed mice.

In this model that we employed for our investigations, the overall ability of Hep3B cells to form tumors was rather weak. Four out of nine mice showed tumor formation, and there was only a small difference in size between the tumors after eleven or after 26 days. Hep3B cells were frequently applied in xenograft tumor studies previously, but in most of the studies 5-10 Mio cells were injected, that is 50-100 times more cells than we applied in our experiments (Ryan et al. 2004; Tang et al. 2010; Tian et al. 2014; Zhao et al. 2013). However, these kinds of studies were intended to test conditions for reducing tumor formation. For our experiments, the small amount of Hep3B cells, which displayed a weak tumor formation ability, was well-suited in the combination with AT-MSCs. The presence of AT-MSCs increased the tumor formation ability of Hep3B cells drastically. All co-injections caused tumors with a much larger volume than the injections of Hep3B cells alone. The injections of AT-MSCs alone were not able to form tumors.

Histologically the 'Hep3B cell-AT-MSC tumors' resembled the structures of the Hep3B cell tumors. They showed typical features of HCC tissue, e.g. macro-trabecular structures, vesicular nuclei and pronounced nucleoli, mitotic figures, basophilic cytoplasm, and intratumoral necrotic areas. Also, the tumors showed positive Ki-67 stainings, which revealed a high proliferative character of the tumors. The tumors were also positive for cytokeratins, which are secreted by epithelial cells. Hep3B cells derive from aberrant hepatocytes, which are, unlike MSCs, epithelial cells. In addition, the tumors showed vessel formation on the inner mouse skin towards the tumor, and the tumor tissue was highly positive for alpha-smooth muscle actin (α-SMA), especially at the tumor margins. A-SMA is a marker for myoepithelial cells, smooth muscle cells and myofibroblasts and thus hints at the presence of vessels (Skalli et al. 1989). Though there is some literature data on the α-SMA expression in MSCs, they reported only low expression levels of α-SMA and only approx. 15 % of an MSC population were positive for α-SMA in immunocytochemical stainings (Hung et al. 2006; Tamama, Sen, & Wells 2008). Therefore, it seems unlikely that the α-SMA stainings of our experiments represented the AT-MSCs since we were not able to detect them in the tumors of assays with green fluorescent protein (GFP)-labeled MSCs, which will be discussed later. Also, the higher distribution of α-SMA-positive cells at the tumor margins implies increasing protrusion/formation of new vessels from the surrounding microenvironment into the tumor.

At least under the applied conditions of the co-injection of 100,000 Hep3B cells and 500,000 AT-MSCs, the AT-MSCs seemed to favor the formation of a Hep3B cell tumor.

Since MSCs are capable of differentiating into a variety of cell lineages, it generates the question of whether they contributed to the Hep3B cell tumor formation in some way. The injection of MSCs alone revealed no growth of a tumor beneath the murine skin after 11-26 days. Hence, it seems that the AT-MSCs did not survive the *in vivo* assay or got incorporated into the murine tissue without a trace. Also, incorporation or fusion with surrounding Hep3B cells could occur in the co-injection model, including taking over of epithelial characteristics. MSCs were demonstrated to fuse with liver tissue in transplantation models and Ferrand et al. showed that BM-MSCs took over epithelial characteristics of gastrointestinal epithelial cells in a co-culture model (Ferrand et al. 2011; Vassilopoulos, Wang, & Russell 2003; Wang et al. 2003). However, engraftment of locally administered MSCs into host tissue was reported to make up 3.5 % of the total administered cells (Rustad & Gurtner 2012). Therefore, it is doubtful that most of the AT-MSCs would persist in the tumor in an either singular or fused state. Moreover, the complete trans-differentiation of the AT-MSCs into hepatocytes seems also doubtful, since direct co-cultures of Hep3B cells and AT-MSCs gave no rise to changes of the stem cells (unpublished data from the group of Prof. B. Christ, University Hospital Leipzig, Germany).
The AT-MSCs' contribution to the tumor via aberrations might be another potential source of tumor cells. There have been reports of spontaneous chromosomal aberrations of *ex vivo* cultured MSCs that led to stem cell-derived tumors *in vivo*. However, the observed events led to sarcoma formation in proximity to vascular smooth muscle cells or were mainly due to long-term cultured MSCs (Hatzistergos et al. 2011; Jeong et al. 2011). In our case, as will be discussed later, long-term-cultured and transduction protocol-exposed AT-MSCs led to a reduced tumor formation in the applied xenotransplantation model.

The observed tumor formations raised the question of how AT-MSCs promoted Hep3B cells' survival and proliferation. The Hep3B cells might have been favored by the presence of AT-MSCs in several ways. Both cell types were mixed and injected as a homogenous suspension underneath the skin of mice. Since the ratio was 5:1 AT-MSCs to Hep3B cells, it is imaginable that most of the Hep3B cells were surrounded by AT-MSCs. Most likely, this larger batch of cells prevented scattering of single Hep3B cells at the point of inoculation and might have kept the tumor cells closer together. This close contact with each other presumably favors the actions of the secreted factors from AT-MSCs and tumor cells, respectively. Though a direct action of conditioned AT-MSC media on Hep3B cells could not be shown at *in vitro* conditions (Winkler et al. 2015), secreted growth factors might still promote

Hep3B cell proliferation *in vivo*. The strong vascularization towards and inside the tumors indicated a well-organized angiogenesis in the tumor microenvironment.

The AT-MSCs were shown to secrete a variety of angiogenesis-promoting and immunoregulatory factors like angiopoietin 1, VEGF, IL-8, IL-6 and MCP-1. As introduced in paragraph 1.2.3 (page 7) and discussed in paragraph 4.4 (page 78), these factors were frequently reported to promote autocrine and paracrine stimulations of HCC-cells and MSCs, as well as the induction of angiogenesis. Single tumor cells will need time and effort to overcome the initial lag phase to reach a stable tumor mass with sufficient oxygen supply. At this stage, the presence of MSCs might promote the Hep3B cells greatly by stimulating surrounding angiogenesis, limiting inflammation and supplying a variety of growth factors, extracellular matrix proteins and proteinases to establish a niche for tumor-initiating cells (Plaks, Kong, & Werb 2015).

Summing up, it is worth to note that, under conditions of the employed *in vivo* mouse model, small numbers of Hep3B tumor cells were proliferating much better when surrounded by AT-MSCs. Events like this might occur when MSCs get inoculated into HCC-affected tissue as means of cellular therapy. Locally the ratio of MSCs and HCC cells will tend towards the MSCs, and few HCC cells might benefit from their new neighbors.

We are the first to show these promoting effects of AT-MSCs on the *in vivo* proliferation of cells from the HCC cell line Hep3B. In a similar approach, Han et al. employed the subcutaneous co-injection of MSCs and the HCC cell line SMMC-7721 into mice. They observed minor contributions of MSCs to the HCC tumor growth but observed major contribution if the MSCs were pretreated with proinflammatory interferon γ (IFN-γ) and tumor necrosis factor α (TNF-α). However, they did not mention the tissue origin of the MSCs and they employed twice as many MSCs and 60 times as many tumors cells. Hence, the number of tumor cells was five times larger than the number of MSCs, thus making it difficult to compare the results to our model due to significant differences in cell counts (Han et al. 2014).

Yang et al. showed similar data for MSCs and gastric cancer cells. Their project was dedicated to investigating the interaction of macrophages and umbilical cord-derived MSCs and their impact on gastric cancer cells. They showed that the co-culture of MSCs with macrophages enhanced the expression and secretion of IL-6, IL-8, MCP-1, VEGF and others by MSCs, which we also detected in supernatants of AT-MSCs. Those macrophage-activated MSCs were able to promote tumor growth of gastric cancer cell and proliferation and migration of gastric epithelial cells. Unstimulated control MSCs were also able to increase tumor proliferation *in vivo*, but with less impact (Yang et al. 2014).

Therefore, the attraction of monocytes to the tumor might be enhanced by MSCs, and the cytokine crosstalk between them and the tumor cells may contribute to the observed enhancement of tumor

growth in the presence of MSCs. This notion is supported by our data showing that MCP-1 was secreted by AT-MSCs (Figure 3-14, page 55) and that its expression was enhanced by PAR_1 stimulation (Figure 3-15, page 56). MCP-1 is a potent monocyte/macrophage attractor and will attract them to inflammation or tumor sites (Deshmane et al. 2009).

AT-MSCs promote initial Hep3B cell tumor formation

The subcutaneous co-injection of Hep3B cells and AT-MSCs into the flank of SCID mice caused a strong formation of tumors. The histologic stainings revealed the epithelial origin and HCC-like polygonal cells in a macro-trabecular pattern, thus implying a Hep3B cell-derived tumor mass. However, one question remained: What happens to the AT-MSCs during tumor formation? Unfortunately, stem cells do not bear single stem cell-specific markers to detect them specifically. Therefore, we labeled the AT-MSCs with green fluorescent protein (GFP) to trace their fate during tumor formation. Some publications stated that stem cells engraft into the liver tissue by cell fusion (Vassilopoulos, Wang, & Russell 2003; Wang et al. 2003). Hence, in the case of persisting AT-MSCs or fused AT-MSC-Hep3B cells, we should detect GFP in the sliced tumors. However, we did not detect green fluorescing cells in the otherwise well-formed tumors. Though this was only one approach, a similar xenotransplantation model was carried out by our collaborators from Leipzig, with no detection of GFP inside the tumor slices, apart from single green fluorescing fragments. Furthermore, our collaborators showed using *in vitro* co-cultures that the Hep3B cells easily outgrow the AT-MSCs after a few days and limit their space for proliferation (Winkler et al. 2015). Therefore, it seemed plausible that the percentage of AT-MSCs would decrease over time in the arising tumor and perhaps proliferating Hep3B cells would limit the proliferation of the AT-MSCs, too.

Based on the tumor volume and the hematoxylin and eosin staining of the presented tumor in Figure 3-23 (page 67), we estimated how many AT-MSCs we could expect in a magnified area (0.1 mm^2) like in the tumor panel if their count would stagnate and persist throughout the formation of the tumor. The particular tumor of Figure 3-23 had an average of approx. 18 nuclei/cells per 200 µm segment, which equals 5832 cells per 0.008 mm^3 and approx. 48 Mio cells for the total tumor volume (66.16 mm^3). If the 500,000 initially injected stem cells would have persisted until the day of the tumor removal, it would have meant that every 96^{th} cell should be an AT-MSC within the displayed images. The area of the tumor cross-section was 5.6 mm^2 large, thus comprising approx. 45,360 cells in total, including 473 potential AT-MSCs. A magnified area (0.1 mm^2) should, therefore, comprise around 8.5 stem cells.

Hence, for the case that the injected AT-MSCs were proliferating or, at least, surviving, we could expect some GFP signal. Perhaps, fixation issues might have caused damage to the GFP and its fluorescence emitting properties, thus leaving the cells invisible under the fluorescence microscope. The

immunohistochemical staining of the tumor slices with a GFP-targeting antibody could shed more light on this hypothesis. However, it might also be plausible that the AT-MSCs did not survive the tumor formation over 24 d. Therefore, the promotion of tumor formation might have been due to initial stimuli on the Hep3B cells and surrounding murine tissue, thus promoting angiogenesis and the formation of a favorable tumor niche and survival of the tumor cells.

PAR_1 gene knockdown in AT-MSCs has no significant effect on Hep3B cell tumor formation

The enhanced Hep3B cell tumor formation under the presence of AT-MSCs may depend on paracrine stem cell-derived stimuli that affect the Hep3B cells and surrounding tissue. As discussed in the previous paragraphs, we were able to show for the first time that PAR_1 activation in AT-MSCs caused an upregulation of MCP-1, IL-8 and IL-6 expression and secretion of especially the latter two. These cytokines are known to exert crucial impacts on *in vivo* tumor formations, hence making the effects of PAR_1 activation in AT-MSCs potential tumor contributors.

For the purpose of assessing the impact of PAR_1 in AT-MSCs on the size of resulting Hep3B cell tumors at *in vivo* conditions, a protocol for knocking down PAR_1 in AT-MSCs was established. The PAR_1 knockdown cells were then subcutaneously co-injected with Hep3B cells into the flank of SCID mice. Tumor formation was compared to co-injections with Hep3B cells and AT-MSCs, which were transduced with control non-target shRNA.

The knockdown protocol included one passage and about two weeks of cell culture. No obvious aberrations and cell changes were observed during this process. As seen in Figure 3-20 (page 61), PAR_1 was knocked down to a remaining presence of approx. 17 % in AT-MSCs. For the purpose of generating a sufficient amount of cells for the *in vivo* studies, the total knockdown and expansion process required two passages and four weeks of culture. Over that time, the stem cells appeared larger, and the rate of proliferation decreased. We tested the cells with flow cytometry and the scatter data revealed that the relative cell volume of the transduced AT-MSCs did not change compared to wild type AT-MSCs. Apparently, the transduced cells were attaching and spreading more than their wild type counterparts. Nevertheless, the AT-MSC-PAR_1KD (knockdown) and AT-MSC-nt (non-target) showed a shifted side scatter in the flow cytometry parameter, thus implying increased granularity or complexity of the cells. All of these observations could indicate the onset of cellular senescence (Muñoz-Espín & Serrano 2014).

The co-injection of Hep3B cells with AT-MSCs of either PAR_1 knockdown or non-target control caused the formation of large, medium and small tumors of comparable sizes in most assayed mice. Some did not show any tumor formation. However, compared to the constant tumor formation obtained by the injection of Hep3B cells with wild type AT-MSCs, the lentivirally-guided modified AT-MSCs appeared to have a diminished ability to form tumors in general. These observations implied that the AT-MSCs

might have succumbed to the long *in vitro* transduction protocol, thus having a reduced impact on the tumor formation, and presumably did not contribute to the tumor by own aberrations as discussed earlier (page 82). Still, their potential was sufficient to promote Hep3B cell tumor formation with HCC-like histologic characteristics in most of the assayed mice.

After all, the obtained tumor volumes of this xenotransplant approach did not show a significant impact of the PAR_1 knockdown in AT-MSCs on the Hep3B cell tumor formation, compared to the control group with the non-target control vector. However, this technique might not take into consideration that the non-target control AT-MSCs had a diminished impact on the tumor formation themselves, compared to the more consistent impacts of wild type AT-MSCs, which could overshadow minor impacts of PAR_1.

5 Conclusions & Outlook

Mesenchymal stem cells (MSCs) provide a valuable resource for the treatment of diseased tissues like chronic wounds or especially liver cirrhosis. However, inflammation- and coagulation-affected tissues produce proteinases that activate proteinase-activated receptors (PARs), which are insufficiently characterized in MSCs. In this context, we characterized the PAR family in adipose tissue-derived (AT)-MSCs. Our results pointed out that PAR_1 was the predominating PAR subtype in AT-MSCs. While PAR_2 and PAR_3 were present and mediated weak responses in the cells, PAR_4 was barely detected and might have no major impact on the AT-MSC's biology.

We showed that PAR_1 played a crucial role in the upregulation of expression and secretion of interleukins (IL) 6 and 8 in AT-MSCs. Our data suggests a major dependence of the PAR_1-elicited elevation on the intracellular free Ca^{2+} level and the Ca^{2+}-dependent protein kinase C (PKC) for cytokine production and secretion. However, further detailed investigations are required to unveil the involved signaling cascades and to clarify to what extent the observed enhanced expression contributes to the elevated secretion of cytokines (Figure 5-1).

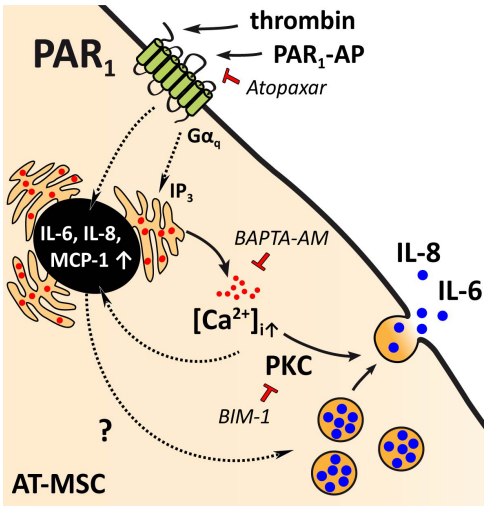

Figure 5-1: Schematic overview of PAR_1's actions in AT-MSCs

The image summarizes the results of our PAR_1 assays in AT-MSCs. Dashed lines represent hypothesized and elsewhere described signaling and may present interesting research targets for the future.

PAR_1 was found to represent the predominantly expressed PAR subtype in AT-MSCs. Stimulation with thrombin or PAR_1-AP caused a strong elevation of the intracellular free Ca^{2+} concentration ($[Ca^{2+}]_i$), an elevated secretion of IL-6 and IL-8 into the supernatant growth medium, and an enhanced expression of IL-6, IL-8 and MCP-1. Those observations were attenuated by pre-treatment with the PAR_1 antagonist Atopaxar. Pre-treatment with the Ca^{2+} chelator BAPTA-AM or the PKC inhibitor BIM-1 attenuated the amounts of secreted IL-6 and IL-8.

In consideration of employing MSCs as means of cell-based therapy of hepatic diseases, we assessed the *in vivo* interaction of AT-MSCs with cells from the hepatocellular carcinoma (HCC) cell line Hep3B. We observed a strong promotion of tumor formation of Hep3B cells if they were subcutaneously co-injected with AT-MSCs into immunodeficient mice. The tumors resembled HCC characteristics and showed no signs of persisting AT-MSCs, thus hinting on a promotion of the tumor formation during early stages. Additional investigations with other HCC cell lines and variations of inoculated cell numbers of the two cell types may shed further light on the controversial issue of MSCs' impact on tumor cells. Nevertheless, we found a plethora of potentially tumor-promoting factors in the supernatants of AT-MSCs. Since PAR_1 was found to promote the secretion of several factors, we hypothesized an influence of PAR_1 in

AT-MSCs on the tumor formation model. However, the lentivirally-guided transduction of shRNA to knockdown PAR_1 in AT-MSCs had no significant effect on the final tumor volume, compared to non-target shRNA transduced cells. The transduction protocol might have caused detrimental effects on the AT-MSCs' survival since both groups showed reduced abilities to form tumors. Hence, different approaches should be considered to verify the data.

In conclusion, we provide data that may help to understand better the curative effects of MSCs for cirrhosis and liver failure. However, chronic liver diseases bear the chance of resulting in the formation of HCC beneath the level of detection at initial medical diagnosis. At these conditions, few tumor cells may benefit greatly from a larger amount of neighboring exogenous stem cells. Additionally, the activation of MSCs inside the tumor microenvironment might increase the secretion of potential tumor promoting factors, as described in the thesis and other publications. PAR_1 might be one of the factors to contribute to the impact of MSCs on diseased tissue.

6 Acknowledgements

The time has come to thank all the authorities, minds, helping hands, and restless supporters that contributed to this work…

My deep gratitude goes to the Deutsche Forschungsgemeinschaft (DFG) and Prof. U. Settmacher for supporting this research project and giving me the opportunity to work on it.
No words mean to express my gratitude to Dr. R. Kaufmann and Prof. F. Böhmer, my guiding beacons of knowledge and wisdom, who always had a helping idea or soothing sense of humor when things went wrong or didn't work out the way we expected.
Thanks to the patients and the hospital in Leipzig that contributed the endless stem cells for making this research possible. Thank you, Prof. B. Christ, for the generous collaboration and courier services and for opening up this intriguing stem cell topic to our group and me. Thank you, Madlen and Sandra, for the continuous preparation of the cells, medium and information that I required, and the kind support in times of late and urgent requests.
Thank you, Jörg and Annette for technical and theoretical support along the bench and lab work and for bringing so much culture, joy and activities into my life.
Thanks to all the people that helped me realize the specialized assays: electron microscopy, Dr. Westermann, Beate; mice assays, Dr. Günther, Yvonne, Elke, Kathrin. You were amazing, and I couldn't ask for any better support! Thank you, Prof. R. Heller, and her group for the continuous support, the opportunity for the side activity as a tutor and for drawing my attention to the vacant PhD position. Another big thank you goes to the ones making life easy in the lab, thank you Dorith, Manu and Ute for providing reliable and clean material.

Thank you to all my fellow students and lab mates for making this period a time of scientific, cultural, culinary and humorous exchange. This time has been amazing!
Franzi, my dearest colleague and courier between our labs, you were always there when I needed specific information and more material from the other lab at short notice. Your restless support, candor and sincerity made this project much easier and saved me lots of time and trouble.
Thank you to my beloved friends and family for supporting me in all conditions of life, mood and matters. I couldn't have done it without you!

Thank you, धन्यवाद, faleminderit, ευχαριστώ, merci, grazie, und einfach nur vielen Dank für die schöne Zeit ☺

Thank you for the cookies!

7 List of figures

8 List of tables

9 References

Adams DH, & Hubscher SG. (2006). *Systemic Viral Infections and Collateral Damage in the Liver*. The American Journal of Pathology, *168*(4), 1057–1059.

Adams MN, Ramachandran R, Yau M-K, Suen JY, Fairlie DP, Hollenberg MD, & Hooper JD. (2011). *Structure, function and pathophysiology of protease activated receptors*. Pharmacology & Therapeutics, *130*(3), 248–282.

Aden DP, Fogel A, Plotkin S, Damjanov I, & Knowles BB. (1979). *Controlled synthesis of HBsAg in a differentiated human liver carcinoma-derived cell line*. Nature, *282*(5739), 615–616.

Ahmed M. (2015). *Non-alcoholic fatty liver disease in 2015*. World Journal of Hepatology, *7*(11), 1450–1459.

Ali SH, & DeCaprio JA. (2001). *Cellular transformation by SV40 large T antigen: interaction with host proteins*. Seminars in Cancer Biology, *11*(1), 15–23.

Al-Khafaji K, Mutyala M, Al-Khafaji N, Harper Y, Ismail I, Hakim H, & Arora RR. (2015). *Protease-Activated Receptor 1 Inhibitors: Novel Antiplatelet Drugs in Prevention of Atherothrombosis*. American Journal of Therapeutics.

Arakaki PA, Marques MR, & Santos MCLG. (2009). *MMP-1 polymorphism and its relationship to pathological processes*. Journal of Biosciences, *34*(2), 313–320.

Aravalli RN. (2010). *Progress in stem cell-derived technologies for hepatocellular carcinoma*. Stem Cells and Cloning : Advances and Applications, *3*, 81–92.

Attwa MH, & El-Etreby SA. (2015). *Guide for diagnosis and treatment of hepatocellular carcinoma*. World Journal of Hepatology, *7*(12), 1632–1651.

Aurich I, Mueller LP, Aurich H, Luetzkendorf J, Tisljar K, Dollinger MM, … Christ B. (2007). *Functional integration of hepatocytes derived from human mesenchymal stem cells into mouse livers*. Gut, *56*(3), 405–415.

Baer PC, & Geiger H. (2012). *Adipose-derived mesenchymal stromal/stem cells: tissue localization, characterization, and heterogeneity*. Stem Cells International, *2012*, 812693.

Bauvois B. (2012). *New facets of matrix metalloproteinases MMP-2 and MMP-9 as cell surface transducers: Outside-in signaling and relationship to tumor progression*. Biochimica et Biophysica Acta (BBA) - Reviews on Cancer, *1825*(1), 29–36.

Bavle RM. (2014). *Eosinophilic nucleoli*. Journal of Oral and Maxillofacial Pathology : JOMFP, *18*(2), 152–154.

Bayo J, Marrodán M, Aquino JB, Silva M, García MG, & Mazzolini G. (2013). *The therapeutic potential of bone marrow-derived mesenchymal stromal cells on hepatocellular carcinoma*. Liver International: Official Journal of the International Association for the Study of the Liver.

Boomsma RA, & Geenen DL. (2012). *Mesenchymal Stem Cells Secrete Multiple Cytokines That Promote Angiogenesis and Have Contrasting Effects on Chemotaxis and Apoptosis*. PLoS ONE, *7*(4).

Borensztajn K, Von Der Thüsen JH, Peppelenbosch MP, & Spek CA. (2010). *The coagulation factor Xa/protease activated receptor-2 axis in the progression of liver fibrosis: a multifaceted paradigm*. Journal of Cellular and Molecular Medicine, *14*(1-2), 143–153.

Brandes RP, Viedt C, Nguyen K, Beer S, Kreuzer J, Busse R, & Görlach A. (2001). *Thrombin-induced MCP-1 Expression Involves Activation of the p22phox-containing NADPH Oxidase in Human Vascular Smooth Muscle Cells*. Thromb Haemost, *85*(6), 1104–1110.

Brass LF, Pizarro S, Ahuja M, Belmonte E, Blanchard N, Stadel JM, & Hoxie JA. (1994). *Changes in the structure and function of the human thrombin receptor during receptor activation, internalization, and recycling.* Journal of Biological Chemistry, *269*(4), 2943–2952.

Bustin SA, Benes V, Garson JA, Hellemans J, Huggett J, Kubista M, … Wittwer CT. (2009). *The MIQE Guidelines: Minimum Information for Publication of Quantitative Real-Time PCR Experiments*. Clinical Chemistry, *55*(4), 611–622.

Chan JKC. (2014). *The Wonderful Colors of the Hematoxylin–Eosin Stain in Diagnostic Surgical Pathology*. International Journal of Surgical Pathology, *22*(1), 12–32.

Chan SL, & Yeo W. (2012). *Targeted therapy of hepatocellular carcinoma: Present and future*. Journal of Gastroenterology and Hepatology, *27*(5), 862–872.

Charles River. (2015). *Fox Chase SCID® Mouse*. Retrieved July 11, 2015, from http://www.criver.com/products-services/basic-research/find-a-model/fox-chase-scid-mouse

Chen J, Ma Y-J, Wang Z, Lin S-S, Xiao F-J, Wang H, Wang L-S, & Guo Z-K. (2014a). *[Promoting effect of thrombin on proliferation of bone marrow-derived mesenchymal stem cells and its mechanisms]*. Zhongguo Shi Yan Xue Ye Xue Za Zhi / Zhongguo Bing Li Sheng Li Xue Hui = Journal of Experimental Hematology / Chinese Association of Pathophysiology, *22*(2), 485–490.

Chen J, Ma Y, Wang Z, Wang H, Wang L, Xiao F, Wang H, Tan J, & Guo Z. (2014b). *Thrombin promotes fibronectin secretion by bone marrow mesenchymal stem cells via the protease-activated receptor mediated signalling pathways*. Stem Cell Research & Therapy, *5*(2), 36.

Chen M, Suzuki A, Borlak J, Andrade RJ, & Lucena MI. (2015a). *Drug-induced liver injury: Interactions between drug properties and host factors*. Journal of Hepatology, *63*(2), 503–514.

Chen Y-X, Zeng Z-C, Sun J, Zeng H-Y, Huang Y-, & Zhang Z-Y. (2015b). *Mesenchymal stem cell–conditioned medium prevents radiation-induced liver injury by inhibiting inflammation and protecting sinusoidal endothelial cells*. Journal of Radiation Research, *56*(4), 700–708.

Choi SH, Kwon O-J, Park JY, Kim DY, Ahn SH, Kim SU, … Han K-H. (2014). *Inhibition of tumour angiogenesis and growth by small hairpin HIF-1α and IL-8 in hepatocellular carcinoma*. Liver International: Official Journal of the International Association for the Study of the Liver, *34*(4), 632–642.

Christ B, Brückner S, & Stock P. (2011). *Hepatic transplantation of mesenchymal stem cells in rodent animal models*. Methods in Molecular Biology (Clifton, N.J.), *698*, 315–330.

Christ B, & Pelz S. (2013). *Implication of hepatic stem cells in functional liver repopulation*. Cytometry. Part A: The Journal of the International Society for Analytical Cytology, *83*(1), 90–102.

Colotta F, Sciacca FL, Sironi M, Luini W, Rabiet MJ, & Mantovani A. (1994). *Expression of monocyte chemotactic protein-1 by*

monocytes and endothelial cells exposed to thrombin. The American Journal of Pathology, *144*(5), 975–985.

Coughlin SR. (2000). *Thrombin signalling and protease-activated receptors*. Nature, *407*(6801), 258–264.

Coughlin SR, & Camerer E. (2003). *PARticipation in inflammation*. The Journal of Clinical Investigation, *111*(1), 25–27.

Cui H, Tan W, Shi J, & Xia Y. (2012). *Recent Development in Thrombin Receptor Antagonist as Novel Antithrombotic Agent*. Open Journal of Medicinal Chemistry, *2*(4), 112–118.

Cunningham CC, & Van Horn CG. (2003). *Energy availability and alcohol-related liver pathology*. Alcohol Research & Health: The Journal of the National Institute on Alcohol Abuse and Alcoholism, *27*(4), 291–299.

Dagouassat M, Suffee N, Hlawaty H, Haddad O, Charni F, Laguillier C, … Charnaux N. (2010). *Monocyte chemoattractant protein-1 (MCP-1)/CCL2 secreted by hepatic myofibroblasts promotes migration and invasion of human hepatoma cells*. International Journal of Cancer, *126*(5), 1095–1108.

Davis HE, Morgan JR, & Yarmush ML. (2002). *Polybrene increases retrovirus gene transfer efficiency by enhancing receptor-independent virus adsorption on target cell membranes*. Biophysical Chemistry, *97*(2–3), 159–172.

Davis HE, Rosinski M, Morgan JR, & Yarmush ML. (2004). *Charged Polymers Modulate Retrovirus Transduction via Membrane Charge Neutralization and Virus Aggregation*. Biophysical Journal, *86*(2), 1234–1242.

DeFea KA, Zalevsky J, Thoma MS, Déry O, Mullins RD, & Bunnett NW. (2000). *beta-arrestin-dependent endocytosis of proteinase-activated receptor 2 is required for intracellular targeting of activated ERK1/2*. The Journal of Cell Biology, *148*(6), 1267–1281.

De Luca A, Lamura L, Gallo M, Maffia V, & Normanno N. (2012). *Mesenchymal stem cell-derived interleukin-6 and vascular endothelial growth factor promote breast cancer cell migration*. Journal of Cellular Biochemistry, *113*(11), 3363–3370.

Deshmane SL, Kremlev S, Amini S, & Sawaya BE. (2009). *Monocyte Chemoattractant Protein-1 (MCP-1): An Overview*. Journal of Interferon & Cytokine Research, *29*(6), 313–326.

Dhillon AS, Hagan S, Rath O, & Kolch W. (2007). *MAP kinase signalling pathways in cancer*. Oncogene, *26*(22), 3279–3290.

Dominici M, Le Blanc K, Mueller I, Slaper-Cortenbach I, Marini F, Krause D, … Horwitz E. (2006). *Minimal criteria for defining multipotent mesenchymal stromal cells. The International Society for Cellular Therapy position statement*. Cytotherapy, *8*(4), 315–317.

Duplantier JG, Dubuisson L, Senant N, Freyburger G, Laurendeau I, Herbert J-M, Desmoulière A, & Rosenbaum J. (2004). *A role for thrombin in liver fibrosis*. Gut, *53*(11), 1682–1687.

Dwyer RM, Potter-Beirne SM, Harrington KA, Lowery AJ, Hennessy E, Murphy JM, Barry FP, O'Brien T, & Kerin MJ. (2007). *Monocyte Chemotactic Protein-1 Secreted by Primary Breast Tumors Stimulates Migration of Mesenchymal Stem Cells*. Clinical Cancer Research, *13*(17), 5020–5027.

El-Serag HB. (2011). *Hepatocellular carcinoma*. The New England Journal of Medicine, *365*(12), 1118–1127.

European Association for the Study of the Liver, & European Organisation for Research and Treatment of Cancer. (2012). *EASL–EORTC Clinical Practice Guidelines: Management of hepatocellular carcinoma*. Journal of Hepatology, *56*(4), 908–943.

Falanga A. (2011). *The Cancer-Thrombosis Connection*. Retrieved August 5, 2014, from http://www.hematology.org/Thehematologist/Mini-Review/1244.aspx

Farazi PA, & DePinho RA. (2006). *Hepatocellular carcinoma pathogenesis: from genes to environment*. Nature Reviews. Cancer, *6*(9), 674–687.

Ferrand J, Noël D, Lehours P, Prochazkova-Carlotti M, Chambonnier L, Ménard A, Mégraud F, & Varon C. (2011). *Human Bone Marrow-Derived Stem Cells Acquire Epithelial Characteristics through Fusion with Gastrointestinal Epithelial Cells*. PLoS ONE, *6*(5), e19569.

Fiorucci S, Antonelli E, Distrutti E, Severino B, Fiorentina R, Baldoni M, … Cirino G. (2004). *PAR1 antagonism protects against experimental liver fibrosis. Role of proteinase receptors in stellate cell activation*. Hepatology, *39*(2), 365–375.

Forte G, Minieri M, Cossa P, Antenucci D, Sala M, Gnocchi V, … Di Nardo P. (2006). *Hepatocyte growth factor effects on mesenchymal stem cells: proliferation, migration, and differentiation*. Stem Cells (Dayton, Ohio), *24*(1), 23–33.

Friedenstein AJ, Gorskaja JF, & Kulagina NN. (1976). *Fibroblast precursors in normal and irradiated mouse hematopoietic organs*. Experimental Hematology, *4*(5), 267–274.

Fujimoto K. (1995). *Freeze-fracture replica electron microscopy combined with SDS digestion for cytochemical labeling of integral membrane proteins. Application to the immunogold labeling of intercellular junctional complexes*. Journal of Cell Science, *108 (Pt 11)*, 3443–3449.

Gaça MDA, Zhou X, & Benyon RC. (2002). *Regulation of hepatic stellate cell proliferation and collagen synthesis by proteinase-activated receptors*. Journal of Hepatology, *36*(3), 362–369.

Gaffney PJ, & Edgell TA. (1995). *The International and "NIH" units for thrombin--how do they compare?* Thrombosis and Haemostasis, *74*(3), 900–903.

Garnier D, Milsom C, Magnus N, Meehan B, Weitz J, Yu J, & Rak J. (2010). *Role of the tissue factor pathway in the biology of tumor initiating cells*. Thrombosis Research, *125 Suppl 2*, S44–50.

Ghosh AK, & Vaughan DE. (2012). *PAI-1 in tissue fibrosis*. Journal of Cellular Physiology, *227*(2), 493–507.

Gieseler F, Ungefroren H, Settmacher U, Hollenberg MD, & Kaufmann R. (2013). *Proteinase-activated receptors (PARs) - focus on receptor-receptor-interactions and their physiological and pathophysiological impact*. Cell Communication and Signaling: CCS, *11*, 86.

Goel HL, & Mercurio AM. (2013). *VEGF targets the tumour cell*. Nature Reviews Cancer, *13*(12), 871–882.

Gordon JR, Zhang X, Stevenson K, & Cosford K. (2000). *Thrombin Induces IL-6 but Not TNFα Secretion by Mouse Mast Cells: Threshold-Level Thrombin Receptor and Very Low Level FcεRI Signaling Synergistically Enhance IL-6 Secretion*. Cellular Immunology, *205*(2), 128–135.

Grishina Z, Ostrowska E, Halangk W, Sahin-Tóth M, & Reiser G. (2005). *Activity of recombinant trypsin isoforms on human proteinase-activated receptors (PAR): mesotrypsin cannot activate epithelial PAR-1, -2, but weakly activates brain PAR-1*. British Journal of Pharmacology, *146*(7), 990–999.

Hamilton JR, Cornelissen I, & Coughlin SR. (2004). *Impaired hemostasis and protection against thrombosis in protease-activated receptor 4-deficient mice is due to lack of thrombin signaling in platelets*. Journal of Thrombosis and Haemostasis: JTH, *2*(8), 1429–1435.

Hansen KK, Saifeddine M, & Hollenberg MD. (2004). *Tethered ligand-derived peptides of proteinase-activated receptor 3 (PAR3) activate PAR1 and PAR2 in Jurkat T cells*. Immunology, *112*(2), 183–190.

Han Z, Jing Y, Xia Y, Zhang S, Hou J, Meng Y, … Wei L. (2014). *Mesenchymal stem cells contribute to the chemoresistance of hepatocellular carcinoma cells in inflammatory environment by inducing autophagy*. Cell & Bioscience, *4*, 22.

Hass R, & Otte A. (2012). *Mesenchymal stem cells as all-round supporters in a normal and neoplastic microenvironment*. Cell Communication and Signaling: CCS, *10*(1), 26.

Hatzistergos KE, Blum A, Ince TA, Grichnik JM, & Hare JM. (2011). *What Is the Oncologic Risk of Stem Cell Treatment for Heart Disease?* Circulation Research, *108*(11), 1300–1303.

Heider I, Schulze B, Oswald E, Henklein P, Scheele J, & Kaufmann R. (2004). *PAR1-Type Thrombin Receptor Stimulates Migration and Matrix Adhesion of Human Colon Carcinoma Cells by a PKC-Dependent Mechanism*. Oncology Research Featuring Preclinical and Clinical Cancer Therapeutics, *14*(10), 475–482.

Herrmann JL, Weil BR, Abarbanell AM, Wang Y, Poynter JA, Manukyan MC, & Meldrum DR. (2011). *IL-6 and TGF-α Costimulate Mesenchymal Stem Cell Vascular Endothelial Growth Factor Production by ERK-, JNK-, and PI3K-Mediated Mechanisms:* Shock, *35*(5), 512–516.

Hilfiker S, & Augustine GJ. (1999). *Regulation of synaptic vesicle fusion by protein kinase C*. The Journal of Physiology, *515*(Pt 1), 1.

Hou Y, Ryu CH, Jun JA, Kim SM, Jeong CH, & Jeun S-S. (2014). *IL-8 enhances the angiogenic potential of human bone marrow mesenchymal stem cells by increasing vascular endothelial growth factor*. Cell Biology International, *38*(9), 1050–1059.

Hsiao ST-F, Asgari A, Lokmic Z, Sinclair R, Dusting GJ, Lim SY, & Dilley RJ. (2012). *Comparative analysis of paracrine factor expression in human adult mesenchymal stem cells derived from bone marrow, adipose, and dermal tissue*. Stem Cells and Development, *21*(12), 2189–2203.

Hung S-C, Kuo P-Y, Chang C-F, Chen T-H, & Ho LL-T. (2006). *Alpha-smooth muscle actin expression and structure integrity in chondrogenesis of human mesenchymal stem cells*. Cell and Tissue Research, *324*(3), 457–466.

Iavarone M, Lampertico P, Iannuzzi F, Manenti E, Donato MF, Arosio E, … Colombo M. (2007). *Increased expression of vascular endothelial growth factor in small hepatocellular carcinoma*. Journal of Viral Hepatitis, *14*(2), 133–139.

Jansen BJH, Gilissen C, Roelofs H, Schaap-Oziemlak A, Veltman JA, Raymakers RAP, … Adema GJ. (2009). *Functional Differences Between Mesenchymal Stem Cell Populations Are Reflected by Their Transcriptome*. Stem Cells and Development, *19*(4), 481–490.

Jeon B-J, Yang Y, Kyung Shim S, Yang H-M, Cho D, & Ik Bang S. (2013). *Thymosin beta-4 promotes mesenchymal stem cell proliferation via an interleukin-8-dependent mechanism*. Experimental Cell Research, *319*(17), 2526–2534.

Jeong J-O, Han JW, Kim J-M, Cho H-J, Park C, Lee N, Kim D-W, & Yoon Y-S. (2011). *Malignant Tumor Formation After Transplantation of Short-Term Cultured Bone Marrow Mesenchymal Stem Cells in Experimental Myocardial Infarction and Diabetic Neuropathy*. Circulation Research, *108*(11), 1340–1347.

Johnson C, Han Y, Hughart N, McCarra J, Alpini G, & Meng F. (2012). *Interleukin-6 and its receptor, key players in hepatobiliary inflammation and cancer*. Translational Gastrointestinal Cancer, *1*(1), 58–70.

Juncker-Jensen A, Deryugina EI, Rimann I, Zajac E, Kupriyanova TA, Engelholm LH, & Quigley JP. (2013). *Tumor MMP-1 Activates Endothelial PAR1 to Facilitate Vascular Intravasation and Metastatic Dissemination*. Cancer Research, *73*(14), 4196–4211.

Kang J-H. (2014). *Protein Kinase C (PKC) Isozymes and Cancer, Protein Kinase C (PKC) Isozymes and Cancer*. New Journal of Science, New Journal of Science, *2014, 2014*, e231418.

Karantza V. (2011). *Keratins in health and cancer: more than mere epithelial cell markers*. Oncogene, *30*(2), 127–138.

Kaufmann R, Hascher A, Mußbach F, Henklein P, Katenkamp K, Westermann M, & Settmacher U. (2012). *Proteinase-activated receptor 2 (PAR2) in cholangiocarcinoma (CCA) cells: effects on signaling and cellular level*. Histochemistry and Cell Biology, *138*(6), 913–924.

Kaufmann R, & Hollenberg MD. (2012). *Proteinase-activated receptors (PARs) and calcium signaling in cancer*. Advances in Experimental Medicine and Biology, *740*, 979–1000.

Kaufmann R, Oettel C, Horn A, Halbhuber K-J, Eitner A, Krieg R, … Settmacher U. (2009). *Met receptor tyrosine kinase transactivation is involved in proteinase-activated receptor-2-mediated hepatocellular carcinoma cell invasion*. Carcinogenesis, *30*(9), 1487–1496.

Kaufmann R, Rahn S, Pollrich K, Hertel J, Dittmar Y, Hommann M, … Settmacher U. (2007). *Thrombin-mediated hepatocellular carcinoma cell migration: Cooperative action via proteinase-activated receptors 1 and 4*. Journal of Cellular Physiology, *211*(3), 699–707.

Kawanami D, Matoba K, Kanazawa Y, Ishizawa S, Yokota T, & Utsunomiya K. (2011). *Thrombin induces MCP-1 expression through Rho-kinase and subsequent p38MAPK/NF-κB signaling pathway activation in vascular endothelial cells*. Biochemical and Biophysical Research Communications, *411*(4), 798–803.

Knecht W, Cottrell GS, Amadesi S, Mohlin J, Skåregärde A, Gedda K, … Bunnett NW. (2007). *Trypsin IV or Mesotrypsin and p23 Cleave Protease-activated Receptors 1 and 2 to Induce Inflammation and Hyperalgesia*. Journal of Biological Chemistry, *282*(36), 26089–26100.

Knight V, Tchongue J, Lourensz D, Tipping P, & Sievert W. (2012). *Protease-activated receptor 2 promotes experimental liver fibrosis in mice and activates human hepatic stellate cells*. Hepatology (Baltimore, Md.), *55*(3), 879–887.

Knowles BB, Howe CC, & Aden DP. (1980). *Human hepatocellular carcinoma cell lines secrete the major plasma proteins and hepatitis B surface antigen*. Science (New York, N.Y.), *209*(4455), 497–499.

Kozawa O, Tokuda H, Kaida T, Matsuno H, & Uematsu T. (1997). *Thrombin Regulates Interleukin-6 Synthesis through Phosphatidylcholine Hydrolysis by Phospholipase D in Osteoblasts*. Archives of Biochemistry and Biophysics, *345*(1), 10–15.

Kreso A, & Dick JE. (2014). *Evolution of the Cancer Stem Cell Model*. Cell Stem Cell, *14*(3), 275–291.

Kuo TK, Hung S-P, Chuang C-H, Chen C-T, Shih Y-RV, Fang S-CY, Yang VW, & Lee OK. (2008). *Stem cell therapy for liver disease: parameters governing the success of using bone marrow mesenchymal stem cells*. Gastroenterology, *134*(7), 2111–2121, 2121.e1–3.

Laird DJ, von Andrian UH, & Wagers AJ. (2008). *Stem cell trafficking in tissue development, growth, and disease*. Cell, *132*(4), 612–630.

Liang X, Ding Y, Zhang Y, Tse H-F, & Lian Q. (2014). *Paracrine Mechanisms of Mesenchymal Stem Cell-Based Therapy: Current Status and Perspectives*. Cell Transplantation, *23*(9), 1045–1059.

Licari LG, & Kovacic JP. (2009). *Thrombin physiology and pathophysiology*. Journal of Veterinary Emergency and Critical Care, *19*(1), 11–22.

Li J, Wang G, Wang C, Zhao Y, Zhang H, Tan Z, Song Z, Ding M, & Deng H. (2007). *MEK/ERK signaling contributes to the maintenance of human embryonic stem cell self-renewal*. Differentiation, *75*(4), 299–307.

Lin C-H, Yu M-C, Chiang C-C, Bien M-Y, Chien M-H, & Chen B-C. (2013a). *Thrombin-induced NF-κB activation and IL-8/CXCL8 release is mediated by c-Src-dependent Shc, Raf-1, and ERK pathways in lung epithelial cells*. Cellular Signalling, *25*(5), 1166–1175.

Lin H, Liu AP, Smith TH, & Trejo J. (2013b). *Cofactoring and Dimerization of Proteinase-Activated Receptors*. Pharmacological Reviews, *65*(4), 1198–1213.

Lin H, & Trejo J. (2013). *Transactivation of the PAR1-PAR2 heterodimer by thrombin elicits β-arrestin-mediated endosomal signaling*. The Journal of Biological Chemistry, *288*(16), 11203–11215.

Li T, & He S. (2006). *Induction of IL-6 release from human T cells by PAR-1 and PAR-2 agonists*. Immunology and Cell Biology, *84*(5), 461–466.

Liu Y, Li P-K, Li C, & Lin J. (2010). *Inhibition of STAT3 Signaling Blocks the Anti-apoptotic Activity of IL-6 in Human Liver Cancer Cells*. Journal of Biological Chemistry, *285*(35), 27429–27439.

Lopez AM, & Hendrickson RG. (2014). *Toxin-Induced Hepatic Injury*. Emergency Medicine Clinics of North America, *32*(1), 103–125.

Ludwicka-Bradley A, Tourkina E, Suzuki S, Tyson E, Bonner M, Fenton JW, Hoffman S, & Silver RM. (2000). *Thrombin Upregulates Interleukin-8 in Lung Fibroblasts via Cleavage of Proteolytically Activated Receptor-I and Protein Kinase C-γ Activation*. American Journal of Respiratory Cell and Molecular Biology, *22*(2), 235–243.

Lu J, Chen B, Li S, & Sun Q. (2014). *Tryptase inhibitor APC 366 prevents hepatic fibrosis by inhibiting collagen synthesis induced by tryptase/protease-activated receptor 2 interactions in hepatic stellate cells*. International Immunopharmacology, *20*(2), 352–357.

Macfarlane SR, Seatter MJ, Kanke T, Hunter GD, & Plevin R. (2001). *Proteinase-activated receptors*. Pharmacological Reviews, *53*(2), 245–282.

Madhusudhan T, Kerlin BA, & Isermann B. (2015). *The emerging role of coagulation proteases in kidney disease*. Nature Reviews Nephrology, *advance online publication*.

Ma F, Chen D, Chen F, Chi Y, Han Z, Feng X, Li X, & Han Z. (2015). *Human Umbilical Cord Mesenchymal Stem Cells Promote Breast Cancer Metastasis by Interleukin-8 and Interleukin-6 Dependent Induction of CD44(+)/CD24(-) Cells*. Cell Transplantation.

Malik N, & Rao MS. (2013). *A Review of the Methods for Human iPSC Derivation*. Methods in Molecular Biology (Clifton, N.J.), *997*, 23–33.

Marin V, Montero-Julian FA, Grès S, Boulay V, Bongrand P, Farnarier C, & Kaplanski G. (2001). *The IL-6-Soluble IL-6Rα Autocrine Loop of Endothelial Activation as an Intermediate Between Acute and Chronic Inflammation: an Experimental Model Involving Thrombin*. The Journal of Immunology, *167*(6), 3435–3442.

Marquardt JU, Andersen JB, & Thorgeirsson SS. (2015). *Functional and genetic deconstruction of the cellular origin in liver cancer*. Nature Reviews Cancer, *15*(11), 653–667.

Martello G, & Smith A. (2014). *The Nature of Embryonic Stem Cells*. Annual Review of Cell and Developmental Biology, *30*(1), 647–675.

Mason SD, & Joyce JA. (2011). *Proteolytic Networks in Cancer*. Trends in Cell Biology, *21*(4).

Ma S, Xie N, Li W, Yuan B, Shi Y, & Wang Y. (2014). *Immunobiology of mesenchymal stem cells*. Cell Death & Differentiation, *21*(2), 216–225.

Matsuoka T, Kogushi M, Kawata T, Kimura A, Chiba K, Musha T, … Hishinuma I. (2004). *1102-48 Inhibitory effect of E5555, an orally active thrombin receptor antagonist, on intimal hyperplasia following balloon injury*. Journal of the American College of Cardiology, *43*(5, Supplement 1), A68.

Maxson S, Lopez EA, Yoo D, Danilkovitch-Miagkova A, & LeRoux MA. (2012). *Concise Review: Role of Mesenchymal Stem Cells in Wound Repair*. Stem Cells Translational Medicine, *1*(2), 142–149.

McLaughlin JN, Shen L, Holinstat M, Brooks JD, DiBenedetto E, & Hamm HE. (2005). *Functional Selectivity of G Protein Signaling by Agonist Peptides and Thrombin for the Protease-activated Receptor-1*. Journal of Biological Chemistry, *280*(26), 25048–25059.

Mercer PF, & Chambers RC. (2013). *Coagulation and coagulation signalling in fibrosis*. Biochimica et Biophysica Acta (BBA) - Molecular Basis of Disease, *1832*(7), 1018–1027.

Mihara M, Hashizume M, Yoshida H, Suzuki M, & Shiina M. (2012). *IL-6/IL-6 receptor system and its role in physiological and pathological conditions*. Clinical Science, *122*(4), 143–159.

Morgan AJ, & Jacob R. (1994). *Ionomycin enhances Ca2+ influx by stimulating store-regulated cation entry and not by a direct action at the plasma membrane.* Biochemical Journal, *300*(Pt 3), 665–672.

Moschonas IC, Goudevenos JA, & Tselepis AD. (2015). *Protease-activated receptor-1 antagonists in long-term antiplatelet therapy. Current state of evidence and future perspectives*. International Journal of Cardiology, *185*, 9–18.

Muñoz-Espín D, & Serrano M. (2014). *Cellular senescence: from physiology to pathology*. Nature Reviews Molecular Cell Biology, *15*(7), 482–496.

Mußbach F, Henklein P, Westermann M, Settmacher U, Böhmer F-D, & Kaufmann R. (2014). *Proteinase-activated receptor 1- and 4-promoted migration of Hep3B hepatocellular carcinoma cells depends on ROS formation and RTK transactivation*. Journal of Cancer Research and Clinical Oncology, *141*(5), 813–825.

Nakamura T, Sakai K, Nakamura T, & Matsumoto K. (2011). *Hepatocyte growth factor twenty years on: Much more than a growth factor*. Journal of Gastroenterology and Hepatology, *26 Suppl 1*, 188–202.

Nakanuma S, Tajima H, Okamoto K, Hayashi H, Nakagawara H, Onishi I, … Harada S. (2010). *Tumor-derived trypsin enhances proliferation of intrahepatic cholangiocarcinoma cells by activating protease-activated receptor-2*. International Journal of Oncology, *36*(4), 793–800.

National Institutes of Health. (2015). *Stem Cell Basics*. Retrieved October 27, 2015, from http://stemcells.nih.gov/info/basics/pages/basics1.aspx

Neuss S, Becher E, Wöltje M, Tietze L, & Jahnen-Dechent W. (2004). *Functional Expression of HGF and HGF Receptor/c-met in Adult Human Mesenchymal Stem Cells Suggests a Role in Cell Mobilization, Tissue Repair, and Wound Healing*. STEM CELLS, *22*(3), 405–414.

Niess H, Bao Q, Conrad C, Zischek C, Notohamiprodjo M, Schwab F, … Bruns CJ. (2011). *Selective targeting of genetically engineered mesenchymal stem cells to tumor stroma microenvironments using tissue-specific suicide gene expression suppresses growth of hepatocellular carcinoma*. Annals of Surgery, *254*(5), 767–774; discussion 774–775.

Nussenbaum F, Herman IM, Nussenbaum F, & Herman IM. (2010). *Tumor Angiogenesis: Insights and Innovations, Tumor Angiogenesis: Insights and Innovations*. Journal of Oncology, Journal of Oncology, *2010, 2010*, e132641.

O'Brien PJ, Prevost N, Molino M, Hollinger MK, Woolkalis MJ, Woulfe DS, & Brass LF. (2000). *Thrombin responses in human endothelial cells. Contributions from receptors other than PAR1 include the transactivation of PAR2 by thrombin-cleaved PAR1*. The Journal of Biological Chemistry, *275*(18), 13502–13509.

O'Shea RS, Dasarathy S, & McCullough AJ. (2009). *Alcoholic Liver Disease*. The American Journal of Gastroenterology, *105*(1), 14–32.

Paradis V. (2013). *Histopathology of hepatocellular carcinoma*. Recent Results in Cancer Research. Fortschritte Der Krebsforschung. Progrès Dans Les Recherches Sur Le Cancer, *190*, 21–32.

Park CW, Kim K-S, Bae S, Son HK, Myung P-K, Hong HJ, & Kim H. (2009). *Cytokine Secretion Profiling of Human Mesenchymal Stem Cells by Antibody Array*. International Journal of Stem Cells, *2*(1), 59–68.

Pathpedia e-Atlas. (2015). *Histopathology images of Hepatocellular carcinoma*. Retrieved October 3, 2015, from http://www.pathpedia.com/education/eatlas/histopathology/liver_and_bile_ducts/hepatocellular_carcinoma.aspx

Phosphosite.org. (2015). *PAR1 (human)*. Retrieved August 12, 2015, from http://www.phosphosite.org/proteinAction.do?id=4882&showAllSites=true

Picot J, Guerin CL, Le Van Kim C, & Boulanger CM. (2012). *Flow cytometry: retrospective, fundamentals and recent instrumentation*. Cytotechnology, *64*(2), 109–130.

Plaks V, Kong N, & Werb Z. (2015). *The Cancer Stem Cell Niche: How Essential Is the Niche in Regulating Stemness of Tumor Cells?* Cell Stem Cell, *16*(3), 225–238.

Ramachandran R. (2012). *Developing PAR1 antagonists: minding the endothelial gap*. Discovery Medicine, *13*(73), 425–431.

Ramachandran R, & Hollenberg MD. (2008). *Proteinases and signalling: pathophysiological and therapeutic implications via PARs and more*. British Journal of Pharmacology, *153 Suppl 1*, S263–282.

Ramachandran R, Noorbakhsh F, Defea K, & Hollenberg MD. (2012). *Targeting proteinase-activated receptors: therapeutic potential and challenges*. Nature Reviews. Drug Discovery, *11*(1), 69–86.

Rasmussen JG, Riis SE, Frøbert O, Yang S, Kastrup J, Zachar V, Simonsen U, & Fink T. (2012). *Activation of protease-activated receptor 2 induces VEGF independently of HIF-1*. PloS One, *7*(9), e46087.

Reagan MR, & Kaplan DL. (2011). *Concise Review: Mesenchymal Stem Cell Tumor-Homing: Detection Methods in Disease Model Systems*. STEM CELLS, *29*(6), 920–927.

Regad T. (2015). *Targeting RTK Signaling Pathways in Cancer*. Cancers, *7*(3), 1758–1784.

Rehermann B, & Nascimbeni M. (2005). *Immunology of hepatitis B virus and hepatitis C virus infection*. Nature Reviews Immunology, *5*(3), 215–229.

Ren Y, Poon RT-P, Tsui H-T, Chen W-H, Li Z, Lau C, Yu W-C, & Fan S-T. (2003). *Interleukin-8 serum levels in patients with hepatocellular carcinoma: correlations with clinicopathological features and prognosis*. Clinical Cancer Research: An Official Journal of the American Association for Cancer Research, *9*(16 Pt 1), 5996–6001.

Riss TL, Moravec RA, Niles AL, Benink HA, Worzella TJ, & Minor L. (2004). *Cell Viability Assays*. In G. S. Sittampalam, N. P. Coussens, H. Nelson, M. Arkin, D. Auld, C. Austin, … J. Weidner (Eds.), *Assay Guidance Manual*. Bethesda (MD): Eli Lilly & Company and the National Center for Advancing Translational Sciences. Retrieved from http://www.ncbi.nlm.nih.gov/books/NBK144065/

Romano M, De Francesco F, Pirozzi G, Gringeri E, Boetto R, Di Domenico M, Zavan B, Ferraro GA, & Cillo U. (2015). *Expression of cancer stem cell biomarkers as a tool for a correct therapeutic approach to hepatocellular carcinoma*. Oncoscience, *2*(5), 443–456.

Rustad KC, & Gurtner GC. (2012). *Mesenchymal Stem Cells Home to Sites of Injury and Inflammation*. Advances in Wound Care, *1*(4), 147–152.

Ryan PC, Jakubczak JL, Stewart DA, Hawkins LK, Cheng C, Clarke LM, … Hallenbeck PL. (2004). *Antitumor efficacy and tumor-selective replication with a single intravenous injection of OAS403, an oncolytic adenovirus dependent on two prevalent alterations in human cancer*. Cancer Gene Therapy, *11*(8), 555–569.

Salameh MA, & Radisky ES. (2013). *Biochemical and structural insights into mesotrypsin: an unusual human trypsin*. International Journal of Biochemistry and Molecular Biology, *4*(3), 129–139.

Schinköthe T, Bloch W, & Schmidt A. (2008). *In vitro secreting profile of human mesenchymal stem cells*. Stem Cells and Development, *17*(1), 199–206.

Schlachterman A, Craft WW, Hilgenfeldt E, Mitra A, & Cabrera R. (2015). *Current and future treatments for hepatocellular carcinoma*. World Journal of Gastroenterology: WJG, *21*(28), 8478–8491.

Scholzen T, & Gerdes J. (2000). *The Ki-67 protein: From the known and the unknown*. Journal of Cellular Physiology, *182*(3), 311–322.

Scholz M, Vogel J-U, Höver G, Kotchetkov R, Cinatl J, Doerr H, & Cinatl J. (2004). *Thrombin stimulates IL-6 and IL-8*

expression in cytomegalovirus-infected human retinal pigment epithelial cells. International Journal of Molecular Medicine.

Serebruany VL, Kogushi M, Dastros-Pitei D, Flather M, & Bhatt DL. (2009). *The in-vitro effects of E5555, a protease-activated receptor (PAR)-1 antagonist, on platelet biomarkers in healthy volunteers and patients with coronary artery disease*. Thrombosis and Haemostasis, *102*(1), 111–119.

Severs NJ. (2007). *Freeze-fracture electron microscopy*. Nature Protocols, *2*(3), 547–576.

Shein HM, & Enders JF. (1962). *Transformation Induced By Simian Virus 40 In Human Renal Cell Cultures, I. Morphology And Growth Characteristics*. Proceedings of the National Academy of Sciences of the United States of America, *48*(7), 1164–1172.

Shin H, Kitajima I, Nakajima T, Shao Q, Tokioka T, Takasaki I, Hanyu N, Kubo T, & Maruyama I. (1999). *Thrombin receptor mediated signals induce expressions of interleukin 6 and granulocyte colony stimulating factor via NF-κB activation in synovial fibroblasts*. Annals of the Rheumatic Diseases, *58*(1), 55–60.

Siehler S. (2009). *Regulation of RhoGEF proteins by G12/13-coupled receptors*. British Journal of Pharmacology, *158*(1), 41–49.

Skalli O, Pelte MF, Peclet MC, Gabbiani G, Gugliotta P, Bussolati G, Ravazzola M, & Orci L. (1989). *Alpha-smooth muscle actin, a differentiation marker of smooth muscle cells, is present in microfilamentous bundles of pericytes.* Journal of Histochemistry & Cytochemistry, *37*(3), 315–321.

Soh UJ, Dores MR, Chen B, & Trejo J. (2010). *Signal transduction by protease-activated receptors*. British Journal of Pharmacology, *160*(2), 191–203.

So KA, Min KJ, Hong JH, & Lee J-K. (2015). *Interleukin-6 expression by interactions between gynecologic cancer cells and human mesenchymal stem cells promotes epithelial-mesenchymal transition*. International Journal of Oncology.

Sonawane ND, Szoka FC, & Verkman AS. (2003). *Chloride Accumulation and Swelling in Endosomes Enhances DNA Transfer by Polyamine-DNA Polyplexes*. Journal of Biological Chemistry, *278*(45), 44826–44831.

Soto AG, Smith TH, Chen B, Bhattacharya S, Cordova IC, Kenakin T, Vaidehi N, & Trejo J. (2015). *N-linked glycosylation of protease-activated receptor-1 at extracellular loop 2 regulates G-protein signaling bias*. Proceedings of the National Academy of Sciences, *112*(27), E3600–E3608.

Soto AG, & Trejo J. (2010). *N-linked glycosylation of protease-activated receptor-1 second extracellular loop: a critical determinant for ligand-induced receptor activation and internalization*. The Journal of Biological Chemistry, *285*(24), 18781–18793.

Stock P, Brückner S, Ebensing S, Hempel M, Dollinger MM, & Christ B. (2010). *The generation of hepatocytes from mesenchymal stem cells and engraftment into murine liver*. Nature Protocols, *5*(4), 617–627.

Studeny M, Marini FC, Champlin RE, Zompetta C, Fidler IJ, & Andreeff M. (2002). *Bone Marrow-derived Mesenchymal Stem Cells as Vehicles for Interferon-β Delivery into Tumors*. Cancer Research, *62*(13), 3603–3608.

Sun Z, Wang S, & Zhao RC. (2014). *The roles of mesenchymal stem cells in tumor inflammatory microenvironment*. Journal of Hematology & Oncology, *7*, 14.

Tamama K, Sen CK, & Wells A. (2008). *Differentiation of Bone Marrow Mesenchymal Stem Cells into the Smooth Muscle Lineage by Blocking ERK/MAPK Signaling Pathway*. Stem Cells and Development, *17*(5), 897–908.

Tanaka N, Morita T, Nezu A, Tanimura A, Mizoguchi I, & Tojyo Y. (2004). *Signaling Mechanisms Involved in Protease-Activated Receptor-1-Mediated Interleukin-6 Production by Human Gingival Fibroblasts*. Journal of Pharmacology and Experimental Therapeutics, *311*(2), 778–786.

Tang TC, Man S, Xu P, Francia G, Hashimoto K, Emmenegger U, & Kerbel RS. (2010). *Development of a Resistance-like Phenotype to Sorafenib by Human Hepatocellular Carcinoma Cells Is Reversible and Can Be Delayed by Metronomic UFT Chemotherapy*. Neoplasia (New York, N.Y.), *12*(11), 928–940.

Taub R. (2004). *Liver regeneration: from myth to mechanism*. Nature Reviews Molecular Cell Biology, *5*(10), 836–847.

Tello-Montoliu A, Tomasello SD, Ueno M, & Angiolillo DJ. (2011). *Antiplatelet therapy: thrombin receptor antagonists*. British Journal of Clinical Pharmacology, *72*(4), 658–671.

ten Cate H, & Falanga A. (2008). *Overview of the postulated mechanisms linking cancer and thrombosis*. Pathophysiology of Haemostasis and Thrombosis, *36*(3-4), 122–130.

Tian S, Hui X, Fan Z, Li Q, Zhang J, Yang X, … Chen H. (2014). *Suppression of hepatocellular carcinoma proliferation and hepatitis B surface antigen secretion with interferon-λ1 or PEG-interferon-λ1*. The FASEB Journal, *28*(8), 3528–3539.

Tokunou T, Ichiki T, Takeda K, Funakoshi Y, Iino N, Shimokawa H, Egashira K, & Takeshita A. (2001). *Thrombin Induces Interleukin-6 Expression Through the cAMP Response Element in Vascular Smooth Muscle Cells*. Arteriosclerosis, Thrombosis, and Vascular Biology, *21*(11), 1759–1763.

Tsochatzis EA, Bosch J, & Burroughs AK. (2014). *Liver cirrhosis*. The Lancet, *383*(9930), 1749–1761.

Ulvik RJ. (2015). *The liver in haemochromatosis*. Journal of Trace Elements in Medicine and Biology, *31*, 219–224.

Vassilopoulos G, Wang P-R, & Russell DW. (2003). *Transplanted bone marrow regenerates liver by cell fusion*. Nature, *422*(6934), 901–904.

Vu TK, Hung DT, Wheaton VI, & Coughlin SR. (1991). *Molecular cloning of a functional thrombin receptor reveals a novel proteolytic mechanism of receptor activation*. Cell, *64*(6), 1057–1068.

Wang H, & Reiser G. (2003). *The role of the Ca2+-sensitive tyrosine kinase Pyk2 and Src in thrombin signalling in rat astrocytes*. Journal of Neurochemistry, *84*(6), 1349–1357.

Wang H, Ubl JJ, Stricker R, & Reiser G. (2002). *Thrombin (PAR-1)-induced proliferation in astrocytes via MAPK involves multiple signaling pathways*. American Journal of Physiology - Cell Physiology, *283*(5), C1351–C1364.

Wang W-W, Ang SF, Kumar R, Heah C, Utama A, Tania NP, … Toh HC. (2013). *Identification of Serum Monocyte Chemoattractant Protein-1 and Prolactin as Potential Tumor Markers in Hepatocellular Carcinoma*. PLoS ONE, *8*(7).

Wang X, Willenbring H, Akkari Y, Torimaru Y, Foster M, Al-Dhalimy M, … Grompe M. (2003). *Cell fusion is the principal source of bone-marrow-derived hepatocytes*. Nature, *422*(6934), 897–901.

Waugh DJJ, & Wilson C. (2008). *The interleukin-8 pathway in cancer*. Clinical Cancer Research: An Official Journal of the American Association for Cancer Research, *14*(21), 6735–6741.

Winkler S, Schmidt L, Leibiger K, Hempel M, Ditze M, Böhmer F, Müller J, Kaufmann R, & Christ B. (2015). *Indirekte Wechselwirkungen zwischen HCC (Hep3B) und humanen mesenchymalen Stammzellen in vitro und in vivo*. Zeitschrift für Gastroenterologie, *53*(01).

Wu F, Wang J, Pu C, Qiao L, & Jiang C. (2015). *Wilson's Disease: A Comprehensive Review of the Molecular Mechanisms*. International Journal of Molecular Sciences, *16*(3), 6419–6431.

Wurster T, & May AE. (2012). *Atopaxar. A novel player in antiplatelet therapy?* Hämostaseologie, *32*(3), 228–233.

Xiu P, Dong X-F, Li X-P, & Li J. (2015). *Clusterin: Review of research progress and looking ahead to direction in hepatocellular carcinoma*. World Journal of Gastroenterology : WJG, *21*(27), 8262–8270.

Xue Y-H, Zhang X-F, Dong Q-Z, Sun J, Dai C, Zhou H-J, … Qin L-X. (2010). *Thrombin is a therapeutic target for metastatic osteopontin-positive hepatocellular carcinoma*. Hepatology, *52*(6), 2012–2022.

Yagi H, & Kitagawa Y. (2013). *The role of mesenchymal stem cells in cancer development*. Frontiers in Genetics, *4*, 261.

Yang T, Zhang X, Wang M, Zhang J, Huang F, Cai J, … Xu W. (2014). *Activation of Mesenchymal Stem Cells by Macrophages Prompts Human Gastric Cancer Growth through NF-κB Pathway*. PLoS ONE, *9*(5), e97569.

Yang ZF, & Poon RTP. (2008). *Vascular changes in hepatocellular carcinoma*. Anatomical Record (Hoboken, N.J.: 2007), *291*(6), 721–734.

Zacharski LR, Hommann M, & Kaufmann R. (2004). *Rationale for clinical trials of coagulation: reactive drugs in hepatocellular carcinoma*. Expert Review of Cardiovascular Therapy, *2*(5), 777–784.

Zhang Z, & Wang F-S. (2013). *Stem cell therapies for liver failure and cirrhosis*. Journal of Hepatology, *59*(1), 183–185.

Zhao P, Metcalf M, & Bunnett NW. (2014). *Biased signaling of protease-activated receptors*. Molecular and Structural Endocrinology, *5*, 67.

Zhao P, Yang X, Qi S, Liu H, Jiang H, Hoppmann S, … Cheng Z. (2013). *Molecular Imaging of Hepatocellular Carcinoma Xenografts with Epidermal Growth Factor Receptor Targeted Affibody Probes, Molecular Imaging of Hepatocellular Carcinoma Xenografts with Epidermal Growth Factor Receptor Targeted Affibody Probes*. BioMed Research International, BioMed Research International, *2013, 2013*, e759057.

Zheng L, & Martins-Green M. (2007). *Molecular mechanisms of thrombin-induced interleukin-8 (IL-8/CXCL8) expression in THP-1-derived and primary human macrophages*. Journal of Leukocyte Biology, *82*(3), 619–629.

Zipori D. (2004). *The nature of stem cells: state rather than entity*. Nature Reviews Genetics, *5*(11), 873–878.

Ehrenwörtliche Erklärung

Hiermit versichere ich,

(1) dass mir die Promotionsordnung der Biologisch-Pharmazeutischen Fakultät bekannt ist,

(2) dass ich die vorliegende Dissertation selbständig angefertigt habe, und alle verwendeten Quellen, Hilfsmittel und persönlichen Informationen als solche gekennzeichnet habe,

(3) dass mich Prof. Dr. F.-D. Böhmer sowie Dr. R. Kaufmann bei der Auswahl und Anfertigung des Materials sowie Manuskriptes unterstützt haben,

(4) dass ich weder die Hilfe eines Promotionsberaters in Anspruch genommen habe, noch andere Personen unmittelbare oder mittelbare geldwerte Leistungen von mir erhalten haben, die im Zusammenhang mit dem Inhalt der vorgelegten Dissertation stehen,

(5) dass ich die Dissertation noch nicht als Prüfungsarbeit für eine staatliche oder andere wissenschaftliche Prüfung eingereicht habe,

(6) dass ich zu keinem Zeitpunkt die gleiche, eine in wesentlichen Teilen ähnliche oder eine andere Abhandlung als Dissertation an einer anderen Hochschule eingereicht habe.

Jena, März 2017